AD-A144 132 MECHANICAL PROPERTIES OF MULTI-YEAR SEA ICE PHASE I TEST RESULTS(U) COLD REGIONS RESEARCH AND ENGINEERING LAB HANOVER NH G F COX ET AL. APR 84 CRREL-84-9 1/2

UNCLASSIFIED F/G 8/12 NL

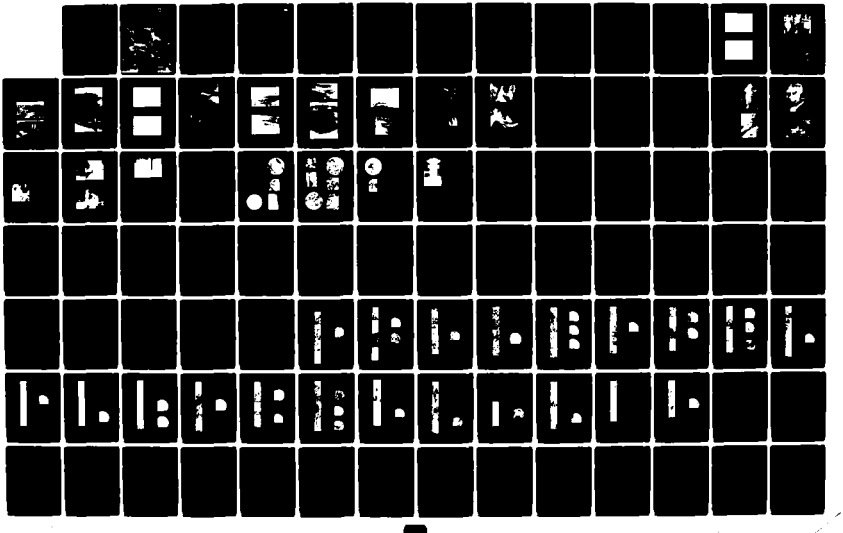

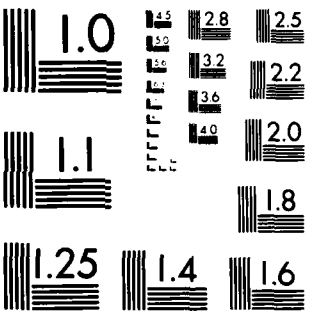

CRREL REPORT 84-9

US Army Corps of Engineers
Cold Regions Research & Engineering Laboratory

Mechanical properties of multi-year sea ice

Phase I: Test results

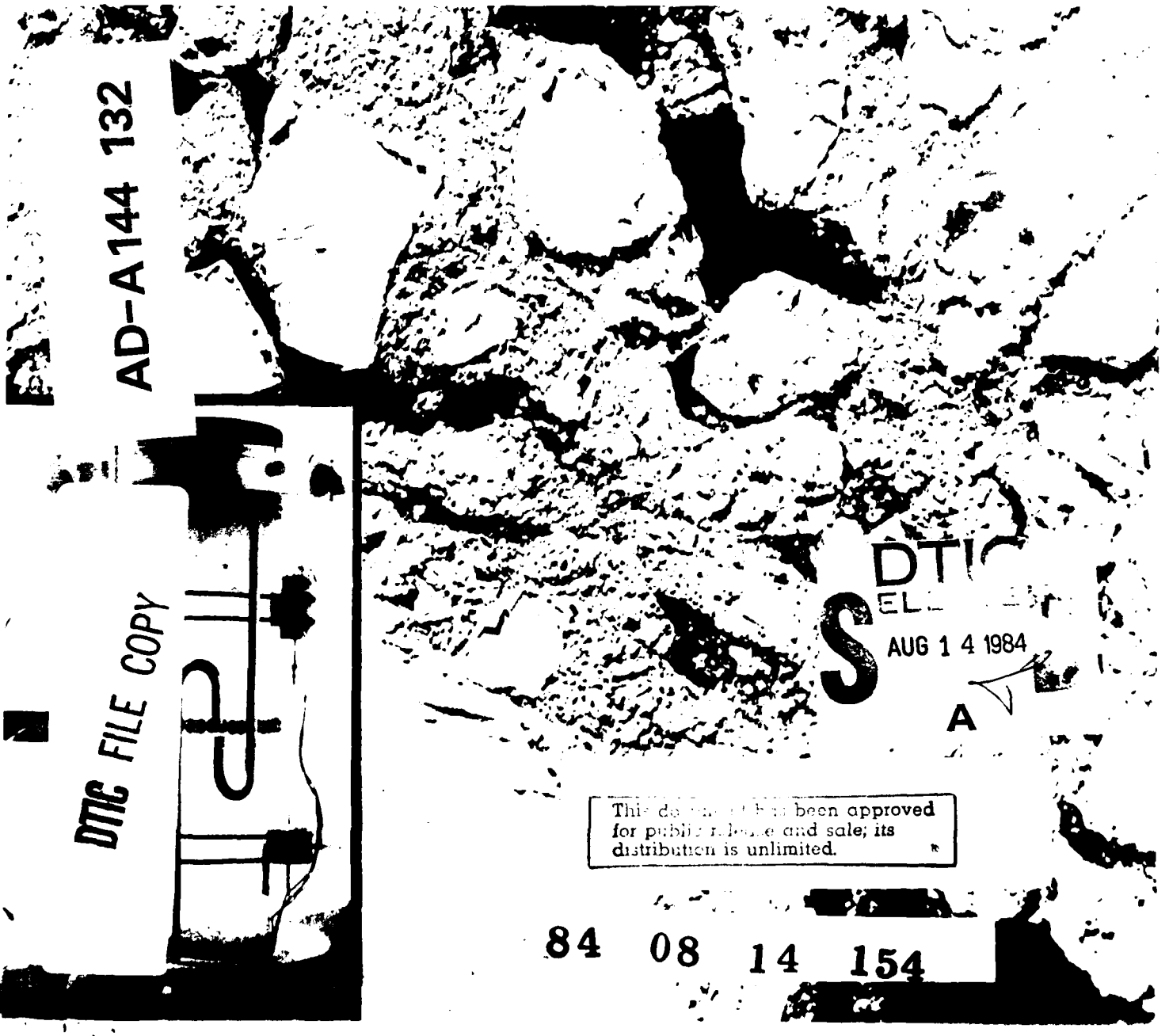

For conversion of SI metric units to U.S./British customary units of measurements consult ASTM Standard E380, Metric Practice Guide, *published by the American Society for Testing and Materials, 1916 Race St., Philadelphia, Pa. 19103.*

Cover: An instrumented test specimen superimposed over aerial photograph of pack ice in the Beaufort Sea.

CRREL Report 84-9

April 1984

Mechanical properties of multi-year sea ice
Phase I: Test results

G.F.N. Cox, J.A. Richter-Menge, W.F. Weeks,
M. Mellor and H. Bosworth

Unclassified

SECURITY CLASSIFICATION OF THIS PAGE (When Data Entered)

REPORT DOCUMENTATION PAGE

READ INSTRUCTIONS BEFORE COMPLETING FORM

1. REPORT NUMBER: CRREL Report 84-9	2. GOVT ACCESSION NO.: AD-A144132
3. RECIPIENT'S CATALOG NUMBER	
4. TITLE (and Subtitle): MECHANICAL PROPERTIES OF MULTI-YEAR SEA ICE Phase I: Test Results	5. TYPE OF REPORT & PERIOD COVERED
6. PERFORMING ORG. REPORT NUMBER	
7. AUTHOR(s): G.F.N. Cox, J.A. Richter-Menge, W.F. Weeks, M. Mellor and H. Bosworth	8. CONTRACT OR GRANT NUMBER(s)
9. PERFORMING ORGANIZATION NAME AND ADDRESS: U.S. Army Cold Regions Research and Engineering Laboratory, Hanover, New Hampshire 03755	10. PROGRAM ELEMENT, PROJECT, TASK AREA & WORK UNIT NUMBERS
11. CONTROLLING OFFICE NAME AND ADDRESS: Shell Development Company, Houston, Texas 77001 and U.S. Geological Survey (now Minerals Management Service) Reston, Virginia 22092	12. REPORT DATE: April 1984
	13. NUMBER OF PAGES: 107
14. MONITORING AGENCY NAME & ADDRESS (if different from Controlling Office)	15. SECURITY CLASS. (of this report): Unclassified
	15a. DECLASSIFICATION/DOWNGRADING SCHEDULE

16. DISTRIBUTION STATEMENT (of this Report)

Approved for public release; distribution unlimited.

17. DISTRIBUTION STATEMENT (of the abstract entered in Block 20, if different from Report)

18. SUPPLEMENTARY NOTES

19. KEY WORDS (Continue on reverse side if necessary and identify by block number)

Ice
Ice properties
Mechanical properties
Sea ice

20. ABSTRACT (Continue on reverse side if necessary and identify by block number)

This report presents the results of the first phase of a test program designed to obtain a comprehensive understanding of the mechanical properties of multi-year sea ice from the Alaskan Beaufort Sea. In Phase I, 222 constant-strain-rate uniaxial compression tests were performed on ice samples from ten multi-year pressure ridges to examine the magnitude and variation of ice strength within and between pressure ridges. A limited number of constant-strain-rate compression and tension tests, constant-load compression tests, and conventional triaxial tests were also performed on ice samples from a multi-year floe to provide preliminary data for developing ice yield criteria and constitutive laws for multi-year sea ice. Data are presented on the strength, failure strain, and modulus of multi-year sea ice under different loading conditions. The statistical variation of ice strength within and between pressure ridges is examined, as well as the effects of ice temperature, porosity, structure, strain rate and confining pressure on the mechanical properties of multi-year sea ice.

DD FORM 1 JAN 73 1473 EDITION OF 1 NOV 65 IS OBSOLETE

Unclassified

SECURITY CLASSIFICATION OF THIS PAGE (When Data Entered)

PREFACE

This report was prepared by Dr. Gordon F.N. Cox, Research Geophysicist, Dr. Wilford F. Weeks, Research Geologist, Jacqueline A. Richter-Menge, Research Civil Engineer, and Hazen W. Bosworth, Physical Science Technician, of the Snow and Ice Branch, Research Division, and Dr. Malcolm Mellor, Research Physical Scientist, of the Experimental Engineering Division, U.S. Army Cold Regions Research and Engineering Laboratory. The study was sponsored by the Shell Development Company and the Minerals Management Service of the Department of Interior with support from the Amoco Production Company, Arco Oil and Gas Company, Chevron Oil Field Research Company, Exxon Production Research Company, Gulf Research and Development Company, Mitsui Engineering and Shipbuilding Company, the National Science Foundation, Sohio Petroleum Company, Texaco, the U.S Department of Energy and the U.S. Coast Guard.

The authors thank Walter Tucker of CRREL and Dr. Jim Dorris of Shell Development Company for technically reviewing the manuscript of this report. In addition the authors are grateful for the support and cooperation provided by Glen Durell, William Burch, Larry Gould, Stephen Decato, Nancy Perron and Carl Martinson.

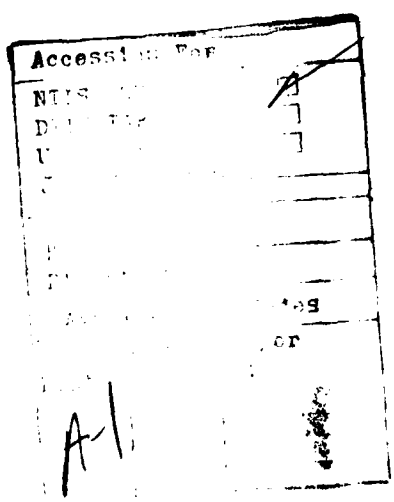

CONTENTS

	Page
Abstract	i
Preface	ii
Introduction	1
Field Sampling	1
Site selection and description	2
Ice sampling procedures	17
Shipping and storage of ice samples	19
Testing Techniques	21
Multi-year Pressure Ridge Tests	21
Ice description	21
Sampling scheme and test variables	25
Uniaxial compressive strength	26
Residual compressive strength	32
Failure strains	33
Initial tangent modulus	36
Statistical Variations in Ice Strength	40
Differences in strength above and below level ice	40
Sources of the variation in strength	41
Shape of the strength histograms	44
Multi-year Floe Ice Tests	45
Ice description	45
Uniaxial compressive strength	46
Constant-load compression tests	46
Constant-strain-rate tension tests	48
Triaxial tests	49
Conclusions	51
Literature Cited	51
Appendix A: Structural profile of a multi-year pressure ridge core	53
Appendix B: Ridge uniaxial compression test data	75
Appendix C: Structural profile of the continuous multi-year floe core	93
Appendix D: Multi-year floe test data	101

ILLUSTRATIONS

Figure

1. Map of Prudhoe Bay showing the general area where the ice samples were collected 2
2. Aerial view of study area 3
3. Aerial view of the multi-year floe that contained ridges 1 and 2 3
4. Core holes A and B on ridge 2 4
5. Surface view of the floe containing ridges 1 and 2 4
6. Surface views of ridge 1 5

Figure		Page
7.	Surface views of ridge 2	6
8.	Aerial view of ridge 2	7
9.	Aerial view of ridge 3	7
10.	Surface views of ridge 4	8
11.	Split portion of ridge 4	9
12.	Aerial view of ridges 4 and 5	9
13.	Surface view of ridge 6	10
14.	Surface view of ridge 7	10
15.	Aerial view of ridge 7	10
16.	Aerial view of ridge 8	11
17.	Surface view of ridge 9	11
18.	Aerial view of ridge 9	12
19.	Aerial view of ridge 10	12
20.	Horizontal coring at an ice quarry	13
21.	Horizontal coring in a split ridge	13
22.	Coring equipment	17
23.	Measuring the ice temperature	17
24.	Logging ice and selecting suitable test samples	18
25.	Logging site	18
26.	Measuring salinity	19
27.	Crushing dry ice for refrigerating ice samples	20
28.	Strapping ice shipping boxes on pallets	20
29.	Ice shipment in cold storage in Anchorage	21
30.	Salinity and schematic structural profile for the continuous multi-year pressure ridge core	22
31.	Thin sections illustrating various ice types	23
32.	Instrumented compression test specimen	26
33.	Uniaxial compressive strength of ridge ice samples vs strain	27
34.	Average uniaxial compressive strength of ridge ice samples vs strain rate at -5 °C (23 °F) and -20 °C (-4 °F)	28
35.	Uniaxial compressive strength vs porosity for ridge ice samples	29
36.	Uniaxial compressive strength vs failure strain for ridge ice samples	34
37.	Initial tangent modulus vs strain rate for ridge ice samples	36
38.	Average initial tangent modulus for ridge ice samples vs strain rate for tests at -5 °C (23 °F) and -20 °C (-4 °F)	37
39.	Initial tangent modulus vs porosity for ridge ice samples	38
40.	Uniaxial compressive strength at -5 °C (23 °F) vs depth for a number of multi-year pressure ridge cores	41
41.	Frequency histogram of regression line slopes of strength vs depth	41
42.	Ice strength frequency histograms	44
43.	Salinity profile and schematic structural profile for continuous multi-year floe core	45
44.	Uniaxial compressive strength of multi-year floe ice samples at -5 °C (23 °F) and -20 °C (-4 °F) vs strain rate	46
45.	Pneumatic loading jig used in constant-load compression tests	47
46.	Constant-load compression test results for the multi-year floe at -5 °C (23 °F) and -20 °C (-4 °F)	47
47.	Uniaxial tensile strength of multi-year floe specimens at -5 °C (23 °F) and -20 °C (-4 °F) vs strain rate	49

Figure Page
48. Triaxial testing equipment 49
49. Average confined compressive strength of multi-year floe samples at different temperatures and strain rates vs confining pressure at failure for confining pressure/axial stress ratios of 0.46, 0.68 and 1.00 .. 50

TABLES

Table
1. Heights and distances between sample sites 5
2. Coring data for the multi-year pressure ridges 14
3. Coring data for the undeformed multi-year ice 16
4. Summary of core and sample recovery information 16
5. Structural classification scheme for multi-year pressure ridge ice samples 23
6. Number of uniaxial compression tests of multi-year ridge ice at different temperatures and strain rates 25
7. Summary of compressive strength data for multi-year pressure ridge ice samples 26
8. Strength, structure and porosity of selected ridge ice samples 31
9. Summary of residual-maximum strength ratios for multi-year pressure ridge ice samples 33
10. Summary of failure strain data for multi-year pressure ridge ice samples 33
11. Summary of initial tangent modulus data for multi-year pressure ridge ice samples 37
12. Statistical characteristics of the uniaxial compressive strength of the samples from above and below the ice 40
13. Analysis for a three-level nested AOV model 42
14. Results of a three-level nested AOV analysis of the variation in compressive strengths, using only cores that had no "missing" samples .. 42
15. Results of a three-level nested AOV analysis of the variation in compressive strengths, including cores with "missing" samples 43
16. Summary of differences in the data sets and AOV results between the cases when no values are missing and when average values are substituted for missing values 44
17. First four moments μ_1, ... μ_4, skewness α_3, kurtosis α_4, and number of strength values n in each of the data sets 45

MECHANICAL PROPERTIES OF MULTI-YEAR SEA ICE

PHASE I: TEST RESULTS

G.F.N. Cox, J.A. Richter-Menge, W.F. Weeks,
M. Mellor and H. Bosworth

INTRODUCTION

Multi-year pressure ridges are thick accumulations of broken ice blocks that have survived at least one melt season. Surface melting and subsequent freezing of the water in the ridge voids produce a massive ice feature with few or no voids. Multi-year pressure ridges in excess of 30 m thick have been observed off the Beaufort Sea coast (Kovacs 1976).

Little is known about the structure and strength of the ice in multi-year pressure ridges. This is surprising because multi-year pressure ridges may govern the design of offshore structures in exposed areas of the Beaufort and northern Chukchi seas. Data on the mechanical properties of this ice are needed so that offshore petroleum exploration can proceed in a safe, cost-effective manner.

This report presents the results from the first phase of a joint government-industry study designed to obtain a comprehensive understanding of the structure and mechanical properties of ice samples from multi-year pressure ridges. The first phase of the study included field sampling in the southern Beaufort Sea, developing a variety of ice testing techniques, and performing 282 uniaxial compression, tension and conventional triaxial tests. Most of the tests were uniaxial compression tests. In subsequent phases of the program the emphasis will shift to tension and triaxial tests.

Ice samples were collected from ten multi-year pressure ridges and from a presumably undeformed multi-year floe. Constant-strain-rate uniaxial compression tests were performed on the ridge ice samples to assess the variations of the ice strength within and between pressure ridges. We conducted these tests at two temperatures and strain rates so that we could also evaluate effects of ice salinity, temperature, porosity, structure and strain rate on the mechanical properties of the ice. The multi-year floe ice samples were used to develop the tension, constant load and triaxial testing techniques that will be used more extensively in subsequent phases of the program.

This report includes a discussion of the field sampling program and the test results and analyses. The development of suitable sample preparation and testing techniques is described in a companion report: "Mechanical Properties of Multi-year Sea Ice: Testing Techniques" (Mellor et al. 1984).

FIELD SAMPLING

The field sampling was performed during the first two weeks of April 1981. On 1 and 2 April reconnaissance flights were flown to observe the distribution of multi-year ice in the Prudhoe Bay area. The area north and west of Reindeer Island was selected as the study area since it contained a wide variety of multi-year floes and was convenient to Deadhorse, our base camp (Fig. 1). Coring and sampling operations began on 3 April and

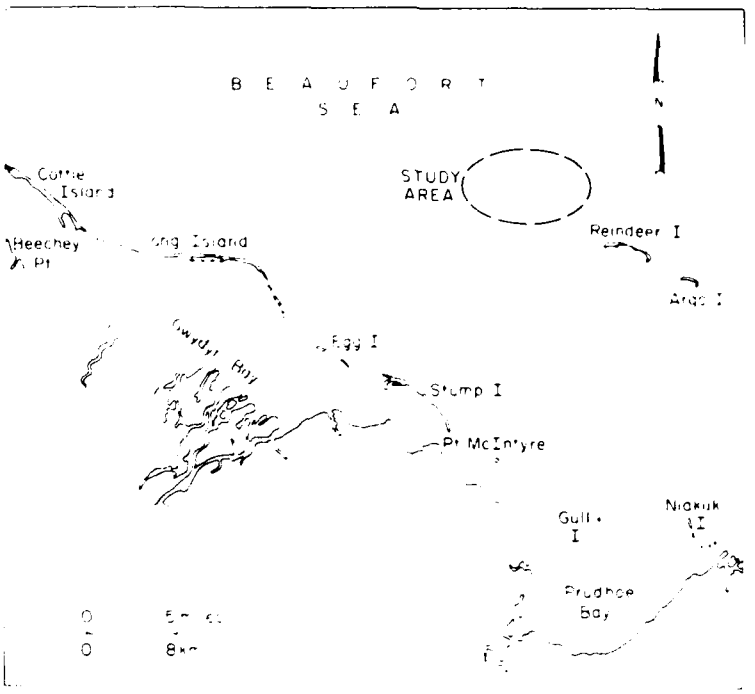

Figure 1. Map of Prudhoe Bay showing the general area where the ice samples were collected.

continued to 15 April. During this period ten multi-year ridges and a presumably undeformed multi-year floe were sampled. We collected continuous cores from one ridge and from the multi-year floe for detailed structural analysis. Paired horizontal and vertical cores were taken at two sites. In all, 329 m of ice were cored and 223 m were shipped to CRREL, resulting in 590 potential test specimens.

Site selection and description

Ten multi-year ridges were sampled on several floes located north and west of Reindeer Island. No attempt was made to determine the exact position of each ridge as there was no reason to believe that position and ridge characteristics are related. All the sampled ridges were part of the fast ice belt and did not appear to be grounded. The multi-year floes containing the ridges were generally rounded and quite varied in size. Some of the larger floes had lateral dimensions of 0.5–1 km. Figures 2 and 3 are general aerial views of some of these floes.

In selecting specific ridges we attempted to include both large and small multi-year ridges. In all cases the ridges we sampled were well-defined linear features that were readily discernible from the air. On each ridge, four cores were obtained, two from each of two sites. Figure 4 shows the pair A and B on ridge 2, separated by 33 cm. The pairs of cores at sites AB and CD on the various ridges were separated by 14–46 m. Table 1 gives A-B, C-D and AB-CD distances and the elevations of the drill sites above level ice in the vicinity of each ridge. On each of the ten ridges the intent was to sample two locations that were far enough apart so that the specimens were clearly from different areas; at each of these locations the two cores were as close to each other as reasonable without developing drilling difficulties. The exact spacings were controlled by the geometries of the various ridges. The surface morphology of the ten ridges was similar: all showed rounded outlines, indicating that they had undergone surface melt; their surfaces were covered with thin snow covers; and the ridge heights were irregular. Figure 3 and 5 show aerial and surface views of the floe containing ridges 1 and 2. Figure 6 shows surface views of ridge 1. A pair of vertical and horizontal cores was also collected on ridge 1, which was also studied by Vaudrey and Associates. Figure 7 shows two surface views of ridge 2, and Figure 8 is an aerial view. Figure 9 is an aerial view of ridge 3 with people on the ice for scale.

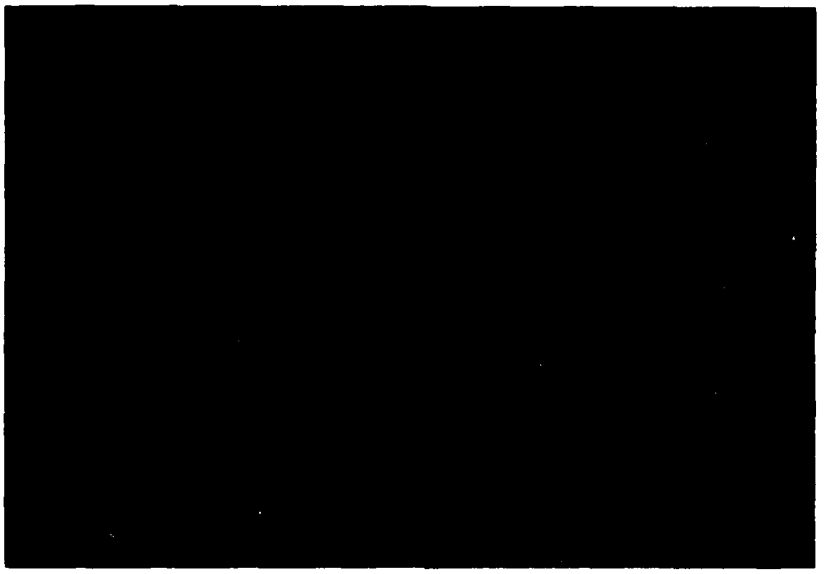

Figure 2. Aerial view of study area.

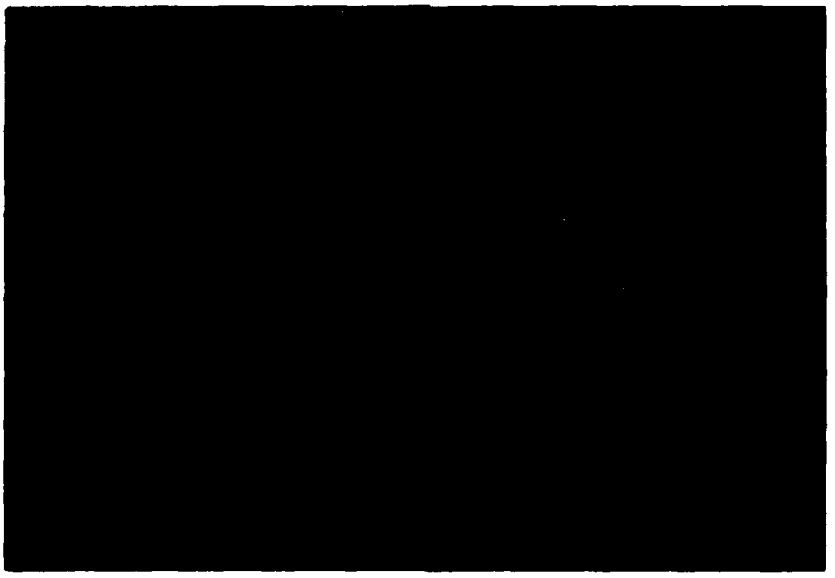

Figure 3. Aerial view of the multi-year floe that contained ridges 1 and 2. The structure is a one-room building installed by Vaudrey and Associates.

Figure 4. Core holes A and B on ridge 2.

Figure 5. Surface view of the floe containing ridges 1 and 2.

Table 1. Heights and distances between sample sites.

Ridge	Height above level ice (m) A, B	C, D	Distance between sites A-B (cm)	C-D (cm)	AB-CD (m)
1	2.1	1.7	45	47	20
2	2.7	1.7	33	41	25
3	2.1	1.8	40	43	30
4	4.0	3.7	63	47	15
5	2.1	1.7	21	24	20
6*	5.2	1.8	—	—	18
7	1.5	0.6	17	21	36
8	1.8	3.7	17	20	27
9	3.7	1.8	21	37	46
10	2.7	2.1	26	22	14

* Ice obtained only at sites A and C.

Figure 6. Surface views of ridge 1.

Figure 7. Surface views of ridge 2.

Figure 8. Aerial view of ridge 2.

Figure 9. Aerial view of ridge 3.

Figure 10. Surface views of ridge 4.

Ridge 4 was large, with the drill sites located 4 and 3.7 m above the surrounding floe (Fig. 10). This ridge was split, exposing its internal structure (Fig. 11). Ridge 5 was lower and located near ridge 4 (Fig. 12). Ridge 6 was the highest ridge sampled, with one drill site 5.2 m above the surrounding ice (Fig. 13). The blocky nature of portions of ridge 6 and the number of voids in the core suggest that this ridge was composed of second-year ice. In fact, the condition of the ice in this ridge was so poor that only one hole was drilled at each site. Ridge 7 was a low ridge that did not possess any particularly distinguishing features (Figs. 14 and 15). Ridge 8 was a long distinctive feature (Fig. 16). Ridges 9 and 10 were both on the same large floe (Figs. 17-19).

Figure 11. Split portion of ridge 4.

Figure 12. Aerial view of ridges 4 and 5

Figure 13. Surface view of ridge 6.

Figure 14. Surface view of ridge 7.

Figure 15. Aerial view of ridge 7.

Figure 16. Aerial view of ridge 8.

Figure 17. Surface view of ridge 9.

Figure 18. Aerial view of ridge 9.

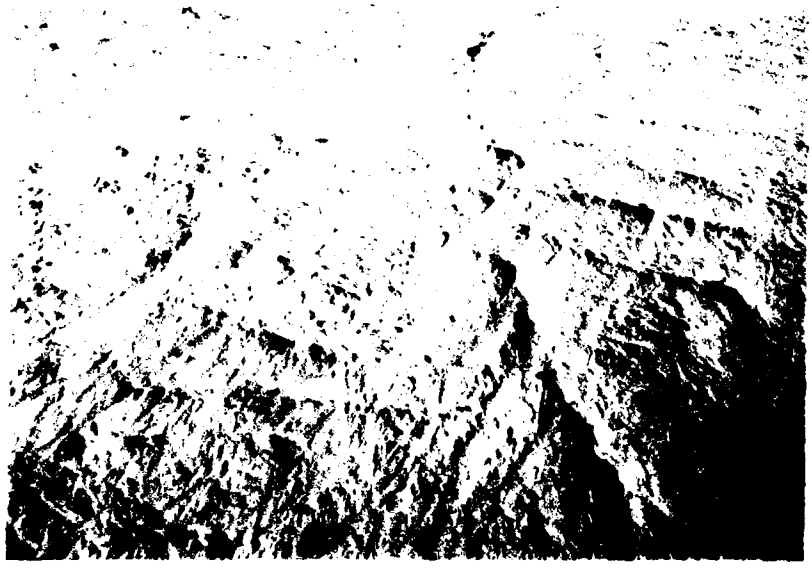

Figure 19. Aerial view of ridge 10.

The presumably undeformed multi-year ice that was cored was near the hut close to ridges 1 and 2 (Fig. 3). We assumed that the ice was undeformed because the sampling area was flat; however, thin sections of the ice core showed columnar ice having a growth direction up to 30° from the vertical. The first set of matching horizontal and vertical cores was from ridge 1, where Vaudrey and Associates had quarried ice for test beams (Fig. 20). The continuous multi-year pressure ridge core collected for petrographic study was obtained nearby. Finally, the second set of matching horizontal and vertical cores was collected from a large ridge that had split, allowing horizontal coring (Fig. 21).

Tables 2, 3 and 4 present data on the length of hole drilled, the estimated number of specimens obtained, and the amount of core that was shipped to CRREL for testing. A total of 467 samples were obtained from multi-year pressure ridges.

Figure 20. Horizontal coring at an ice quarry.

Figure 21. Horizontal coring in a split ridge.

We had planned to collect at least six samples from each drill site (there were four drill sites on each ridge), but we actually collected from 8 to 16 at each site. We also planned to collect two samples from above level ice (ridge sail) and four samples from below level ice (ridge keel) at each site. This requirement was met and usually exceeded at all sites except 7C and D, where a low freeboard prevented us from collecting more than one sample above level ice at each site, and at 4A and B, where a high freeboard prevented us from collecting more than two samples below level ice at each site. About 120 samples were collected from the presumably undeformed multi-year floe.

Table 2. Coring data for the multi-year pressure ridges.

Ridge no.	Site	Ridge height (m)	Depth of penetration (m)	Approximate no. of samples: Above level ice	Below level ice	Total	Core length retained (m)
1	A	2.1	4.75	6	6	12	4.70
	B	2.1	5.65	4	10	14	5.19
	C	1.7	4.30	3	6	9	3.73
	D	1.7	4.22	3	6	9	3.48
2	A	2.7	4.53	6	5	11	3.77
	B	2.7	5.09	6	6	12	4.82
	C	1.7	5.14	3	8	11	4.44
	D	1.7	5.37	4	5	9	3.61
3	A	2.1	5.47	3	8	11	3.99
	B	2.1	4.07	5	4	9	3.76
	C	1.8	4.46	4	6	10	3.76
	D	1.8	3.99	4	5	9	3.57
4	A	4.0	4.68	9	2	11	4.63
	B	4.0	4.78	10	2	12	4.78
	C	3.7	5.82	7	5	12	4.31
	D	3.7	5.63	9	5	14	5.63
5	A	2.1	5.38	7	8	15	5.28
	B	2.1	4.30	6	5	11	4.30
	C	1.7	5.92	4	10	14	5.47
	D	1.7	5.88	3	10	13	5.29
6	A	5.2	7.29	7	6	13	4.60
	C	1.8	6.29	5	9	14	5.14
7	A	1.5	5.92	4	9	13	4.81
	B	1.5	6.93	3	13	16	6.30
	C	0.6	6.07	1	8	9	3.01
	D	0.6	5.76	1	9	10	3.30
8	A	1.8	4.68	4	5	9	3.23
	B	1.8	5.45	4	8	12	4.16
	C	3.7	6.25	6	5	11	3.86
	D	3.7	7.00	4	6	10	3.27

Table 2 (cont'd).

Ridge no.	*Site*	*Ridge height (m)*	*Depth of penetration (m)*	*Approximate no. of samples*			*Core length retained (m)*
				Above level ice	*Below level ice*	*Total*	
9	A	3.7	5.70	7	4	11	3.63
	B	3.7	5.12	7	3	10	3.28
	C	1.8	5.45	4	7	11	3.63
	D	1.8	4.98	4	5	9	2.97
10	A	2.7	5.81	3	6	9	2.94
	B	2.7	4.99	4	4	8	2.64
	C	2.1	5.73	3	8	11	3.63
	D	2.1	5.99	3	7	10	3.63
Total			204.84			424	156.54
		Paired horizontal and vertical cores					
Horizontal 1	1		4.06			7	2.31
	2		3.02			5	1.66
Vertical 1	1		2.18			4	1.32
	2		2.30			3	1.02
	3		2.31			2	0.66
	4		2.11			3	1.34
Horizontal 2	1		3.26			5	1.65
	2		3.27			3	0.99
Vertical 2	1		3.30			2	0.66
	2		3.21			1	0.33
	3		2.30			3	0.99
	4		3.18			5	1.65
Total			34.50			43	14.58
Thin-section and salinity core			8.18				8.02
Grand total			247.52			467	179.14

Table 3. Coring data for the undeformed multi-year ice.

Site	*Length cored (m)*	*No. of samples*	*Length retained (m)*
C1	3.35	2	0.66
C2	3.56	7	2.31
C3	3.31	7	2.31
C4	3.35	6	1.98
C5	3.17	6	1.98
C6	3.32	5	1.65
C7	3.31	5	1.65
C8	3.14	5	1.65
C9	3.31	6	1.98
C10	3.27	6	1.98
C11	3.00	6	1.98
C12	3.29	5	1.65
C13	3.20	5	1.65
C14	3.28	4	1.35
C15	3.13	5	1.65
C16	3.35	6	1.98
C17	3.10	4	1.35
C18	3.34	5	1.65
C19	3.34	5	1.65
C20	3.23	4	1.35
C21	3.17	7	2.31
C22	3.30	5	1.65
C23	3.13	4	1.35
C24	3.14	5	1.65
Total	78.09	123	40.74
Thin-section and salinity core	3.18		3.18
Grand total	81.27		43.92

Table 4. Summary of core and sample recovery information.

Ice cored	*Length cored (m)*	*Length retained (m)*	*Percentage retained*	*Approximate no. of samples*
	Multi-year pressure ridges			
Vertical holes	204.84	156.54	76	424
Paired vertical and horizontal cores	34.50	14.58	42	43
Thin-section and salinity core	8.18	8.02	87	—
	Undeformed multi-year ice			
Thin-section and salinity core	3.18	3.18	100	—
Vertical holes	78.09	40.74	52	123
Total	328.79	223.06		590

There were large variations in the percentage of collected ice that was actually retained (Table 4). These variations are readily explainable. Two cores were taken strictly to provide ice for determining ice temperature, salinity and internal structure. All of these cores were retained (except for a small, badly shattered segment that was judged unusable, even for these purposes). At first only one person was available to log the ice cores from the multi-year pressure ridges. As core logging was the slowest part of the sampling procedure, time was not available to trim all samples to size. Therefore, an appreciable amount of extra ice was loaded for additional thin section and salinity analyses. Later, when the multi-year floe was being sampled, two persons were logging cores, samples were trimmed to 33-cm lengths, and it was not necessary to collect additional ice. A sample recovery rate of 60% is probably a reasonable figure to use in planning future programs involving vertical coring. The low recovery rate from two sites where paired vertical and horizontal cores were collected (42%) was caused by the poor quality of the ice.

Ice sampling procedures

Drilling

Ice cores 4¼ in. (10.8 cm) in diameter were obtained with a fiberglass coring auger specifically designed and built for this study. The auger was driven by a ¼-in., ¼-h.p. electric drill (Fig. 22). Power was supplied by a 1700-W generator. The cores were obtained at depth by attaching CRREL auger extension rods to the core barrel. To prevent the extension rods and core barrel down the hole from vibrating, spacers having outside diameters of 5.625 in. (14.3 cm) were attached around the extension rods. The new, larger-diameter auger produced high-quality ice cores up to 120 cm in length. Details on the core barrel design are given in Rand (In prep.).

Core measurements

Immediately after the core was retrieved from the ice, a temperature reading was taken in the bottom of the core. A hole was drilled into the center of the core with an electric hand drill, and a thermistor probe was inserted in the ice (Fig. 23). While the temperature equilibrated, the length of core was measured and 33-cm-long strength test samples were selected (Fig. 24). Generally, one to three test samples were obtained from each ice core. Ice containing core dog gouges was rejected, while ice containing healed natural cracks was re-

Figure 22. Coring equipment.

Figure 23. Measuring the ice temperature.

Figure 24. Logging ice and selecting suitable test samples.

Figure 25. Logging site. Note core tubes and salinity containers.

tained for testing. The samples were cut to length with a coarse-toothed pruning saw. The lower 5 cm of each core, from which the ice temperature was obtained, was also usually saved for an ice salinity measurement. This ice was placed in numbered 1-qt freezer containers. Pieces less than 33 cm long were measured and discarded. At least 33 cm of ice would be needed for easy matching to final test specimen dimensions. Both discarded and test ice were catalogued for length and depth. The positions of the temperature and salinity samples were also noted so that temperature and salinity profiles could later be plotted. We then placed the test ice in numbered core tubes, taking note of the core tube number and the position of the test ice in the tube (Fig. 25). The core tubes were packed in wooden boxes lined with insulation for shipment to Deadhorse.

In Deadhorse the ice salinity samples were melted, and salinities were determined with a conductivity bridge (Fig. 26). The core tubes were transferred to insulated boxes for shipment to CRREL in Hanover.

Figure 26. Measuring salinity.

Shipping and storage of ice samples

Shipping and storage of the ice core samples were important parts of the ice sampling program. Samples were temporarily stored in Deadhorse and Anchorage, and shipped from Deadhorse to Anchorage and on to Hanover.

When the ice was sampled, the air temperatures in the Prudhoe Bay area remained below -15 °C. Since the ambient temperatures were close to the $NaCl \cdot 2H_2O$ eutectic, -22.9 °C, and because the multi-year ice had a low salinity, usually less than 4 °/oo, no special measures were taken to refrigerate the samples, either on the ice or in Deadhorse. No brine drainage from the core samples was observed. Had it been unseasonably warm, the cores would have been packed in dry ice immediately after removing them from the ice floe.

Upon removal from the ice, the cores were cut to length, catalogued and packed in core tubes. In Deadhorse, gaps in the core tubes were packed with paper to protect the core ends from damage during shipment. The core tubes were then placed in insulated shipping boxes. These boxes were constructed of heavy-weight, wax-coated cardboard, with 3-in.-thick styrofoam on the bottom, sides and top. Each box could accommodate six 1-m-long tubes, snow for packing, and dry ice for refrigeration.

When ten or more shipping boxes were filled with core samples, a shipment of dry ice was ordered from Anchorage. To avoid delays in shipment, the dry ice was shipped to Deadhorse by cargo air freight. When the dry ice arrived in Deadhorse, the ice core boxes were taken to the air cargo terminal, where they were packed with snow and dry ice. Two to three inches of snow were packed on top of the core tubes to prevent thermal cracking of the cores, which could result from direct contact with the dry ice. Then two blocks of dry ice were crushed and spread over the top of the snow in each box (Fig. 27). Each block of dry ice originally weighed 25 lbs. About 8 lbs were lost in shipment to Deadhorse due to sublimation. Thus, each shipping box was sent to Anchorage with about 35 lbs of dry ice.

To minimize shipping damage and to facilitate handling, the boxes were strapped to wooden pallets (Fig. 28). Two boxes were placed on each pallet. Instructions were given to the shipper not to stack the pallets more than two high. "Freeze" stickers were also placed on the boxes to alert shippers that the boxes should be refrigerated if they were delayed in shipment. To prevent the ice from being delayed in Deadhorse or Fairbanks, the ice was usually sent priority air freight to Anchorage. Three ice shipments were made from Deadhorse to Anchorage. An expediting firm in Anchorage was alerted prior to each ice shipment. They were provided with shipping information, such as air bill number and number of boxes. The expediter met each shipment as it arrived in Anchorage, inspected the dry ice, and moved the ice to a cold-storage facility at a seafood processing plant (Fig. 29). Storage temperatures were maintained at -30 °C.

Figure 27. Crushing dry ice for refrigerating ice samples.

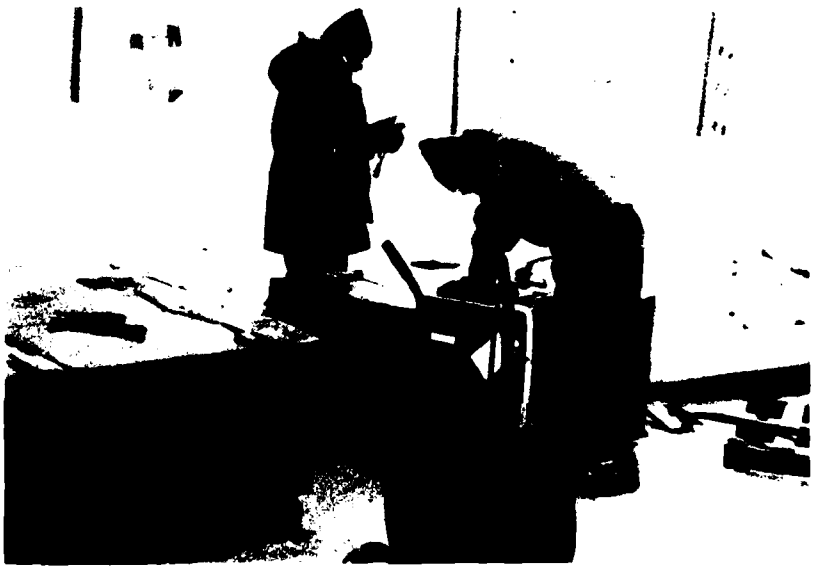

Figure 28. Strapping ice shipping boxes on pallets.

Figure 29. Ice shipment in cold storage in Anchorage.

All of the shipping boxes still contained dry ice when they arrived in Anchorage. However, about half the dry ice in each box was lost after a 36-hour wait in Deadhorse and a 3-hour flight to Anchorage (which stopped in Fairbanks).

At the end of the field sampling program, two CRREL employees went to Anchorage to prepare the ice samples for shipment to Hanover. Each of the boxes was opened and repacked with 75 lbs of dry ice, and the boxes were rebanded to the pallets. The ice was then shipped priority air freight to Boston, where it was met by CRREL employees with a refrigerated truck. The ice was then taken to CRREL and stored at -30°C.

TESTING TECHNIQUES AND PROCEDURES

Sample preparation and testing techniques were developed to perform quality uniaxial compression and tension tests at a constant strain rate, uniaxial compression tests at a constant load, and conventional triaxial tests at a constant strain rate. During this development, different sample geometries, platens, strain-measurement transducers, and loading devices were evaluated. These efforts are described in a companion report (Mellor et al. 1984). Close attention was given to the practices recommended by Hawkes and Mellor (1970) for the uniaxial testing of rock, and the IAHR ice-testing standardization group (Schwarz et al. 1981).

MULTI-YEAR PRESSURE RIDGE TESTS

Ice description

Prior to this investigation no detailed structural analyses had been performed on ice samples from multi-year pressure ridges. It is therefore appropriate to examine the structure, salinity and density of the ice so that the test results can be properly evaluated. As it is often difficult to differentiate between the original fabric and the deformation fabric of a tested specimen, a continuous core was obtained from a multi-year pressure ridge specifically for structural analysis. A simple structural classification scheme was also devised from continuous core and sample thin sections for investigating the effects of ice structure on strength.

From our understanding of pressure ridge formation and consolidation mechanisms we would expect to find a variety of ice types in a multi-year pressure ridge. A given core may contain small to large fragments of columnar sheet ice blocks; slush, snow and granular ice in the frozen voids between the sheet ice blocks; and even some freshwater ice derived from summer melting. We would expect large blocks of sheet ice in compression ridges and small fragments of sheet ice in shear ridges, depending on how the ridge was formed.

The structural profile of the 8.2-m-long, multi-year ridge continuous core is given in Appendix A. If the keel-to-sail ratio was 3.3 (Kovacs 1983), this ridge was 12.9 m thick. The profile was prepared by splicing photographs of vertical-ice thin sec-

tions taken in crossed polarized light. A few photographs of horizontal thin sections are also included. A second vertical profile (which is not included here) of the same core was also prepared from thin sections obtained at right angles to the first profile to aid in determining the structural type and orientation of the crystals.

The upper 140 cm of the core consists of isotropic, fine-grained (<2 mm) to medium-grained (2–6 mm) granular ice. At about 140 cm there is a transition to fine- to medium-grained columnar crystals having no well-defined orientation. This ice, which is mixed with some fine granular material, continues to about 167 cm, where a 3-cm, fine-grained band begins. Below the band the columnar crystals become elongated in a direction 25° from the vertical. At 185 cm the direction of elongation again becomes irregular, and the crystals are mixed with fine-grained material. Some fine granular grains are present in well-defined bands. From 210 to 260 cm the columnar crystals are medium-grained to coarse-grained (>6 mm) and are elongated 10° from the vertical.

At about 260 cm there is a striking change in the fabric. A 100-cm-thick layer of brecciated ice is found consisting of columnar and granular fragments up to 5 cm in diameter surrounded by fine- to medium-grained granular ice. Samples of the granular material had porosities of about 500 °/oo and salinities of 0.04 °/oo. It is surprising to find such porous ice below sea level, as one would expect porous ice to be saturated with seawater and have a higher salinity. The larger fragments consist of either columnar sea ice or columnar freshwater ice. The freshwater ice was probably derived from a frozen melt pond that was incorporated into the ridge.

From 360 to 460 cm the core consists largely of isotropic fine and medium granular material with a few isolated patches of brecciated ice. This is followed by about 90 cm of medium- and coarse-grained columnar crystals generally showing no preferred orientation. Fine-grained, healed cracks are also present in the ice. At 550 cm a 15-cm-thick layer of brecciated ice begins. The layer is similar to the brecciated ice above, but the columnar fragments are smaller.

The remainder of the core consists of columnar ice. From 565 to 600 cm columnar crystals are coarse-grained and have no preferred orientation. At about 600 cm the c-axes of the crystals become horizontal, and between 700 and 800 cm the c-axes show strong alignment in the horizontal plane. The crystals are medium- to coarse-grained. The bottom 20 cm of the core consists of coarse-grained crystals having c-axes close to horizontal, with no preferred alignment.

About one-third of the core consists of columnar ice, most of which is near the bottom of the core (Fig. 30). The upper portion of the core consists largely of granular ice, mixed granular and columnar ice, and pulverized, brecciated ice. Overall, the ice structure is highly variable, and we would expect the mechanical properties of the ice to be equally variable.

The salinity profile (Fig. 30) shows a characteristically low salinity in the upper portion of the ridge caused by flushing of the brine during the melt season (Cox and Weeks 1974). At depth the salinity is generally greater, except for the brecciated ice, which has a low salinity. These observations from the continuous core are consistent with the salinity measurements of the tested specimens. Samples from the ridge sails had an average salinity of 0.7 °/oo, while samples from the ridge keels had an average salinity of 1.5 °/oo. The mean salinity of all the test samples was 1.3 ± 0.8 °/oo.

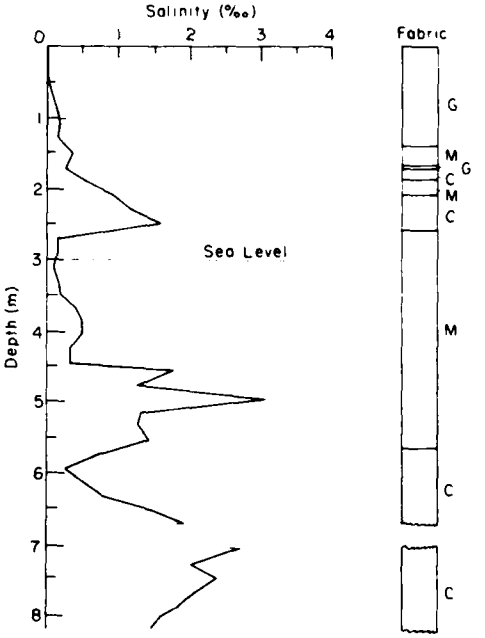

Figure 30. Salinity and schematic structural profile for the continuous multi-year pressure ridge core. G = granular ice, C = columnar ice; M = mixed granular and columnar ice.

The ice in the sails also had a lower density. The average density of the test samples from the ridge sails was 0.875 Mg/m³ (54.6 lbs/ft³). The keel samples had an average density of 0.899 Mg/m³ (56.1 lbs/ft³). Densities were determined at -20°C (-4°F). The lower density of the sail samples can be attributed to their higher porosity and lower salinity.

Based on the ice structure in the continuous core and the test specimens, a simple ice structure classification scheme was devised to help in examining the effects of ice structure on strength (Table 5). Existing ice classification methods, such as those of Michel (1978) and Cherepanov (1974), are not appropriate because they do not consider deformed ice. Figure 31 illustrates the structural

Table 5. Structural classification scheme for multi-year pressure ridge ice samples.

Ice type	*Code*	*Structural characteristics*
Granular	I	Isotropic, equiaxed crystals
Columnar	II	Elongated, columnar grains
	IIA	Columnar sea ice with c-axes normal to growth direction; axes may not be aligned
	IIB	Columnar sea ice having random c-axis orientation (Transition ice)
	IIC	Columnar freshwater ice; may be either anisotropic or isotropic
Mixed	III	Combination of Types I and II
	IIIA	Largely Type II with granular veins
	IIIB	Largely Type I with inclusions of Type I or II ice (Brecciated ice).

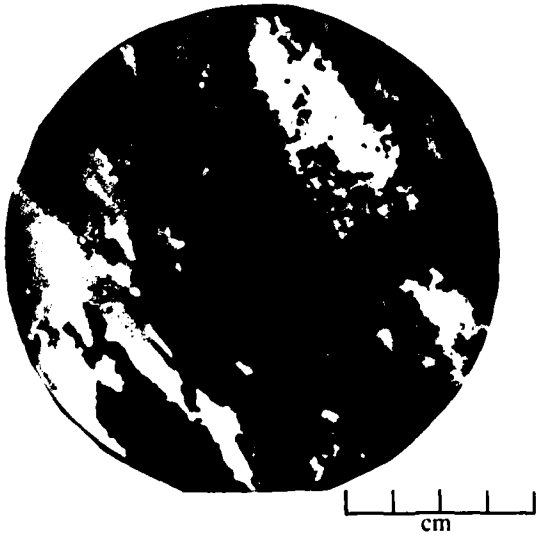

Horizontal Section (Aligned)

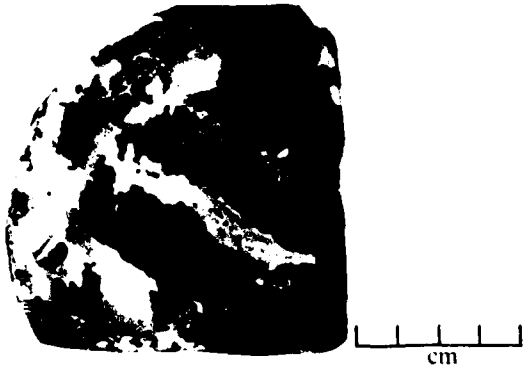

Horizontal Section (Unaligned)

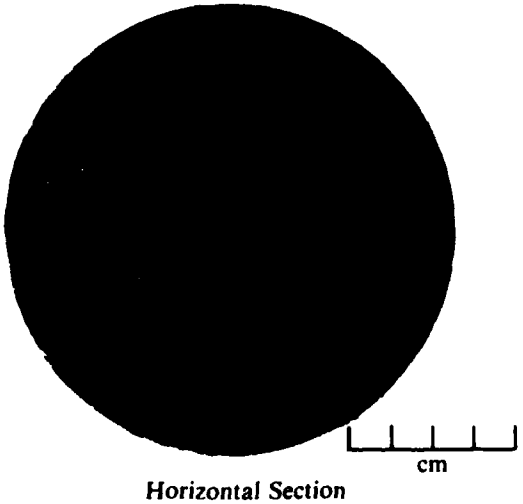

Horizontal Section

a. Granular ice (Type I).

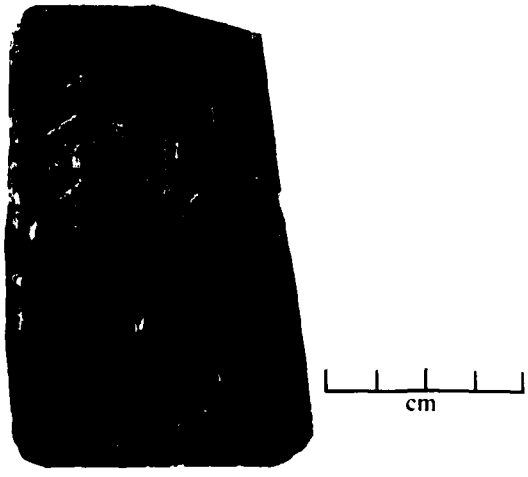

Vertical Section (0° Elongation)

b. Columnar sea ice (Type IIA).

Figure 31. Thin sections illustrating various ice types.

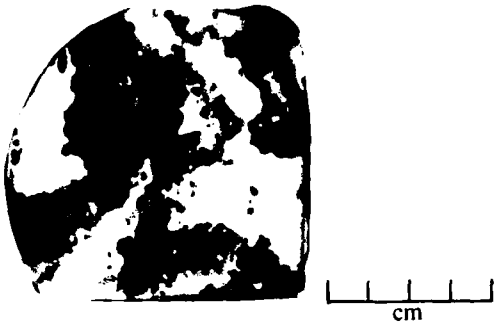

Horizontal Section

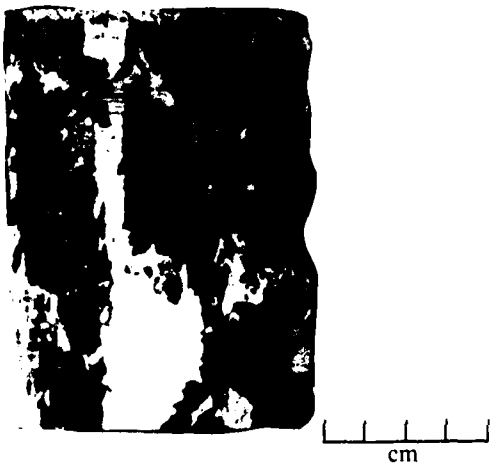

Vertical Section

c. Columnar transition sea ice (Type IIB).

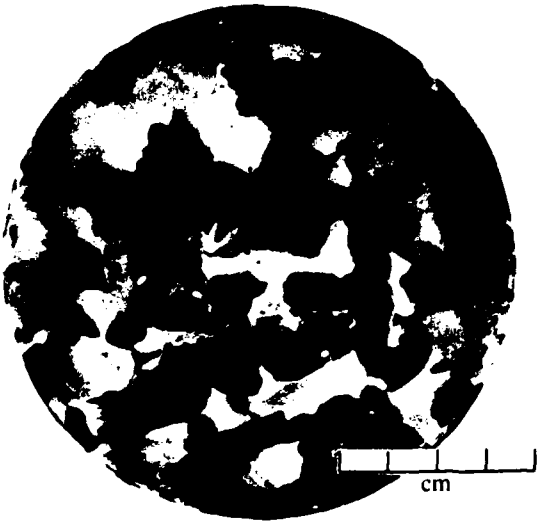

Horizontal Section

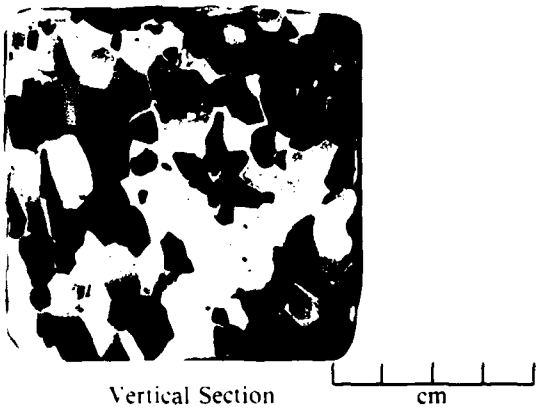

Vertical Section

d. Columnar freshwater ice (Type IIC).

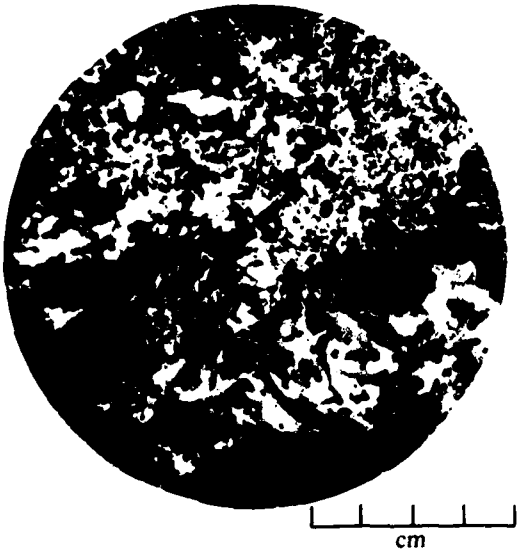

Horizontal Section

e. Mixed ice (Type III).

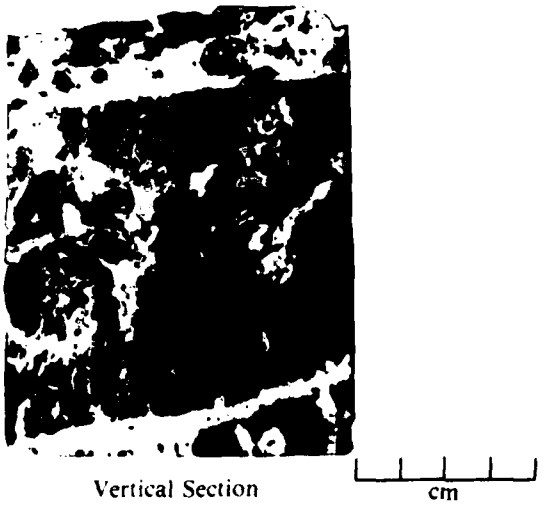

Vertical Section

f. Mixed ice, columnar with granular veins (Type IIIA).

Figure 31 (cont'd). Thin sections illustrating various ice types.

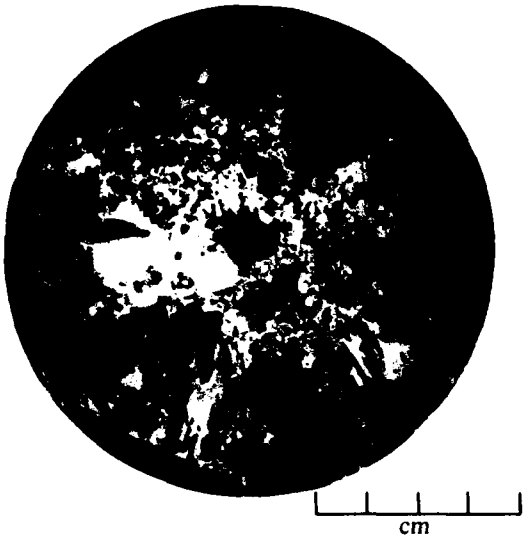

Horizontal Section

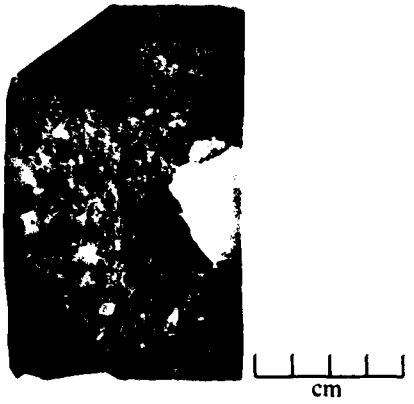

Vertical Section

g. Mixed, brecciated ice (Type IIIB).

Figure 31 (cont'd).

characteristics of each ice type in our classification scheme.

The classification scheme does not consider any genetic criteria; however, the origin of each type may be postulated. Granular ice may be derived from snow or slush ice, frazil, granulation of sheet ice during the ridge building process, or freezing in the void spaces in the ridge during consolidation. Columnar ice is probably largely derived from the parent sheet ice, which was deformed to form the ridge. It may also form at the base of the ridge by congelation growth after the ridge was formed. The mixed ice probably originated during building and consolidation. Mixtures of granular and columnar (Type III) ice may form in the ridge voids. Type IIIA ice includes healed fractures, and Type IIIB ice is probably the cataclastic product of ice blocks ground from the parent sheet.

Sampling scheme and test variables

Uniaxial compression tests were performed on the ice samples obtained from the ten multi-year pressure ridges to examine the magnitude and variation of ice strength both within and between pressure ridges. For each of the four core sites on each ridge, we tried to test two samples from the ridge sail (above level ice) and four samples from the ridge keel (below level ice). The tests were conducted at two strain rates and two temperatures so that the effects of these variables on the mechanical properties of the ice could also be evaluated. These temperatures and strain rates were chosen to bracket the conditions that would be expected in the ice off the Alaska coast under normal operating conditions. We tested 222 samples (Table 6).

Table 6. Number of uniaxial compression tests of multi-year ridge ice at different temperatures and strain rates.

	Number of tests		
	10^{-3}/s	10^{-1}/s	Total
-5 °C (23 °F)	69	71	140
-20 °C (4 °F)	41	41	82
Total	110	112	222

All of the compression tests were performed on a closed-loop electrohydraulic testing machine. The machine had two actuators with capacities of 1.1 and 0.11 MN and a fast-response, high-flow-rate servovalve. The load frame of the machine had a capacity of 2.2 MN. Test strain rates were controlled by monitoring the full sample strain with an extensometer, which was attached to phenolic-resin end caps bonded to the test specimens (Fig. 32). The tests were programmed to continue to 5% full sample strain to examine the post-yield behavior and residual strength of the ice. Since this resulted in considerable deformation of the test specimen, strain rates could not be controlled by transducers mounted on the ice. Test temperatures were controlled to within 0.5 °C by placing the sample in an environmental chamber mounted on the testing machine. The lower machine platen was also refrigerated to eliminate thermal gradient problems.

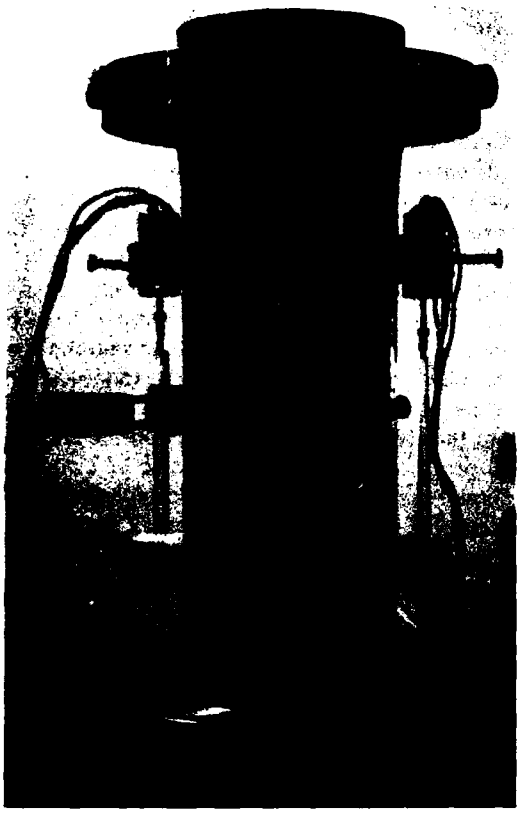

Figure 32. Instrumented compression test specimen.

In addition to monitoring loads and full-sample strains during each test, axial strains were measured with a pair of direct-current distance transducers (DCDTs) mounted on the center of the sample. In a few of the tests, circumferential strains were measured in the middle of the sample with a roller chain and extensometer; however, these data were rejected because the roller chain and extensometer could not be seated properly on the sample when the displacement was very small. Data were recorded on an XY plotter, a strip chart, and an FM magnetic tape recorder.

We prepared cylindrical specimens from the 10.7-cm-diameter core. Samples were first cut to length on a band saw, and the ends were milled square on a milling machine to produce a 25.4-cm-long test specimen. Phenolic end caps were bonded to the sample ends, and the sample was turned to a diameter of 10.2 cm on a lathe. The finished sample also had slight fillets on the ends to minimize stress concentrations near the end planes. Every effort was made to produce properly sized, precision-machined test samples. Details of the sample preparation techniques and the testing equipment are given in Mellor et al. (1984).

At the conclusion of the tests we determined strength and modulus values from the force-displacement curves and compared them to the brine volume, porosity and structure of the ice. In addition, statistical analyses were performed on the ice strength data to examine the variation of ice strength within and between pressure ridges.

Uniaxial compressive strength

The results from the constant-strain-rate, uniaxial compression tests are given in Appendix D. The compressive strengths of the specimens, or the peak stress endured during each of the tests, are plotted against strain rate in Fig. 33. The plots show considerable scatter; this is not surprising because the structure and porosity of the multi-year ridge samples are highly variable. Average strength values are given in Table 7 and plotted against strain rate in Figure 34, which also compares our data to those of other investigators.

The results indicate that the uniaxial compressive strength of vertical sea ice samples from multi-year pressure ridges increases with increasing strain rate and decreases with increasing temperature. These trends are consistent with the test data for horizontal first-year sea ice samples reported by Wang (1979). The shaded area in Figure 34 represents the variation in ice strength of horizontal samples of first-year columnar, oriented-columnar, and granular sea ice in different load-

Table 7. Summary of compressive strength data for multi-year pressure ridge ice samples.

	Maximum		*Minimum*		*Mean and standard deviation*		*Numbers of samples*
	(MPa)	*(lbf/in.²)*	*(MPa)*	*(lbf/in.²)*	*(MPa)*	*(lbf/in.²)*	
-5 °C (23 °F)							
10^{-1}/s	7.52	1090	0.47	68	2.34 ± 1.08	340 ± 157	71
10^{-3}/s	10.90	1580	2.39	346	6.06 ± 1.63	879 ± 237	69
-20 °C (-4 °F)							
10^{-1}/s	4.26	617	1.17	170	2.79 ± 0.69	404 ± 100	41
10^{-3}/s	12.68	1838	7.03	1020	9.63 ± 1.39	1396 ± 202	41

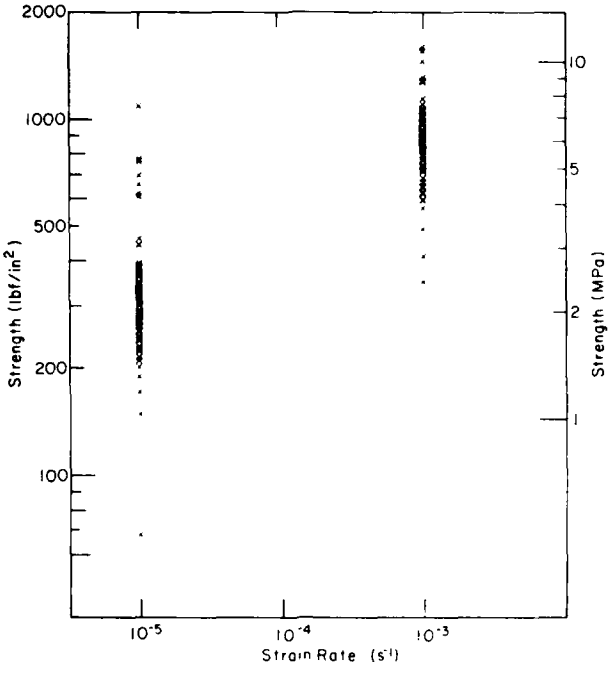

a. Tests conducted at -5°C (23°F).

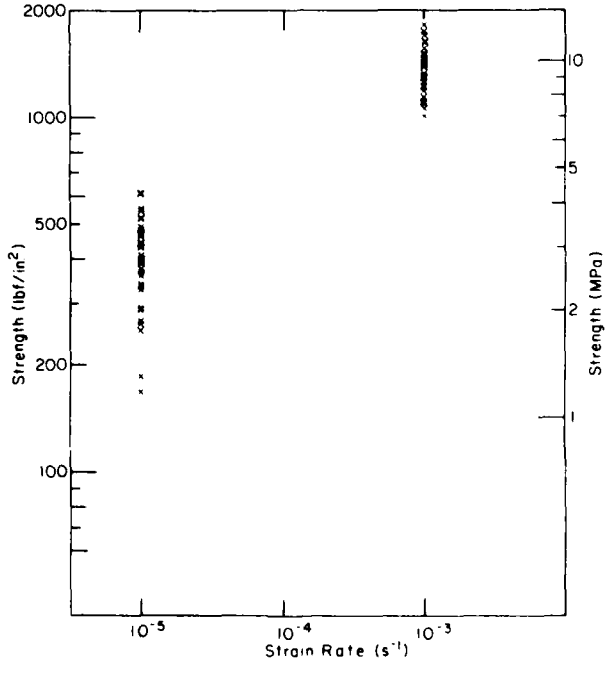

b. Tests conducted at -20°C (-4°F).

Figure 33. Uniaxial compressive strength of ridge ice samples vs strain rate.

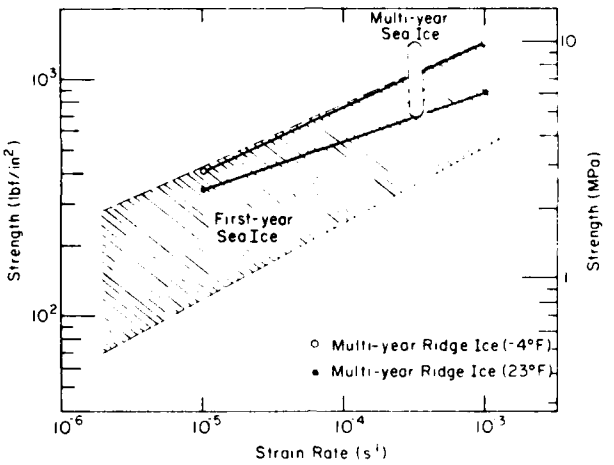

Figure 34. Average uniaxial compressive strength of ridge ice samples vs strain rate at -5 °C (23 °F) and -20 °C (-4 °F). Data for first-year sea ice (Wang 1979) at -10 °C (14 °F) and data for multi-year sea ice (Frederking and Timco 1980) at -26 °C (-15 °F) are included for comparison.

ing directions at -10 °C (14 °F). The strength of the vertical ridge ice samples is comparable to the strength of granular first-year sea ice and horizontal, columnar, oriented first-year sea ice in the hard fail direction. Our data also agree closely with the multi-year sea ice strength values at -26 °C (-15 °F) obtained by Frederking and Timco (1980).

Previous investigations of the strength of first-year sea ice have shown a decrease in ice strength with increasing brine volume (Schwarz and Weeks 1977). Presumably, as the brine volume increases, fewer ice bonds need to be broken before the ice fails (Weeks and Assur 1969). We found little or no correlation between the strength of the multi-year pressure ridge samples and the brine volume. However, this is not surprising because the multi-year ice had a low salinity and a high air content.

A more reasonable measure of the ice porosity is the sum of the brine and air volumes of the ice. Since sample air volumes are difficult to measure (Nakawo 1983) and time consuming to calculate, they have usually been neglected in analyses of sea ice strength. Equations were therefore developed for readily calculating the air volume of sea ice samples, given the ice density, salinity and temperature. The equations are given in Cox and Weeks (1982).

The compressive strength of the ridge samples is plotted against the total porosity of the ice in Figure 35. At all four test conditions the ice strength decreases with increasing ice porosity. This trend appears to be most pronounced at the higher strain rate, 10^{-1}/s, where flaws and cavities play a more important role in brittle ice failure. For a given strain rate and porosity there is also a significant increase in strength with decreasing temperature. Again, this trend appears to be more pronounced at 10^{-3}/s.

In addition to strain rate, temperature and porosity, the strength and mechanical properties of ice are greatly affected by the ice structure. Both Peyton (1966) and Wang (1979) show large variations in the strength of first-year sea ice depending on the grain size and crystal orientation. Schwarz and Weeks (1977) reviewed and discussed the effects of ice structure on the strength of first-year sea ice.

To evaluate the effects of structure on the strength of the multi-year ridge ice samples, we examined the results from the first 78 compression tests at -5 °C (23 °F). Of these 78 tests, 39 were at a strain rate of 10^{-4}/s and 39 were at 10^{-1}/s. For each strain rate the five strongest, the five weakest, and five intermediate-strength samples were chosen for detailed structural analysis.

The structural analysis was performed by preparing thin sections of both the tested samples and the end pieces adjacent to the test specimen. The end pieces were studied to help determine structural characteristics of the specimen that were not caused by testing. Horizontal thin sections were prepared from ice at the top, middle and bottom

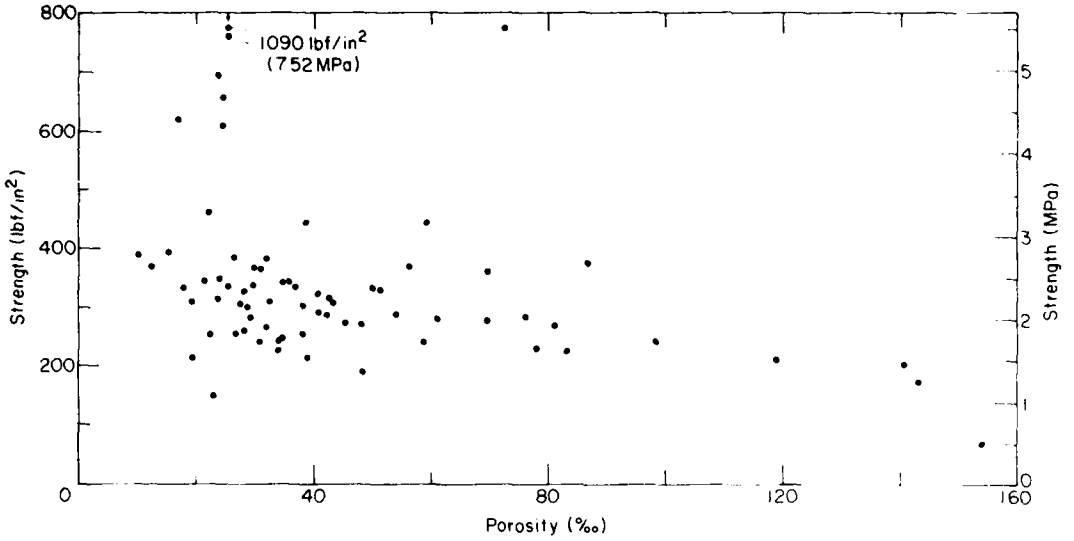

a. Tests conducted at 10^{-4}/s and -5 °C (23 °F).

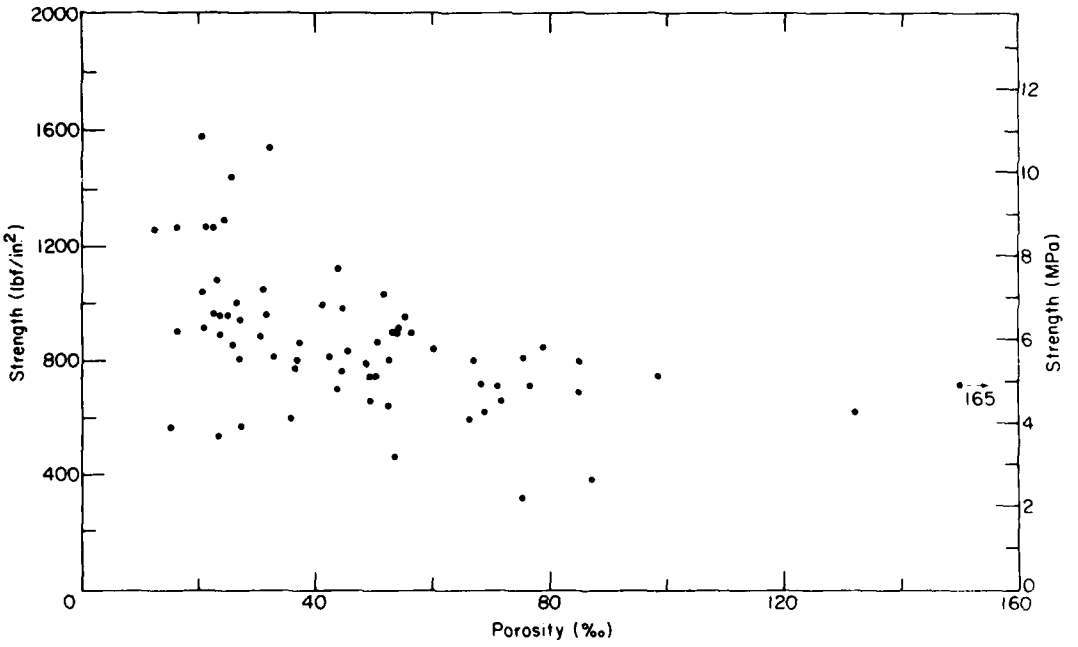

b. Tests conducted at 10^{-1}/s and -5 °C (23 °F).

Figure 35. Uniaxial compressive strength vs porosity for ridge ice samples.

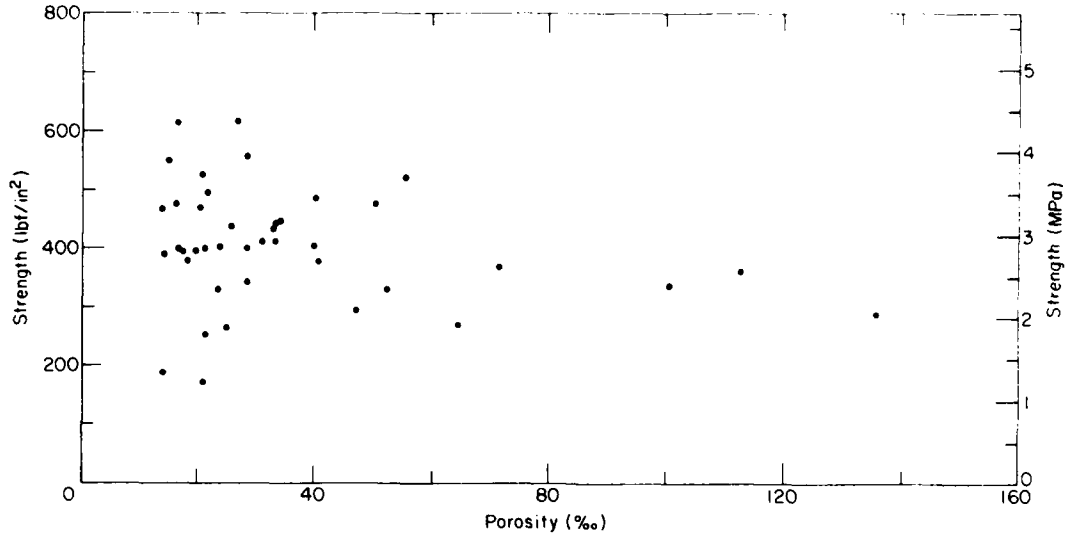

c. Tests conducted at 10^{-5}/s and -20°C (-4°F).

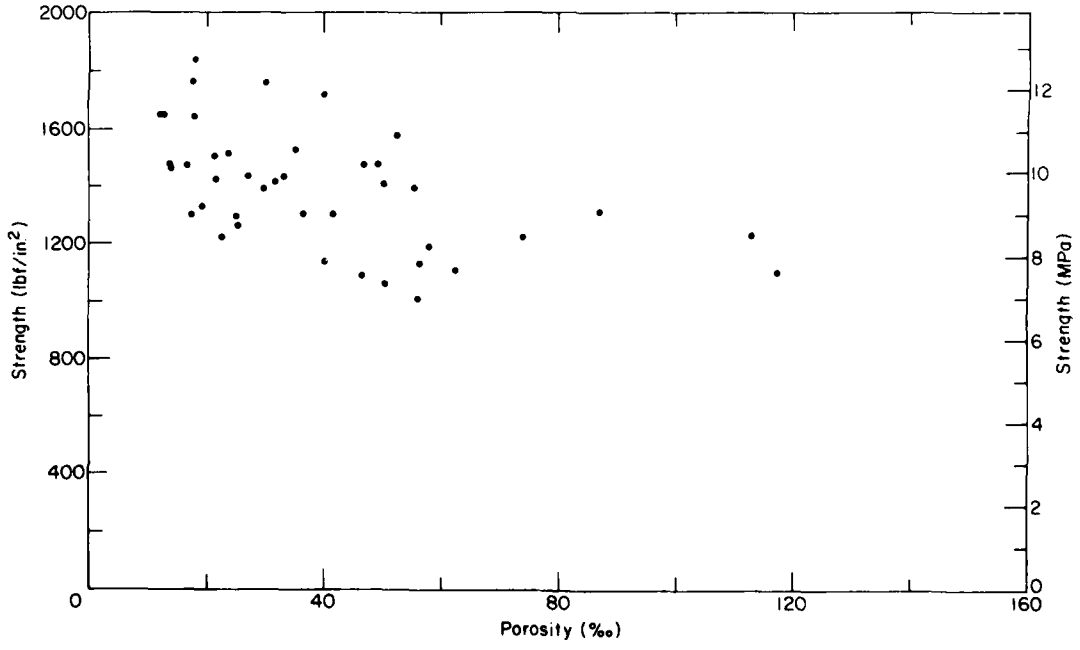

d. Tests conducted at 10^{-1}/s and -20°C (-4°F).

Figure 35 (cont'd). Uniaxial compressive strength vs porosity for ridge ice samples.

of the test sample, provided that the sample was not destroyed during the test. The remainder of the sample was sectioned vertically in two perpendicular cuts. We determined the ice type, grain size, and crystal orientation by studying photographs of the horizontal and vertical thin sections taken in crossed-polarized light. We also examined photographs of the test specimen taken immediately after the test to document the failure characteristics of the ice.

The strength, structure and porosity of the selected samples are given in Table 8. In both the 10^{-3} and 10^{-5}/s tests columnar specimens with crystal axes elongated parallel (0–20°) to the loading direction (Type IIA) were consistently the strongest. Of these samples, specimens with aligned c-axes were stronger than those having random, planar c-axis orientations. Columnar samples with elongated crystals oriented parallel to the plane of maximum shear (30–60° to the loading direction) had intermediate and low strengths. Randomly oriented columnar ice (Type IIB) had intermediate strengths.

Samples containing granular ice (Type I) or a mixture of granular and columnar ice (Type III) consistently had intermediate or low strength values. The structure alone is not clearly related to strength for these types of ice. However, the weakest samples generally had much higher porosities than the intermediate-strength specimens.

Our observations on the structural variation of ice strength for the columnar samples agree with the findings of Peyton (1966) and Wang (1979) for first-year sea ice. However, our multi-year granular ice samples were much weaker than the columnar ice samples loaded in the hard fail direction; Wang's granular sea ice samples were about as strong as his oriented columnar ice samples in the hard fail direction. The strengths of the granular samples in both studies were similar, but the majority of our columnar samples were loaded parallel to the growth direction, while Wang tested ice perpendicular to the growth direction. Peyton's work indicates that this can account for a two-fold difference in strength, where the samples loaded parallel to the growth direction are strongest.

Table 8. Strength, structure and porosity of selected ridge ice samples.

Sample number	Strength (MPa)	Strength (lbf/in.²)	Ice type*	Grain size (mm)	Porosity (o/oo)
		Tested at 10^{-3}/s and -5°C (23°F)			
High Strength					
R1B-320/346	7.52	1090	IIA-Aligned 0° Elongation	55 × 10	25.3
R5B-075/101	5.34	774	IIA-Aligned 5° Elongation	17 × 6	72.3
R1B-429/455	4.80	696	IIA 5° Elongation	15 × 10	23.7
R8A-432/458	4.53	657	IIA-Aligned 5° Elongation	30 × 5	24.5
R5A-165/191	4.27	619	IIA 0° Elongation	15 × 3	16.9
R7A-342/368	4.19	607	IIC 0° Elongation	2-20	24.4
Intermediate Strength					
R3B-363/387	2.72	394	IIIB	<1	15.3
R2A-140/165	2.68	388	I	2	10.1
R5B-341/367	2.54	368	I	<1	56.1
R7A-059/082	2.49	361	I	<1	69.5
R8B-499/526	240	348	IIB	20 × 5	23.8
Low Strength					
R7B-241/267	1.58	229	III	5	77.8
R1A-226/252	1.48	214	IIA 40° Elongation	25 × 15	19.4
R1A-399/425	1.48	214	III	—	38.9
R2B-094/121	1.18	171	IIIB	<1	143
R7A-263/286	0.47	68	IIIA 40° Elongation	35	154

Table 8 (cont'd).

Sample number	Strength (MPa)	Strength (lbf/in.²)	Ice type*	Grain size (mm)	Porosity (o/oo)
			Tested at 10^{-3}/s and -5°C (23°F)		
High Strength					
R1A-300/326	10.90	1580	IIA-Aligned 0° Elongation	55 × 10	20.3
R7B-440/466	10.62	1540	IIA-Aligned 5° Elongation	45 × 10	32.0
R8B-466/493	9.93	1440	IIA-Aligned 15° Elongation	50 × 15	25.6
R8A-384/410	8.94	1297	IIA 0° Elongation	40 × 10	24.2
R2A-285/310	8.76	1270	IIA 10° Elongation	25 × 15	22.3
R1A-175/201	8.76	1270	IIA 80° Elongation	—	16.2
R5B-141/167	8.76	1270	IIA 0° Elongation	45 × 25	21.1
Intermediate Strength					
R3B-331/357	6.70	971	IIIB	< 1	31.4
R3A-188/213	6.69	970	III	5	23.5
R3A-401/427	6.38	925	III	< 1	21.0
R1B-216/241	6.31	915	IIA 40° Elongation	35 × 20	16.3
R4B-299/325	6.28	910	III	2-10	56.2
R4B-420/466	6.28	910	IIIA	35 × 10	53.0
Low Strength					
R8B-300/326	4.05	587	III	—	15.1
R7B-175/201	3.84	557	IIC 50° Elongation	5	23.3
R7B-072/098	3.36	487	III	—	53.4
R2A-110/135	2.81	408	I	< 1	86.9
R8A-033/059	2.39	346	IIIA	—	75.2

* The elongation direction for the columnar ice samples refers to the angle between the columns, or elongated axes, and the loading direction (vertical).

Residual compressive strength

The uniaxial compressive strength tests on the multi-year pressure ridge samples were programmed on the testing machine to continue to 5% full sample strain to examine the residual strength and post-yield behavior of the ice. The residual strength is defined here as the stress on the sample at 5% strain assuming the specimen has a constant 10.16-cm (4.000-in.) diameter. Average values of the residual-maximum strength ratio of the ridge samples under different loading conditions are given in Table 9.

All but eight of the tests at 10^{-3}/s continued to 5% strain. Three tests at -20°C (-4°F) failed, and five tests were ended early because of experimental difficulties. At 10^{-3}/s and -20°C (-4°F) 18 of 41 tests continued to 5% strain. The data suggest that as either the strain rate increases or the temperature decreases, the ice tends to become more brittle and less ductile. Additional tests at different strain rates are needed to define the ductile-brittle transition at each temperature of interest.

At a strain rate of 10^{-5}/s the residual strength was quite high, about two-thirds of the peak stress. For the tests that continued to 5% strain at 10^{-3}/s the residual strength was about one-fifth of the peak stress. Further work on the nonsimultaneous loading of ice on wide structures may show that residual strength is an important design parameter at low rates of ice movement.

Table 9. Summary of residual-maximum strength ratios for multi-year pressure ridge ice samples.

	Residual-maximum strength ratios			*Tests continuing to 5% strain*	
	Maximum	*Minimum*	*Mean and standard deviation*	*Number*	*Percentage*
-5 °C (23 °F)					
10^{-1}/s	1.000	0.173	0.688 ± 0.166	68	96
10^{-3}/s	0.421	0.074	0.198 ± 0.078	43	62
-20 °C (-4 °F)					
10^{-1}/s	0.970	0.315	0.642 ± 0.162	36	88
10^{-3}/s	0.746	0.047	0.194 ± 0.148	18	44

Failure strains

Average failure strains at the maximum stress for different tests conditions are given in Table 10. The strains were calculated from the average of the DCDT measurements on the sample. As anticipated, the failure strain decreased with increasing strain rate at a given temperature. As the strain rate increased, the ice became more brittle and tolerated less strain before it failed. We would also expect the failure strain to decrease at a given strain rate as the ice gets colder; however, the 10^{-3}/s tests did not show this trend. The standard deviations show that we did not have enough samples to draw any significant conclusions about the variation of failure strain with temperature.

Figure 36 shows plots of strength vs failure strain. Each point corresponds to the peak of the stress-strain curve for each of the tests. The scatter in the data clearly demonstrates the variability in the mechanical properties of the ice, even at given temperatures and strain rates. The structure and porosity of the ice are obviously important. In the 10^{-3}/s tests there is a positive correlation between ice strength and failure strain. At 10^{-1}/s there is no apparent correlation.

Table 10. Summary of failure strain data for multi-year pressure ridge ice samples.

	Failure strain (%)			
	Maximum	*Minimum*	*Mean and standard deviation*	*Number of samples*
-5 °C (23 °F)				
10^{-1}/s	0.83	0.06	0.38 ± 0.17	71
10^{-3}/s	0.20	0.05	0.13 ± 0.03	69
-20 °C (4 °F)				
10^{-1}/s	0.73	0.10	0.31 ± 0.14	41
10^{-3}/s	0.25	0.05	0.19 ± 0.04	41

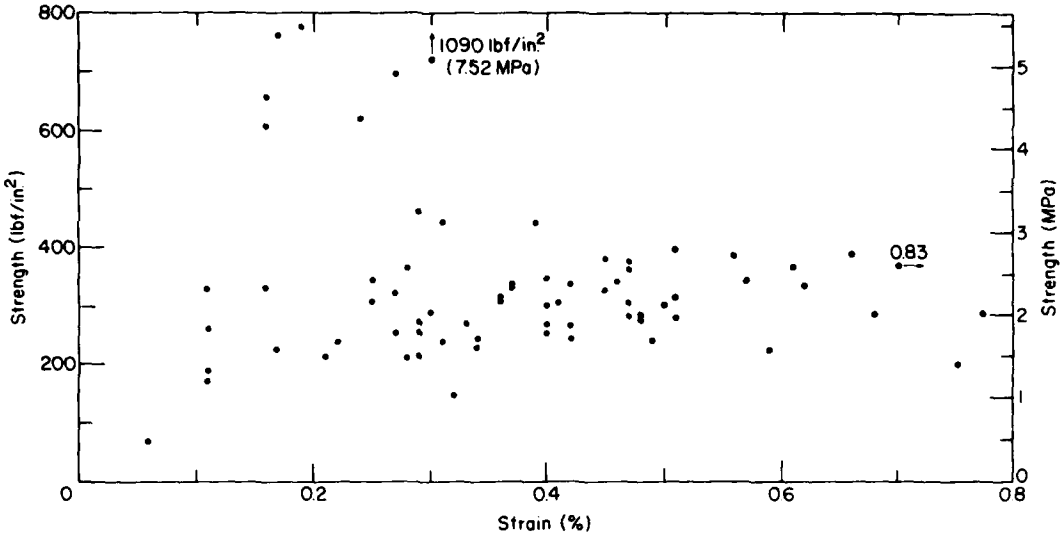

a. Tests conducted at 10^{-1}/s and -5°C (23°F).

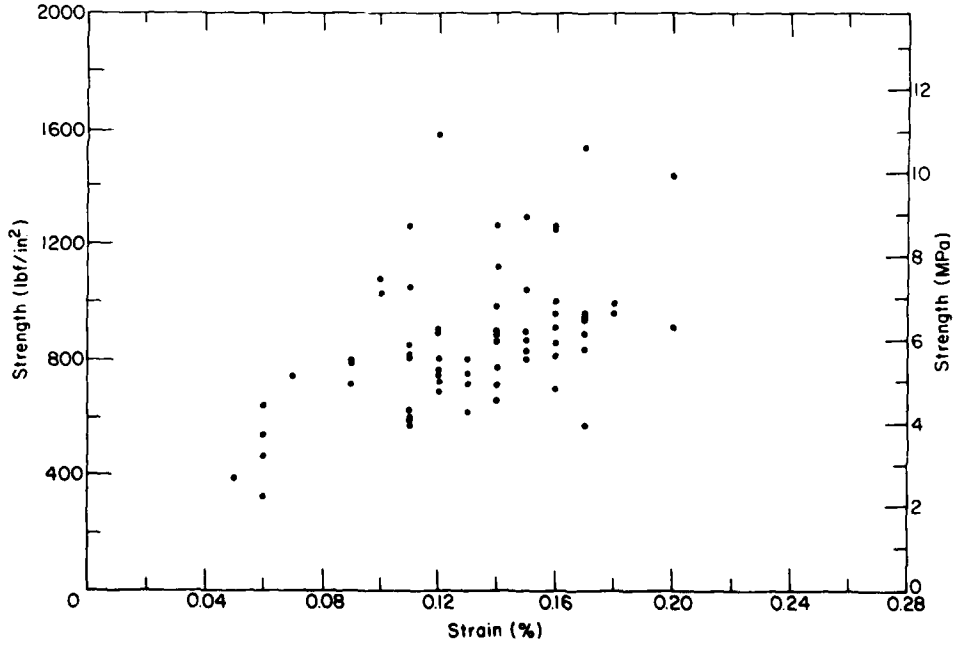

b. Tests conducted at 10^{-1}/s and -5°C (23°F).

Figure 36. Uniaxial compressive strength vs failure strain for ridge ice samples.

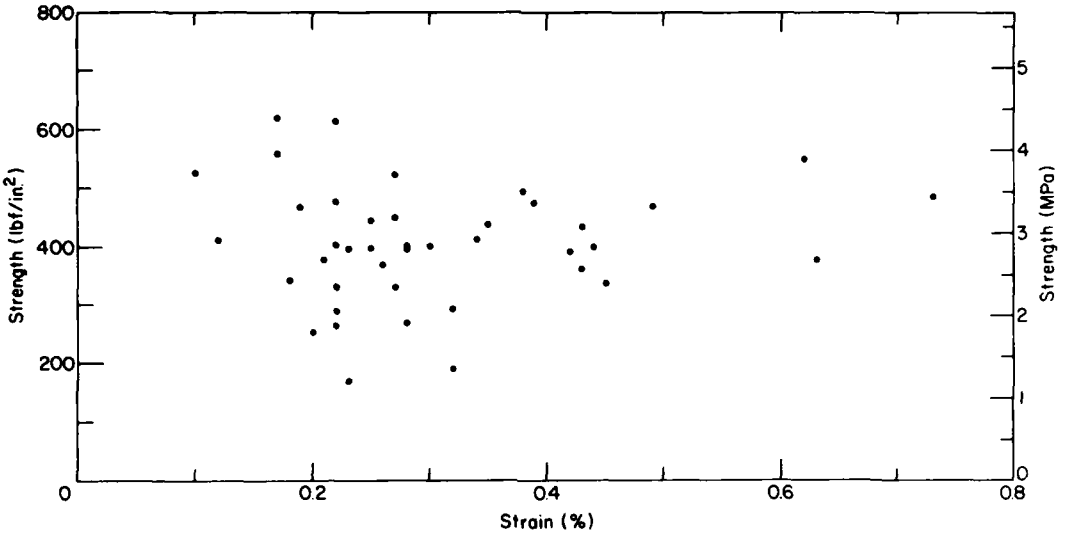

c. Tests conducted at 10^{-5}/s and -20°C (-4°F).

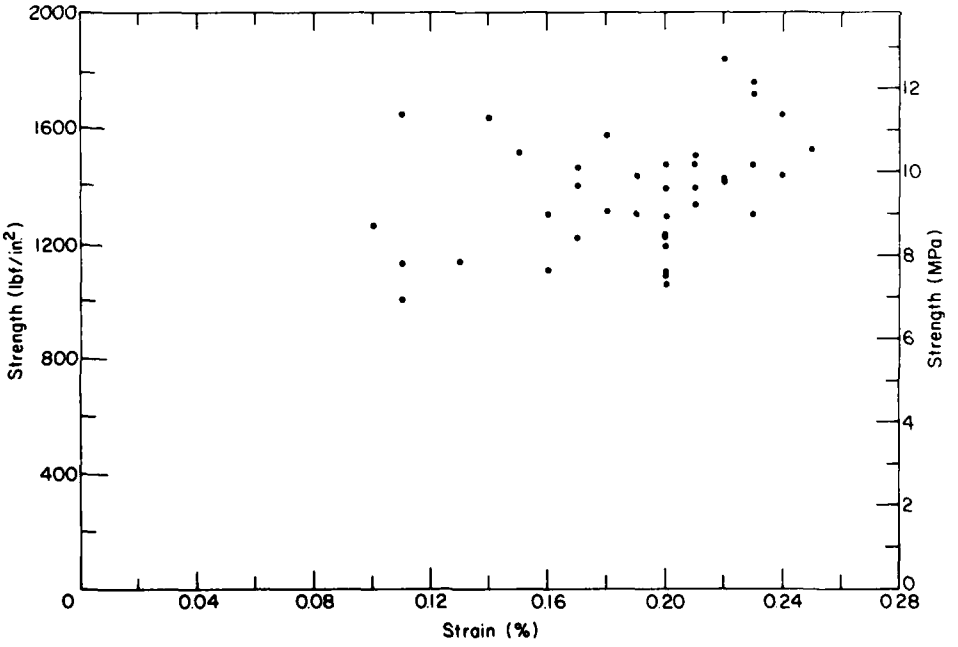

d. Tests conducted at 10^{-1}/s and -20°C (-4°F).

Figure 36 (cont'd).

Initial tangent modulus

We estimated the initial tangent modulus of each ridge samples from the initial slope of the force-displacement curve for each compression test. In a few tests where seating of the actuator on the sample was not uniform, the linear portion of the curve immediately after seating was used to determine the modulus. Axial displacement was determined from the average displacement of the DCDTs mounted on the sample. The initial tangent modulus is plotted against strain rate in Figure 37. As with the strength data the modulus

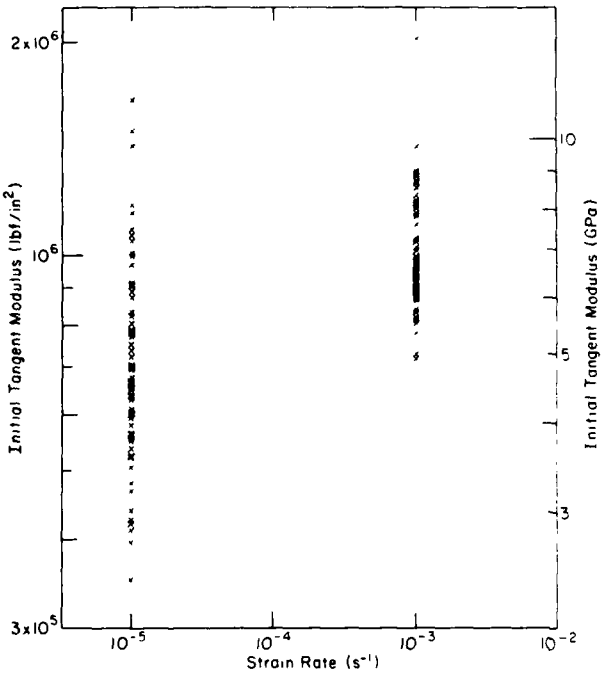

a. Tests conducted at -5 °C (23 °F).

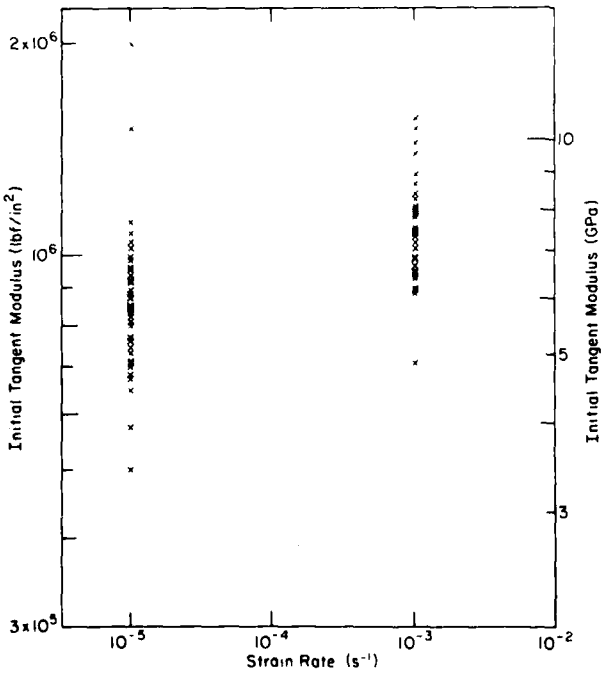

b. Tests conducted at -20°C (-4°F).

Figure 37. Initial tangent modulus vs strain rate for ridge ice samples.

data show considerable scatter due to variations in ice structure and porosity. Average modulus values are given in Table 11 and are plotted against strain rate in Figure 38. The results show that the modulus increased with strain rate and decreased with temperature. For a given temperature and strain rate, these values agree closely with those of Traetteberg et al. (1975) for freshwater columnar and granular ice. The 10^{-3}/s results are also comparable to dynamic, seismic determinations of Young's modulus for sea ice (Schwarz and Weeks 1977). Because of the large scatter of the modulus data, the trends with temperature are not statistically significant.

Schwarz and Weeks (1977) reported that Young's modulus of sea ice decreases with increasing brine volume. For multi-year sea ice we would expect a similar decrease with increasing porosity. The initial tangent modulus of the ridge samples is plotted against porosity in Figure 39. At 10^{-3}/s the modulus decreased with increasing porosity; at 10^{-5}/s no relation is evident. These observations are similar to those made when examining the strength porosity data (Fig. 35). Structural defects such as cracks and cavities apparently have a greater effect on the ice modulus and strength at high strain rates, where the ice is more brittle. Due to time constraints no effort was made to examine the variation of ice modulus with structure.

Table 11. Summary of initial tangent modulus data for multi-year pressure ridge ice samples.

	Initial Tangent Modulus						
	Maximum		*Minimum*		*Mean and standard deviation*		*Number of samples*
	(GPa)	*(10^3 lbf/in.^{2})*	*(GPa)*	*(10^3 lbf in.$^{-2}$)*	*(GPa)*	*(10^3 lbf/in.$^{-2}$)*	
-5 °C (23 °F)							
10^{-3}/s	10.34	1.500	2.41	0.350	5.02 ± 1.57	0.728 ± 0.228	70
10^{-5}/s	9.86	1.430	4.95	0.718	6.99 ± 1.12	1.014 ± 0.162	70
-20 °C (-4 °F)							
10^{-3}/s	10.48	1.520	3.45	0.500	5.95 ± 1.19	0.863 ± 0.172	40
10^{-5}/s	10.38	1.570	4.89	0.709	7.62 ± 1.19	1.105 ± 0.173	40

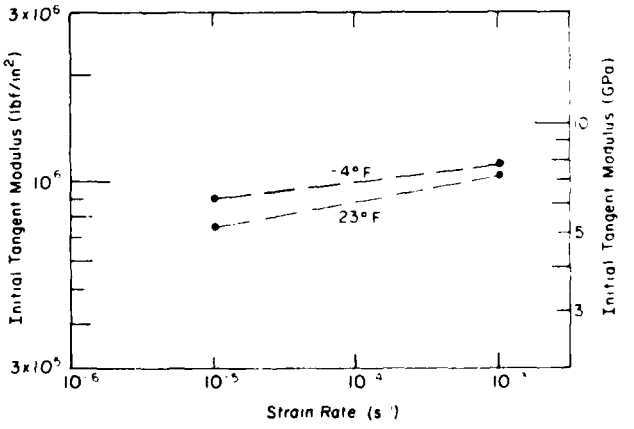

Figure 38. Average initial tangent modulus of ridge ice samples vs strain rate for tests at -5 °C (23 °F) and -20 °C (-4 °F).

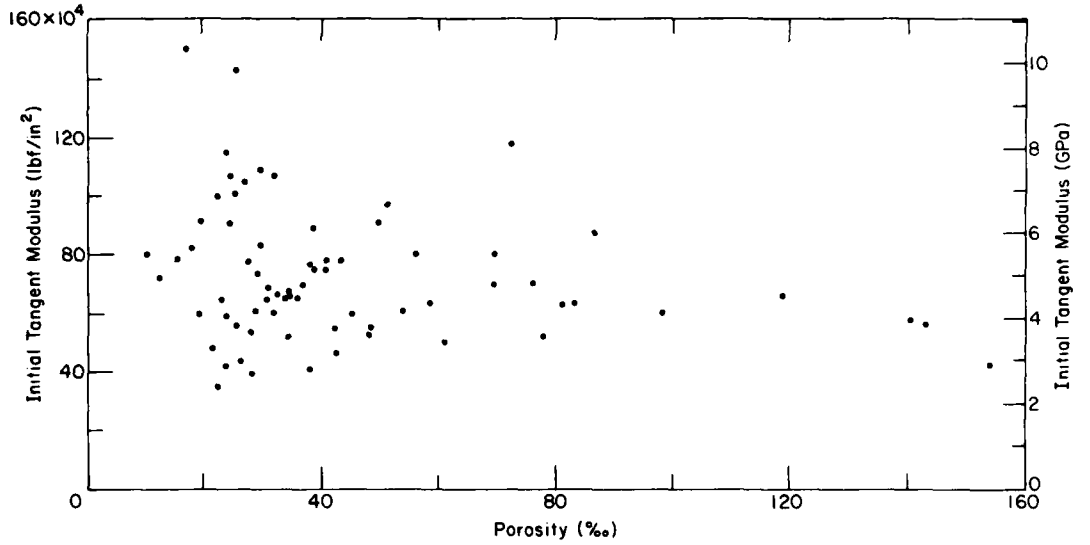

a. Tests conducted at 10^{-4}/s and -5°C (23°F).

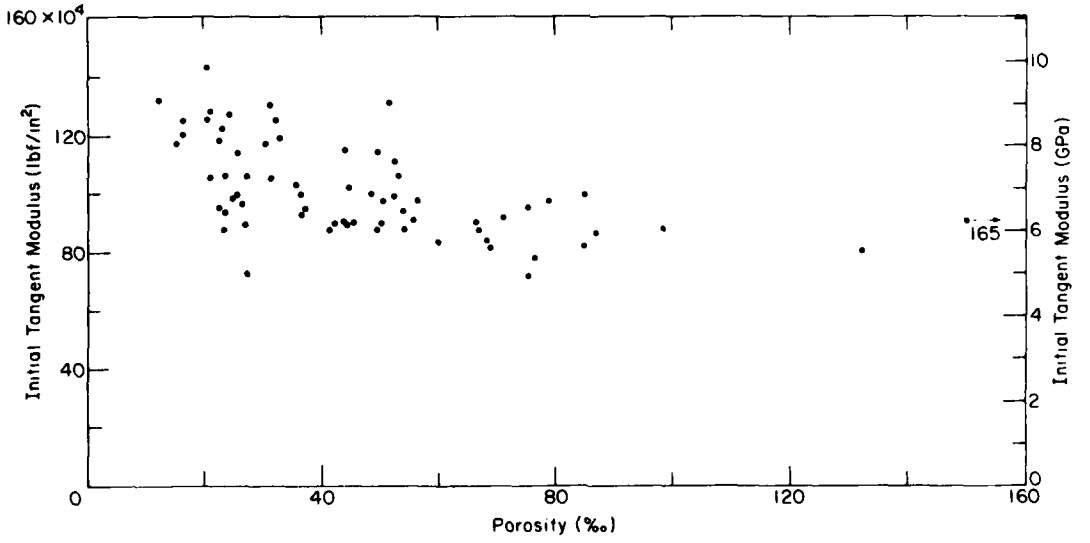

b. Tests conducted at 10^{-1}/s and -5°C (23°F).

Figure 39. Initial tangent modulus vs porosity for ridge ice samples.

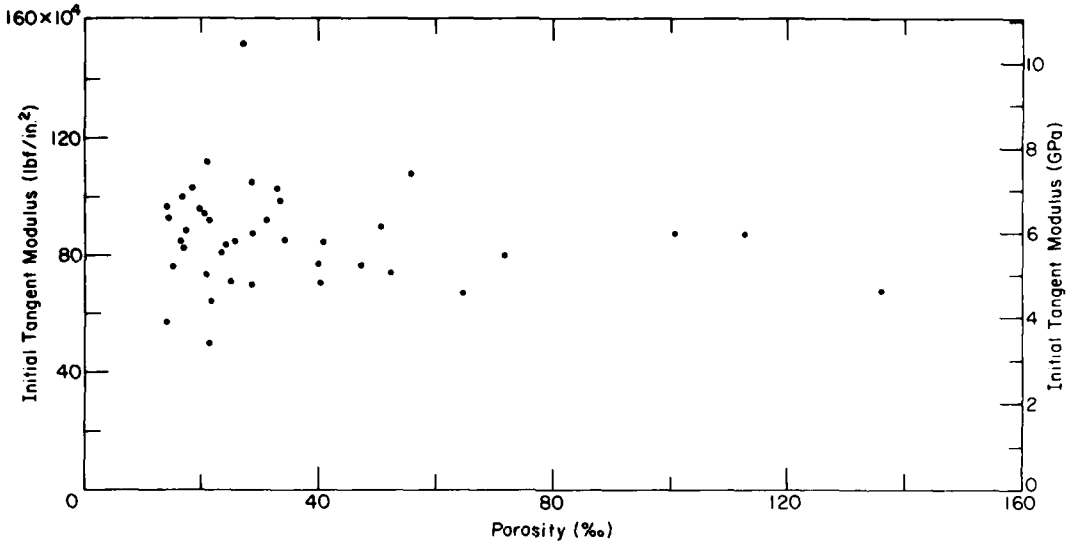

c. Tests conducted at 10^{-5}/s and -20°C (-4°F).

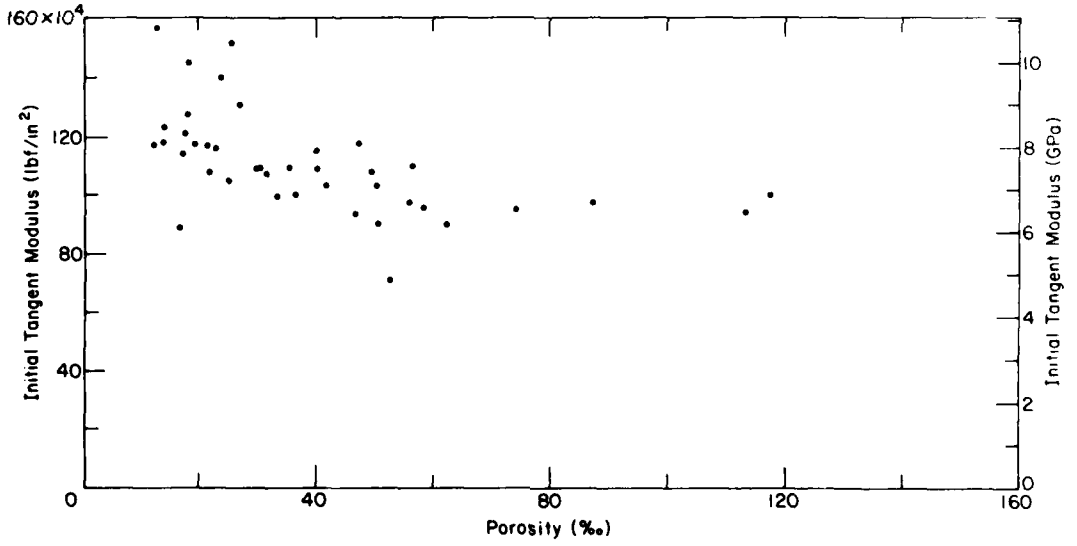

d. Tests conducted at 10^{-5}/s and -20°C (-4°F).

Figure 39 (cont'd).

STATISTICAL VARIATIONS IN ICE STRENGTH

Statistical analyses were performed to examine the variation of ice strength of the multi-year pressure ridge samples. We were interested in determining if there were any significant differences in ice strength between samples collected from the ridge sails and keels (above and below the surrounding level ice) and if there were any consistent trends of ice strength with depth. We were also interested in assessing the variation in ice strength between ridges, between cores located side by side on a given ridge, and between samples from the same core. We prepared histograms for examining the frequency distribution of ice strength at each of the four test conditions.

Differences in strength above and below level ice

When each core was obtained, the elevation of the top of the core relative to the upper surface of the surrounding level ice was determined. This allowed us to classify the ice in each core as above level ice or below level ice, a classification that approximately corresponds to above sea level and below sea level (the level ice elevations in the study area would not be expected to vary by more than 0.2 m from sea level). Using this basic division of samples the data for the two strain rates and the two temperatures can be tested for differences. Table 12 summarizes the properties of these data sets, with each set subdivided into above-level-ice and below-level-ice portions. The hypothesis that is tested is whether or not there is any reason, based on the available data, to doubt that the above- and below-level-ice samples have the same yield strength population means (i.e., H_o: $\mu_a = \mu_b$, where μ is the population mean and the subscripts a and b indicate above and below level ice).

Using a two-tailed t-test we found for all four areas that there is no reason to doubt that both the above- and below-level-ice samples have the same population means, even if we accept a 20% chance of being wrong. It is interesting to speculate about the reasons for this result. The average salinity of the ice from the ridge sails is 0.8 °/oo lower than the salinity of ice from the ridge keels (Fig. 30); this by itself would cause the keel ice to be weaker. However, this is offset by a higher gas volume in the ridge sails. In fact, the total porosity (gas and brine) of the sail ice is roughly 40% higher than the porosity of the keel ice. This, of course, should result in weaker sail ice. We believe that the lack of such a trend is caused by the large variations in ice strength that are produced by changes in the internal structure of the ice. These structural changes occur essentially at random throughout an ice core and do not correlate with the location of a sample relative to sea level, so they tend to obscure any differences that might exist between the strength of the ice in the upper and lower portions of multi-year ridges. This is important, as we can now combine both the above- and below-level-ice samples into one population in the Analysis of Variance (AOV) that follows.

The vertical variation in strength has also been examined in another way. For each of the 74 cores from which two or more samples were obtained, a plot was made of strength vs the depth of the sample measured below the upper ice surface. Figure 40 is an example of these plots. For each core the slope of the linear regression line of strength vs depth was then determined. Figure 41 shows a frequency histogram of the resulting slope values; the histogram is symmetrical with a mean of essential-

Table 12. Statistical characteristics of the uniaxial compressive strength of the samples from above and below level ice. *Symbols are as follows:* $\bar{\sigma}_c$ = average; s = standard deviation; n = number of tests; t = value of the t-test for differences between means. Strength values are in lbf/in.² and (MPa).

	Above level ice			*Below level ice*			*Difference*		*t for 0.05*	*t for 0.20*
	$\bar{\sigma}_c$	s	n	$\bar{\sigma}_c$	s	n	*between means*	t	*significance level*	*significance level*
-5 °C (23 °F)										
10^{-1}/s	338	140	21	343	170	48	5	0.11	2.00	1.29
	(2.33)	(0.97)		(2.36)	(1.17)		(0.03)			
10^{-3}/s	837	236	25	902	240	44	65	1.10	2.00	1.29
	(5.77)	(1.63)		(6.22)	(1.65)		(0.45)			
-20 °C (4 °F)										
10^{-1}/s	428	106	15	379	121	24	49	1.26	2.03	1.30
	(2.95)	(0.73)		(2.61)	(0.83		(0.34)			
10^{-3}/s	1425	227	15	1377	187	26	49	0.72	2.03	1.30
	(9.83)	(1.57)		(9.49)	(1.29)		(0.34)			

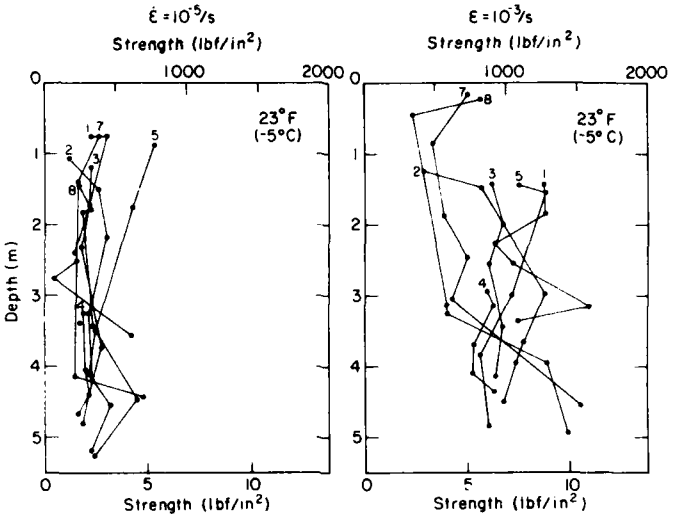

Figure 40. Uniaxial compressive strength at -5°C (23°F) vs depth for a number of multi-year pressure ridge cores. The number at the top of each profile is the ridge number from which the samples were obtained.

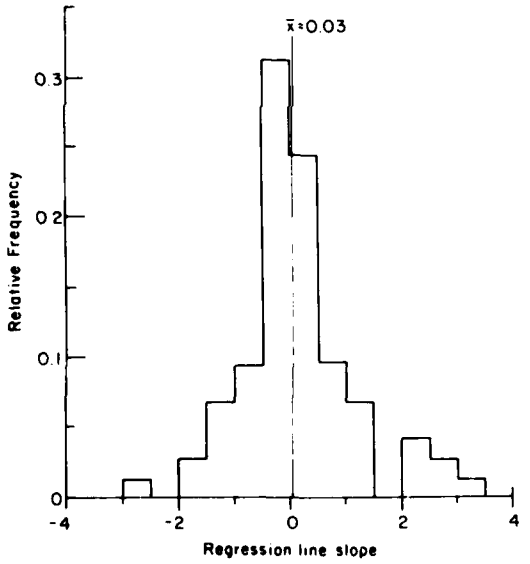

Figure 41. Frequency histogram of regression line slopes of strength vs depth.

ly zero. There clearly is no reason to believe that there is a systematic variation in strength with depth in the sampled multi-year pressure ridges. This, of course, does not mean that the upper and lower portions of in situ ridges necessarily have the same strength; during the ice growth season the near-surface ice is commonly stronger because of its lower temperature.

Sources of the variation in strength

We initially planned to collect test samples from exactly the same levels in collocated cores (i.e. located as close together as practical) from each ridge. This did not prove possible because of problems with gouges and breaks in the cores. Instead, because of the erratic location of the gouges in each core, vertical locations of the samples in each core were approximately random This, coupled with the fact that there was no systematic difference between the strength values of the above- and below-level-ice samples, makes it possible to study the observed strength variation by using a three-level AOV model. In this model the total sample variance is partitioned into the variance components contributed by differences 1) between ridges, 2) between pairs of cores collocated on a given ridge, and 3) between samples from the same core.

The linear AOV model assumed is

$$x_{ijk} = \mu + v_i + y_{ij} + z_{ijk}$$

with $i = 1...r$, $j = 1...t$, and $k = 1...n$. *Here* μ is the grand mean, v_i corresponds to the ridge effect, y_{ij} to the effect of collocated cores within the same ridge, and z_{ijk} to the effect of samples within the same core. The parameters v_i, y_{ij} and z_{ijk} are assumed to be normally distributed, with zero means and variances ψ^2, ω^2 and σ^2, respectively. Table 13 gives the computational relations for this model, and Table 14 gives the results for the four

Table 13. Analysis for a three-level nested AOV model.

Source of variance	*Sums of squares*	*Degrees of freedom*	*Mean squares*	*E (Mean squares)*
Between ridges	$nt\sum_{i}^{r}(\bar{x}_{i...}-\bar{x}_{...})^2$	$r-1$	s_r^2	$\sigma^2+n\omega^2+nt\psi^2$
Between cores at a site	$n\sum_{i}\sum_{j}^{r\ t}(\bar{x}_{ij.}-\bar{x}_{j..})^2$	$r(t-1)$	s_t^2	$\sigma^2+n\omega^2$
Between samples from the same core	$\sum_{i}\sum_{j}\sum_{k}^{r\ t\ n}(x_{ijk}-\bar{x}_{ij.})^2$	$rt(n-1)$	s_n^2	σ^2
Total	$\sum_{i}\sum_{j}\sum_{k}^{r\ t\ n}(x_{ijk}-\bar{x}_{...})^2$	$rtn-1$		

Table 14. Results of a three-level nested AOV analysis of the variation in compressive strengths, using only cores that had no "missing" samples. There are n samples from each core, t pairs of cores on each ridge, and r ridges. Strength values are given in lbf/in.^{2} and (MPa).

	Source of variation	*Sum of squares*	*Degrees of freedom*	*Mean squares*	*Expected mean squares*	*r,t,n*	$\hat{\sigma}$	$\hat{\omega}$	$\hat{\psi}$	H_0: $\omega^2=0$ F	$F_{0.95}$	H_0: $\psi^2=0$ F	$F_{0.95}$
-5 °C (23 °F)													
10^{-1}/s	Between ridges	247,178 (111.7)	4	61,795 (2.94)	$\sigma^2+3\omega^2+6\psi^2$	5,2,3	180 (1.24)	90 (0.62)	29 (0.20)	1.74	2.71	1.10	5.19
	Between cores at a site	283,245 (13.47)	5	56,651 (2.69)	$\sigma^2+3\omega^2$								
	Between samples within cores	650,369 (30.92)	20	32,518 (1.55)	σ^2								
10^{-3}/s	Between ridges	118,693 (5.64)	2	59,347 (2.82)	$\sigma^2+3\omega^2+6\psi^2$	3,2,3	412 (2.84)	210 (1.45)	61 (0.42)	0.22	3.49	1.61	9.55
	Between cores at a site	110,852 (5.27)	3	36,951 (1.76)	$\sigma^2+3\omega^2$								
	Between samples within cores	2,034,966 (96.7)	12	169,581 (8.06)	σ^2								
-20 °C (-4 °F)													
10^{-1}/s	Between ridges	48,027 (2.28)	3	16,009 (0.76)	$\sigma^2+3\omega^2+6\psi^2$	4,2,3	127 (0.88)	69 (0.48)	119 (0.82)	0.11	3.01	8.80*	6.59
	Between cores at a site	7,276 (0.35)	4	1,819 (0.09)	$\sigma^2+3\omega^2$								
	Between samples within cores	259,603 (12.34)	16	16,225 (0.77)	σ^2								
10^{-3}/s	Between ridges	279,144 (13.27)	2	139,572 (6.63)	$\sigma^2+3\omega^2+6\psi^2$	3,2,2	209 (1.44)	50 (0.34)	121 (0.83)	1.17	3.49	2.72	9.55
	Between cores at a site	154,017 (7.32)	3	51,339 (2.44)	$\sigma^2+3\omega^2$								
	Between samples within cores	525,533 (24.98)	12	43,794 (2.08)	σ^2								

* *Significant at the 5% level; however, this is not significant at the 1% level, where* $F_{0.99}=16.69$.

test conditions. In Table 14 we have only used data when a complete set of three samples (one from above level ice and two from below level ice) were available for a given core. Because of breakage and gouging this reduces the number of degrees of freedom between ridges to between 2 and 4. The results indicate that in all cases there is no reason to doubt the hypothesis that ω^2 equals zero (*i.e. that there is no significant variation between cores at the same site*).

Several cores in each data set were, for a variety of reasons, missing one sample. To avoid discarding the two samples in each core with a missing sample (as we did in the previous analysis), we also

Table 15. Results of a three-level nested AOV analysis of the variation in compressive strengths, including cores with "missing" samples. When one of the three values from a core was missing, it was replaced by the average of the other two values. The total number of missing values in each data set is indicated by M; r is the number of ridges, t is the number of collocated cores, and n is the number of samples in each core. Strength values are given in lbf/in.^{2} and (MPa).

	Source of variation	Sum of squares	Degrees of freedom	Mean squares	Expected mean squares	M,r,t,n	$\hat{\sigma}$	$\hat{\omega}$	$\hat{\psi}$	H_0: $\omega^2 = 0$ F	$F_{0.95}$	H_0: $\psi^2 = 0$ F	$F_{0.95}$
-5 °C (23 °F)													
10^{-3}/s	Between ridges	327,008 (15.55)	6	54,501 (2.59)	$\sigma^2 + 3\omega^2 + 6\psi^2$	2,7,2,3	169 (1.17)	71 (0.49)	43 (0.30)	1.52	2.36	1.25	3.87
	Between cores at a site	304,106 (14.46)	7	43,444 (2.07)	$\sigma^2 + 3\omega^2$								
	Between samples within cores	798,045 (37.94)	28	28,502 (1.35)	σ^2								
10^{-1}/s	Between ridges	882,608 (41.96)	6	147,101 (6.99)	$\sigma^2 + 3\omega^2 + 6\psi^2$	4,7,2,3	288 (1.99)	114 (0.79)	131 (0.90)	0.53	2.36	3.35	3.87
	Between cores at a site	307,389 (14.61)	7	43,913 (2.08)	$\sigma^2 + 3\omega^2$								
	Between samples within cores	2,315,585 (110.08)	28	82,699 (3.93)	σ^2								
-20 °C (-4 °F)													
10^{-3}/s	Between ridges	89,114 (4.24)	5	17,823 (0.85)	$\sigma^2 + 3\omega^2 + 6\psi^2$	4,6,2,3	106 (0.73)	37 (0.26)	42 (0.29)	0.65	2.51	2.44	4.39
	Between cores at a site	43,889 (2.09)	6	7,315 (0.35)	$\sigma^2 + 3\omega^2$								
	Between samples within cores	271,357 (12.90)	24	11,307 (0.54)	σ^2								
10^{-1}/s	Between ridges	428,698 (20.38)	5	85,740 (4.08)	$\sigma^2 + {}^1\omega^2 + 6\psi^2$	5,6,2,3	171 (1.18)	45 (0.31)	129 (0.89)	1.21	2.51	2.41	4.39
	Between cores at a site	213,321 (10.14)	6	35,554 (1.69)	$\sigma^2 + 3\omega^2$								
	Between samples within cores	704,850 (33.51)	24	29,369 (1.40)	σ^2								

completed an approximate analysis in which we replaced each of the missing values with the mean of the other observations from the same core (Table 15). The inserted values therefore made no contribution to the residual sum of squares. This analysis indicates that in all cases there is no reason to doubt the hypotheses that there is no significant variation between cores at the same site and that there is no significant variations between ridges. Table 16 summarizes the differences in the results of the two analyses. The main factor contributing to the observed variance is associated with differences within cores. This is not surprising, considering the extreme local variability in the structure of the ice in multi-year pressure ridges (the variance between cores at a site and between ridges was always much less than that within cores). In more than 50% of the cases, however, the variance associated with differences between ridges was larger than that observed between cores in the same ridge. Again these results are reasonable. In ridges where the block sizes are either large or very small, we might expect a low variance from collocated cores. In ridges where the blocky structure is intermediate in size, the variance would presumably be higher.

These results do not mean that we believe that all multi-year pressure ridges have identical strengths. As a first-year ridge is gradually metamorphosed into a multi-year ridge, the voids in the ridge are slowly sealed with ice, presumably increasing the bulk strength of the ridge. In fact, one of the ridges sampled (ridge 6) contained many large voids, which caused the core recovery to be so poor that we moved to another ridge. We believe that this ridge had been through only one melt season, and as a result many of the voids had not rehealed. We have also sampled a ridge (which is not included in the present data set) that contained many large gas bubbles. The ridges in-

Table 16. Summary of differences in the data sets and AOV results between the cases when no values are missing and when average values are substituted for missing values. Strength values are in lbf/in.² and (MPa).

	No. of missing values	No. of ridges	Estimated standard deviation: Within cores, $\hat{\sigma}^2$	Between cores at a site, $\hat{\omega}^2$	Between ridges, $\hat{\psi}^2$	$H_0: \omega^2 = 0$ F	$F_{0.95}$	$H_0: \psi^2 = 0$ F	$F_{0.95}$
-5 °C (23 °F)									
10^{-1}/s	0	5	180 (1.24)	90 (0.62)	29 (0.20)	1.74	2.71	1.10	5.19
	2	7	169 (1.17)	71 (0.49)	43 (0.30)	1.52	2.36	1.25	3.87
10^{-3}/s	0	3	412 (2.84)	210 (1.45)	61 (0.42)	0.22	3.49	1.61	9.55
	4	7	288 (1.99)	114 (0.79)	131 (0.90)	0.53	2.36	3.35	3.87
-20 °C (-4 °F)									
10^{-1}/s	0	4	127 (0.88)	69 (0.48)	119 (0.82)	0.11	3.01	8.80*	6.59
	4	6	106 (0.73)	37 (0.26)	42 (0.30)	0.65	2.51	2.44	4.39
10^{-3}/s	0	3	209 (1.44)	50 (0.34)	121 (0.83)	1.17	3.49	2.72	9.55
	5	6	171 (1.18)	45 (0.31)	129 (0.89)	1.21	2.51	2.41	4.39

* Significant at the 5% level; however, this is not significant at the 1% level, where $F_{0.99}(3,4) = 16.69$.

cluded in the present data set had well-rounded surface profiles and are believed to be several years old. Also, for several of the ridges, we were able to examine the surfaces of fractures traversing the ridge in order to ascertain that the ridge was composed of massive ice that was nearly void-free. Therefore, we believe that our data set is reasonably representative of old, solid, well-healed pressure ridges and that even in these ridges the homogenization processes associated with aging are not sufficient to erase the large differences in mechanical properties caused by local structural differences within the ice.

Shape of the strength histograms

Histograms were also prepared in order to examine the frequency distribution of ice strength at each of the four test conditions. Figure 42 shows histograms based on the four data sets, and Table 17 presents the first four moments (μ_1, μ_2, μ_3, μ_4), the skewness (α_3) and the kurtosis (α_4) for each data set. For symmetrical distributions, such as the normal, $\alpha_3 = 0$. The kurtosis is a measure of the peakedness of the distribution, with higher values indicating a distribution that is more peaked than normal and lower values indicating a distribution that is broader than normal. At the higher strain rates (10^{-3}/s) both sets of data show a positive skew, but only in the tests performed at −5 °C is the skew large enough to suggest that the parent population was not normal. The −5 °C tests are also more peaked than normal, while the −20 °C tests are less peaked. It is not possible to test these deviations for significance, as applicable tables do not exist. At the lower strain rate (10^{-5}/s) the −5 °C tests show a pronounced positive skew and peakedness, while the −20 °C tests, although showing a slight negative skew, do not appear to be appreciably nonnormal. We therefore conclude that there is no observational basis for suggesting that either high test temperatures or low strain rates themselves are associated with a stength histogram of a particular shape.

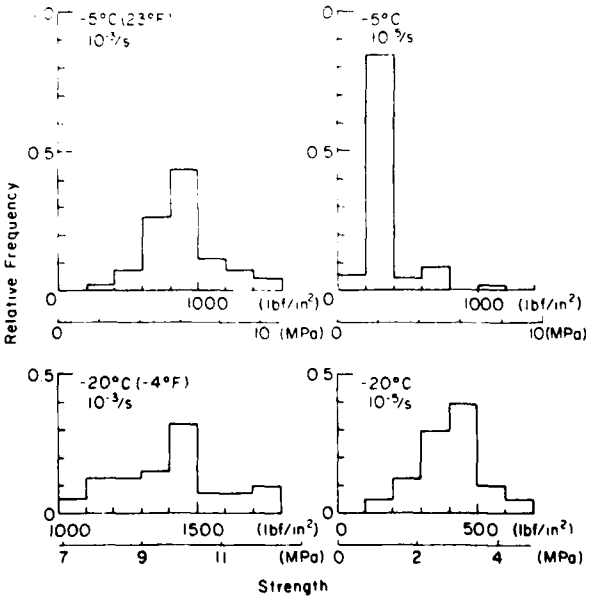

Figure 42. Ice strength frequency histograms.

Table 17. First four moments $\mu_1,\ldots\mu_4$, skewness α_3, kurtosis α_4, and number of strength values n in each of the data sets. Strength values are given in lbf/in.^{2} and (MPa).

	μ_1	μ_2	μ_3	μ_4	α_3	α_4	n
-5 °C (23 °F)							
10^{-1}/s	341	25,356	9,201,861	6,213,168,250	2.28	9.66	69
	(2.35)	(174.8)					
10^{-3}/s	879	56,249	9,396,181	1.26×10^{10}	0.70	3.98	69
	(6.06)	(387.8)					
-20 °C (-4 °F)							
10^{-1}/s	404	10,039	-104,606	301,536,360	-0.10	2.99	39
	(2.78)	(69.2)					
10^{-3}/s	1,394	39,525	1,103,267	3,608,530,000	0.14	2.31	41
	(9.61)	(272.5)					

MULTI-YEAR FLOE ICE TESTS

The major research objective of Phase I was to obtain a preliminary understanding of the structure and uniaxial compressive strength of ice samples from multi-year pressure ridges. In addition, methods were also to be developed to conduct uniaxial tension tests at constant strain rates, uniaxial compression tests at constant loads, and conventional triaxial tests at constant axial strain rates. These tests will be used extensively during subsequent phases of the test program.

The techniques and equipment for performing the tension, constant load compression, and triaxial tests developed in this study are described in the companion report by Mellor et al. (1984). The test methods and some initial results are briefly described in this report. Multi-year ice samples from a presumably undeformed area were used to evaluate these techniques. Because of the limited number of tests for each test type and condition, and because of budget constraints, the tests results have not been thoroughly analyzed. Structural analyses have not been performed on the test specimens.

Ice description

Twenty-five cores of multi-year sea ice were obtained from a relatively flat area near ridges 1 and 2. We were not interested in penetrating through the floe, so the cores were limited to about 3 m in length. One continuous core was taken exclusively for analyzing structure and salinity and was not cut up for test specimens.

A structural profile of the continuous core is given in Appendix C. The profile was prepared in the same manner as the pressure ridge structural profile described earlier. The upper 9 cm of the core consists of fine-grained slush or snow ice underlain by randomly oriented columnar ice. From 45 to 170 cm the columnar ice exhibits a prefered, nearly horizontal c-axis orientation. Because the elongated axes of the crystals are not exactly vertical, we suspect that the ice sheet had probably been deflected by a nearby pressure ridge. At 170 cm we encounter a thin layer of fine granular ice, followed by a thin layer of columnar congelation ice. Beneath 190 cm the core has a coarse platey structure mixed with fine granular ice. The salinity profile for this core and a schematic structural profile are presented in Figure 43.

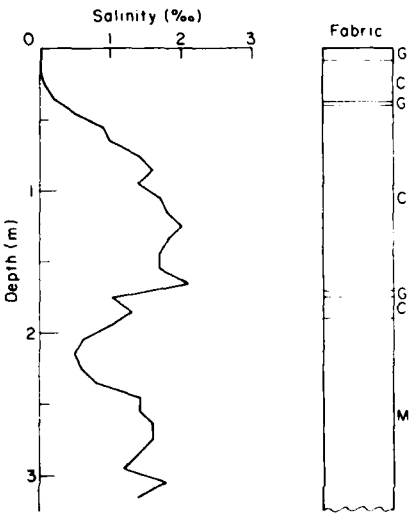

Figure 43. Salinity profile and schematic structural profile for the continuous multi-year floe core. C = columnar ice; G = granular ice; M = mixed granular and columnar ice.

The test samples from the floe had an average salinity of 1.7 ± 0.5‰, comparable to the salinities of the multi-year pressure ridge keel samples. The average density of the floe samples at −20°C was 0.910 ± 0.006 Mg/m³.

We prepared thin sections for most of the multi-year floe test specimens, but we have not yet performed structural analyses. Several columnar samples had crystal c-axes that were close to 45° to the loading direction. Other than increasing the variability in ice properties, this suggests that the presumably undeformed sampling area on the floe was in fact part of the adjacent pressure ridge flank.

Uniaxial compressive strength

Eleven constant-strain-rate, uniaxial compression tests were performed on the floe ice samples so that their properties could later be compared to those of the ridge specimens. Some 10^{-2}/s tests were also conducted in preparation for Phase II of the program. The test specimens were prepared, instrumented and tested in the same manner as the ridge samples.

The strength data are plotted in Figure 44. Strength, moduli and other properties for each specimen are given Appendix D. In general the ice strength increases with increasing strain rate and decreasing temperature. The data also show considerable scatter because of the variation in ice structure and crystal orientation.

Constant-load compression tests

Constant-load compression tests were performed on the closed-loop testing machine and on a specially designed pneumatic loading jig. The closed-loop testing machine was used for high-load tests at stresses of 2.07 and 4.14 MPa (300 and 600 lbf/in.²), while the pneumatic loading jig was used for the small-load test at 0.69 MPa (100 lbf/in.²). Samples loaded on the testing machine were prepared and instrumented in the same manner as the ridge compression specimens.

The pneumatic loading jig was based on a design developed by Mellor and Cole (1982). It consisted of a loading frame and a Bellofram pneumatic actuator, which was used to apply the load to the sample (Fig. 45). Sample strains were measured by a pair of DCDTs mounted between the end caps on the specimen and were recorded on a digital, paper tape recorder. Axial strains were not measured on the sample, as the constant-load tests performed on the testing machine showed that full sample strains and sample strains up to and beyond yielding were essentially equal. The loading jig was placed in an environmental chamber inside a coldroom. The chamber was heated to maintain a constant temperature during each test. Details on the instrumentation and test equipment are given in Mellor et al. (1984).

Nine constant-load compression tests were performed at different loads and temperatures. The results are given in Appendix D and plotted in

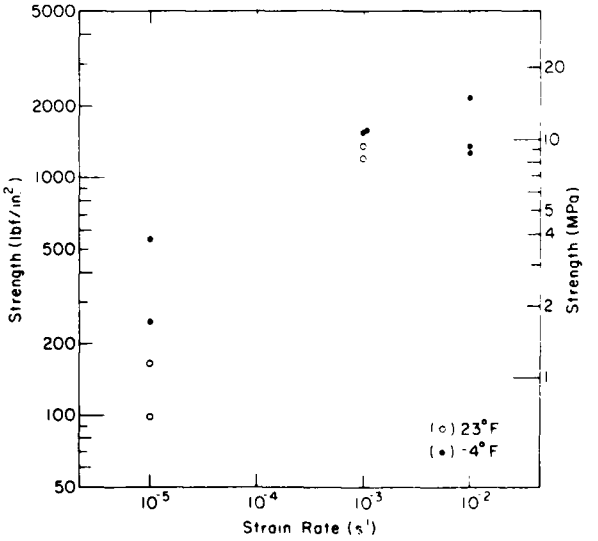

Figure 44. Uniaxial compressive strength of multi-year floe ice samples at -5°C (23°F) and -20°C (-4°F) vs strain rate.

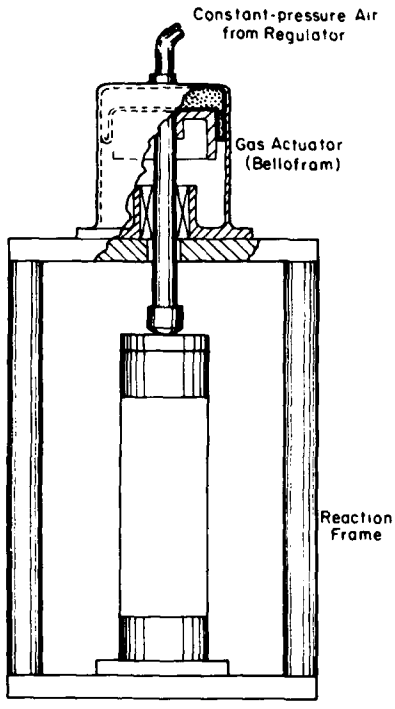

Figure 45. Pneumatic loading jig used in constant-load compression tests.

Figures 46. The strain-rate minimum for each of the tests was determined by differentiating each strain-time curve. The failure strain was defined as the strain at the strain-rate minimum, marking the onset of tertiary creep.

The strain-rate minimum of each test is plotted against the applied stress in Figure 46a. In general the strain-rate minimum increases as the stress increases; however, there is considerable scatter in the data due to variations in the ice structure. The strain-rate minimum is plotted against the failure strain in Figure 46b. Unlike the results on polycrystalline freshwater ice by Mellor and Cole (1982), ductile yielding occurs at strains of about 0.2–0.3%, not at 1%. However, the failure strains in the constant-load tests generally agree with the failure strains in the constant-strain-rate tests, supporting the correspondence between constant-load and constant-strain-rate tests for ice suggested by Mellor (1980). Despite the scatter in the test data, the strain-rate minimum in each of the tests varies inversely with the time to failure (Fig. 46c). This suggests that the ice behavior prior to the onset of tertiary creep can be described by a Burgers rheological model (Mellor 1980). A Burgers model consists of a series combination of the Kelvin-Voigt and Maxwell models.

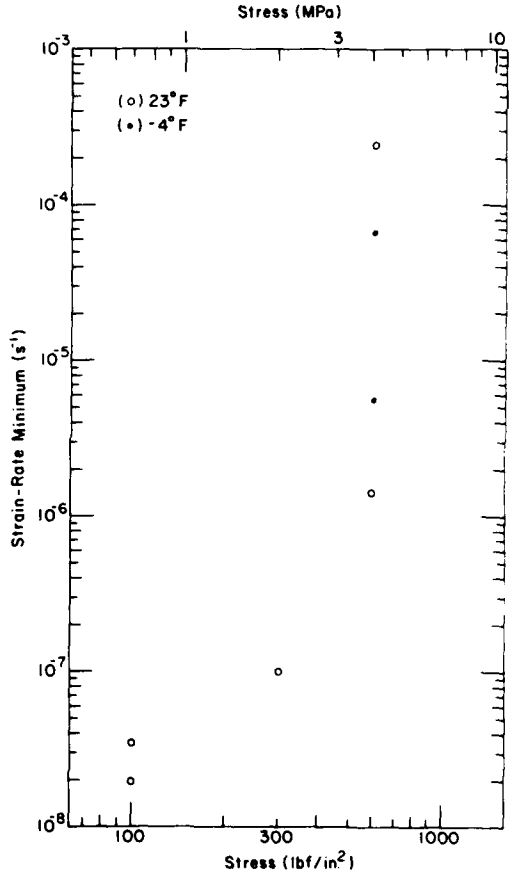

a. Strain-rate minimum vs applied stress.

Figure 46. Constant-load compression test results for the multi-year floe at -5 °C (23 °F) and -20 °C (-4 °F).

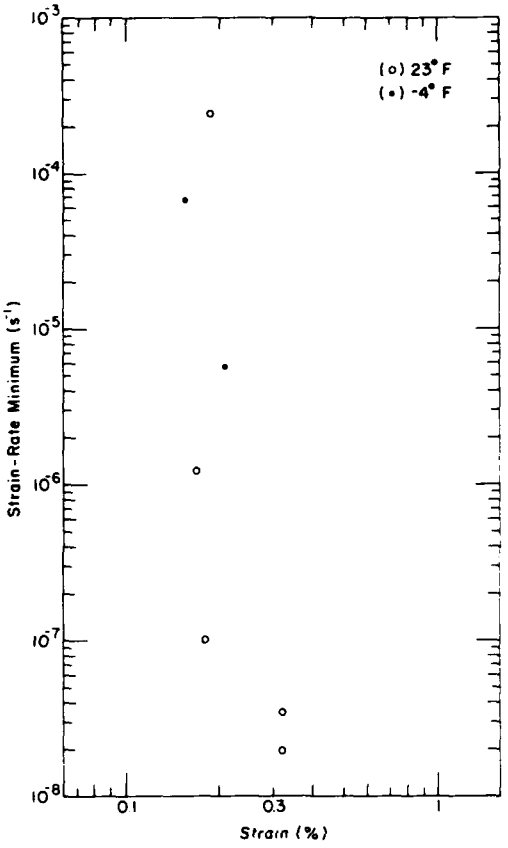

b. Strain-rate minimum vs failure strain.

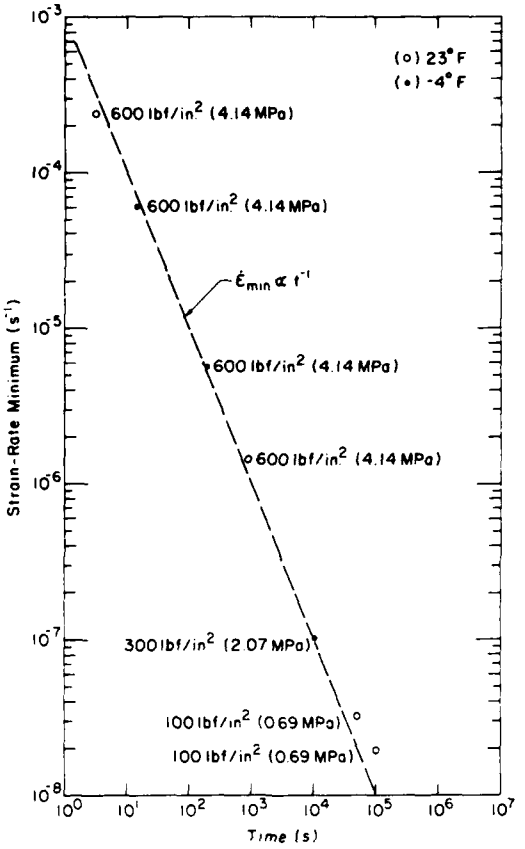

c. Strain-rate minimum vs time to failure.

Figure 46 (cont'd). Constant-load compression test results for the multi-year floe at -5°C (23°F) and -20°C (-4°F).

Constant-strain-rate tension tests

Constant-strain-rate tension tests were performed on capped, dumbbell test specimens at two strain rates (10^{-5} and 10^{-3}/s) and two temperatures (−5° and −20°C). The dumbbell specimens were prepared from 25.4-cm-long, 10.2-cm-diameter core samples in a similar manner as the compression test specimens; however, the diameter of the central portion of the specimen was further reduced to 8.9 cm. The smaller neck diameter was chosen to prevent failure at the end-cap bond. A series of strength tests were performed to evaluate the maximum neck diameter that would ensure that failure would be in the central portion of the sample. To minimize stress concentrations in the sample, the fillets on each end of the dumbbell specimen had a radius of two neck diameters, or 17.8 cm.

The tests were conducted on the closed-loop testing machine, where the strain rate was controlled by an extensometer mounted between the end caps. The capped samples were attached to the machine's cross heads with a pair of spherical universal joints, one mounted on each end of the sample. These ball joints were used by Currier (1981), who investigated the tensile strength of freshwater polycrystalline ice. In a few of the later tests, axial strains were also measured on the reduced central portion of the sample with a pair of DCDTs. Additional information on sample preparation, equipment and tension testing can be found in Mellor et al. (1984).

The results from the tension tests are given in Appendix D and plotted in Figure 47. Compared to compressive strength, the tensile strength of the multi-year floe samples shows little variation with temperature and strain rate. Michel (1978) found similar trends for replicate freshwater polycrystalline ice samples. Our results are surprising because there is considerable variation in ice structure between samples. Tests on freshwater polycrystalline ice show that the ice strength varies by a factor of

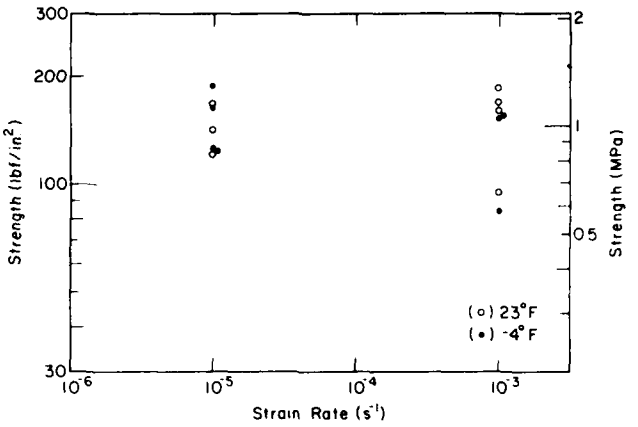

Figure 47. Uniaxial tensile strength of multi-year floe specimens at -5°C (23°F) and -20°C (-4°F) vs strain rate.

three, depending on the grain size (Michel 1978). The average tensile strength of all our tests was 1.00 ± 0.22 MPa (145 ± 32 lbf/in.²). Typically the samples failed at a strain of about 0.01–0.02%. The full-sample failure strains measured between the end caps are comparable to the failure strains measured on the reduced sections of the samples. We would expect the sample strains of the reduced sections to be higher. Possibly there is some excessive yielding at the bond between the ice and the end cap.

Triaxial tests

Conventional triaxial tests were performed on the closed-loop testing machine using the triaxial cell shown in Figure 48. The cell was designed so that the confining radial pressure on the sample could be ramped in constant proportion to the applied axial stress. For a right circular cylindrical specimen the ratio of the confining pressure to the axial stress is determined by the ratio of the diameter of the piston entering the cell (sample diameter) to the diameter of the piston in the upper cylinder. Two ratios of confining pressure to axial stress were used: 0.46 and 0.68. The larger ratio was obtained by placing a collar in the upper piston and using a smaller-diameter piston. Strain rates were controlled by an extensometer attached between the cell and the upper cylinder. The triaxial specimens were prepared in the same manner as the constant-strain-rate compression ridge ice samples. Additional details on the triaxial cell can be found in Mellor et al. (1984).*

* Recent work has shown that specimen end caps made from phenolic resin are too soft for triaxial testing when axial displacement is measured outside the pressure cell. Aluminum end caps have been substituted. Displacement transducers must also be mounted on the specimen to obtain reliable modulus data.

Because the compression test specimens had a dumbbell shape, we must correct for the axial tensile forces of the fluid on the sample when we compute the axial stresses:

$$\sigma_{cor} = F/A_s\,[1-K/A_s\,(A_c-A_s)]$$

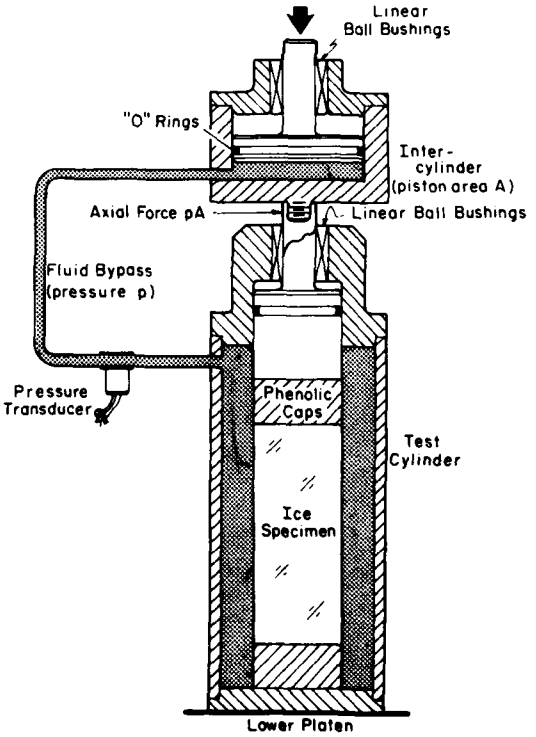

Figure 48. Triaxial testing equipment.

where σ_{cor} = corrected axial stress
F = external measured force
A_s = area of the reduced section of the sample
K = ratio of A_s to the area of the piston in the upper cylinder
A_c = area of the end cap.

The triaxial tests results are presented in Appendix D and are summarized in Figure 49, where the average triaxial strength for each test condition is plotted against the confining pressure at failure. Tests were conducted at two strain rates (10^{-5} and 10^{-3}/s), two temperatures (−5° and −20°C), and two confining pressure-axial stress ratios (0.46 and 0.68). The tests at 10^{-3}/s and −20°C with a confining pressure ratio of 0.68 were projected to exceed the capacity of our system (~ 20 MPa axial stress) and were not conducted. Two other tests were continued well beyond the design limits of the system and resulted in damage to the triaxial cell.

The plotted results actually reresent a portion of the ice yield surface in the compression-compression quadrant in stress-stress space. As the temperature decreases or strain rate increases, the size of the yield surface increases. The data again show considerable scatter; however, the structure of the multi-year floe ice is highly variable. The average results generally agree with the triaxial test results of Jones (1982), who investigated the confined compressive strength of freshwater polycrystalline ice at −11°C and different strain rates.

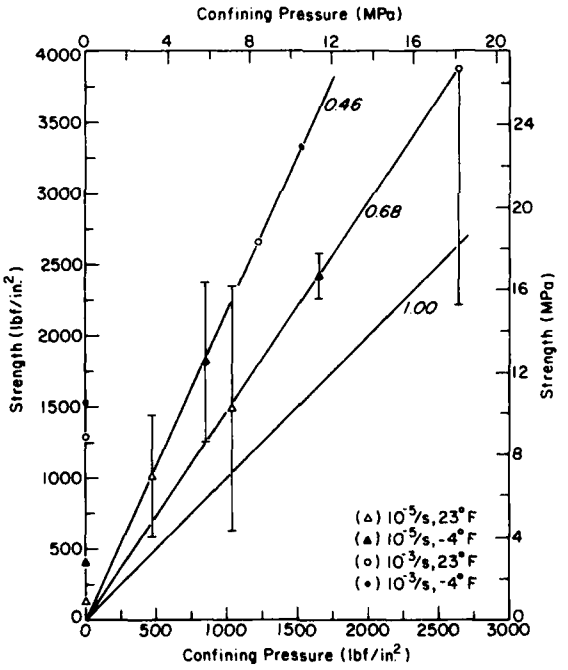

Figure 49. Average confined compressive strength of multi-year floe samples at different temperatures and strain rates vs confining pressure at failure for confining pressure/axial stress ratios of 0.46, 0.68 and 1.00. The bars denote one standard deviation from the mean.

CONCLUSIONS

The results of Phase I of this investigation have provided a preliminary understanding of the structure and mechanical properties of multi-year sea ice. Data are now available for the preliminary design of structures to be used in exposed areas of the Beaufort Sea. However, considerable work remains to be done before reliable constitutive relations can be developed for detailed ice-structure analyses. Not only do additional tests have to be performed at different temperatures and loading conditions, a greater emphasis has to be placed on the effect of ice structure on the ice mechanical properties. Both the strength and modulus ice data show more scatter than can be explained by variations in ice temperature, porosity, test load, strain rate or confining pressure. Before the results of Phase I can be fully applied, we need to categorize the structure of each test specimen. More structural analyses should also be planned in subsequent phases of the program.

LITERATURE CITED

Cherepanov, N.V. (1974) Classification of ice of natural water bodies. *Ocean 74, Proceedings of the IEEE International Conference on Engineering in the Ocean Environment, 21-23 August 1974, Halifax, Nova Scotia,* **1**:97-101.

Cox, G.F.N. and W.F. Weeks (1974) Salinity variations in sea ice. *Journal of Glaciology,* **13**(67):109-120

Cox, G.F.N. and W.F. Weeks (1982) Equations for determining the gas and brine volumes in sea ice samples. USA Cold Regions Research and Engineering Laboratory, CRREL Report 82-30. ADA122779.

Currier, J.H. (1981) The brittle to ductile transition in polycrystalline ice under tension. M.S. thesis, Thayer School of Engineering, Dartmouth College, Hanover, New Hampshire.

Frederking, R.M.W. and G.W. Timco (1980) NRC ice property measurements during the Canmar Kigoriak trials in the Beaufort Sea, Winter 1979-80. National Research Council of Canada, Division of Building Research, NRCC 18722.

Hawkes, I. and M. Mellor (1970) Uniaxial testing in rock mechanics laboratories. *Engineering Geology,* **4**(3):177-285.

Jones, S.J. (1982) The confined compressive strength of polycrystalline ice. *Journal of Glaciology,* **28**(98):171-178.

Kovacs, A. (1983) Characteristics of multi-year pressure ridges. *Proceedings of the Seventh International Conference on Port and Ocean Engineering under Arctic Conditions, Helsinki, Finland, 5-9 April 1983.* Vol. 3.

Kovacs, A. (1976) Grounded ice in the fast ice zone along the Beaufort Sea coast of Alaska. USA Cold Regions Research and Engineering Laboratory, CRREL Report 76-32. ADA031352.

Mellor, M. (1980) Mechanical properties of polycrystalline ice. *Physics and Mechanics of Ice, Proceedings of the International Union of Theoretical and Applied Mechanics Symposium, Copenhagen, August 6-10, 1979.* New York:Springer-Verlag, pp. 217-245.

Mellor, M. and D.M. Cole (1982) Deformation and failure of ice under constant stress or constant strain rate. *Cold Regions Science and Technology,* **5**:201-219.

Mellor, M., G.F.N. Cox and H.W. Bosworth (1984) Mechanical properties of multi-year sea ice: Testing techniques. *USA Cold Regions Research* and Engineering Laboratory, CRREL Report 84-8.

Michel, B. (1978) *Ice Mechanics.* Quebec City:Les Presses de l' Universite' Laval.

Nakawo, M. (1983) Measurements on air porosity of sea ice. *Annals of Glaciology,* **4**:204-208.

Peyton, H.R. (1966) Sea ice strength. Geophysical Institute, University of Alaska, Report UAG-182.

Rand, J. (In prep.) The CRREL 4-inch ice coring auger. USA Cold Regions Research and Engineering Laboratory, Special Report.

Schwarz, J., R. Frederking, V. Gavillo, I.G. Petrov, K.-I. Hirayama, M. Mellor, P. Tryde and K.D. Vaudrey (1981) Standardized testing methods for measuring mechanical properties of ice. *Cold Regions Science and Technology,* **4**:245-253.

Schwarz, J. and W.F. Weeks (1977) Engineering properties of ice. *Journal of Glaciology,* **19(8)**:449-530.

Traetteberg, A., L.W. Gold and R. Frederking (1975) The strain rate and temperature dependence of Young's modulus of ice. *Proceedings of the Third International Symposium of Ice Problems, 18-21 August 1975, Hanover, New Hampshire,* International Association of Hydraulic Research, Committee on Ice Problems, pp. 449-486.

Wang, Y.S. (1979) Sea ice properties. Technical Seminar on Alaskan Beaufort Sea Gravel Island Design, 18 October 1979, Exxon Company, U.S.A., Houston, Texas.

Weeks, W.F. and A. Assur (1969) Fracture of lake and sea ice. USA Cold Regions Research and Engineering Laboratory, Research Report 269. ADA697750

APPENDIX A: STRUCTURAL PROFILE OF A MULTI-YEAR PRESSURE RIDGE CORE

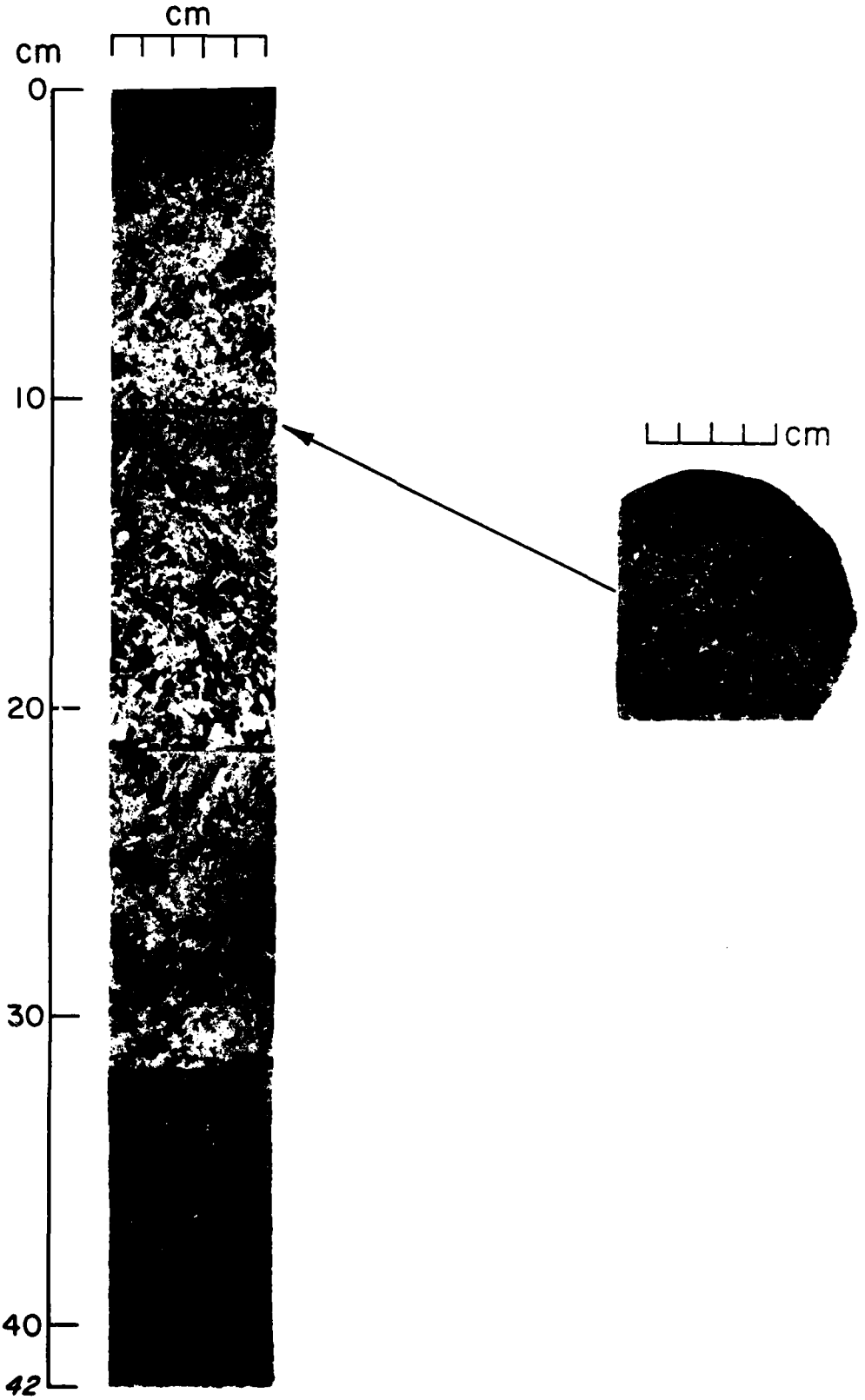

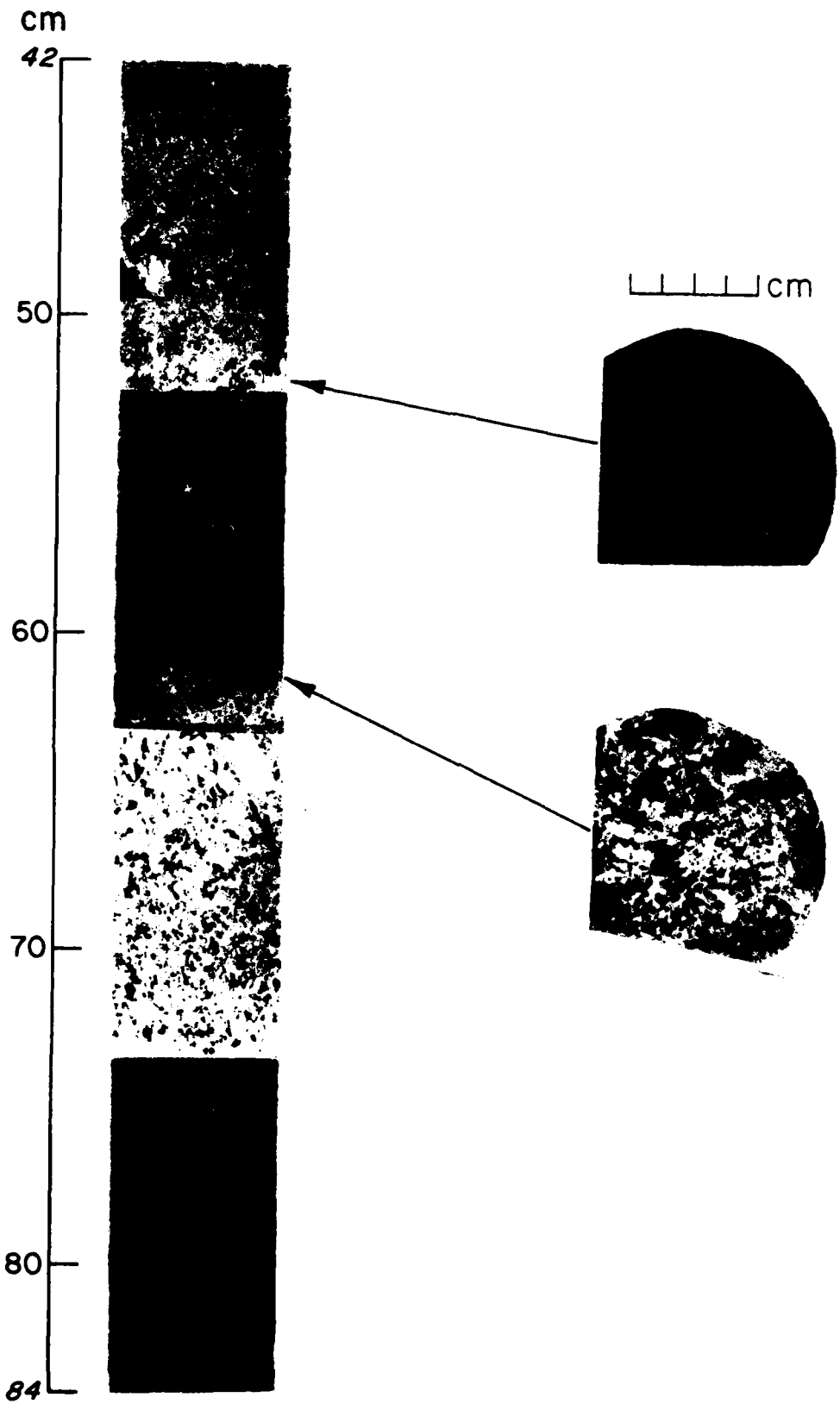
cm
42
50
60
70
80
84
cm

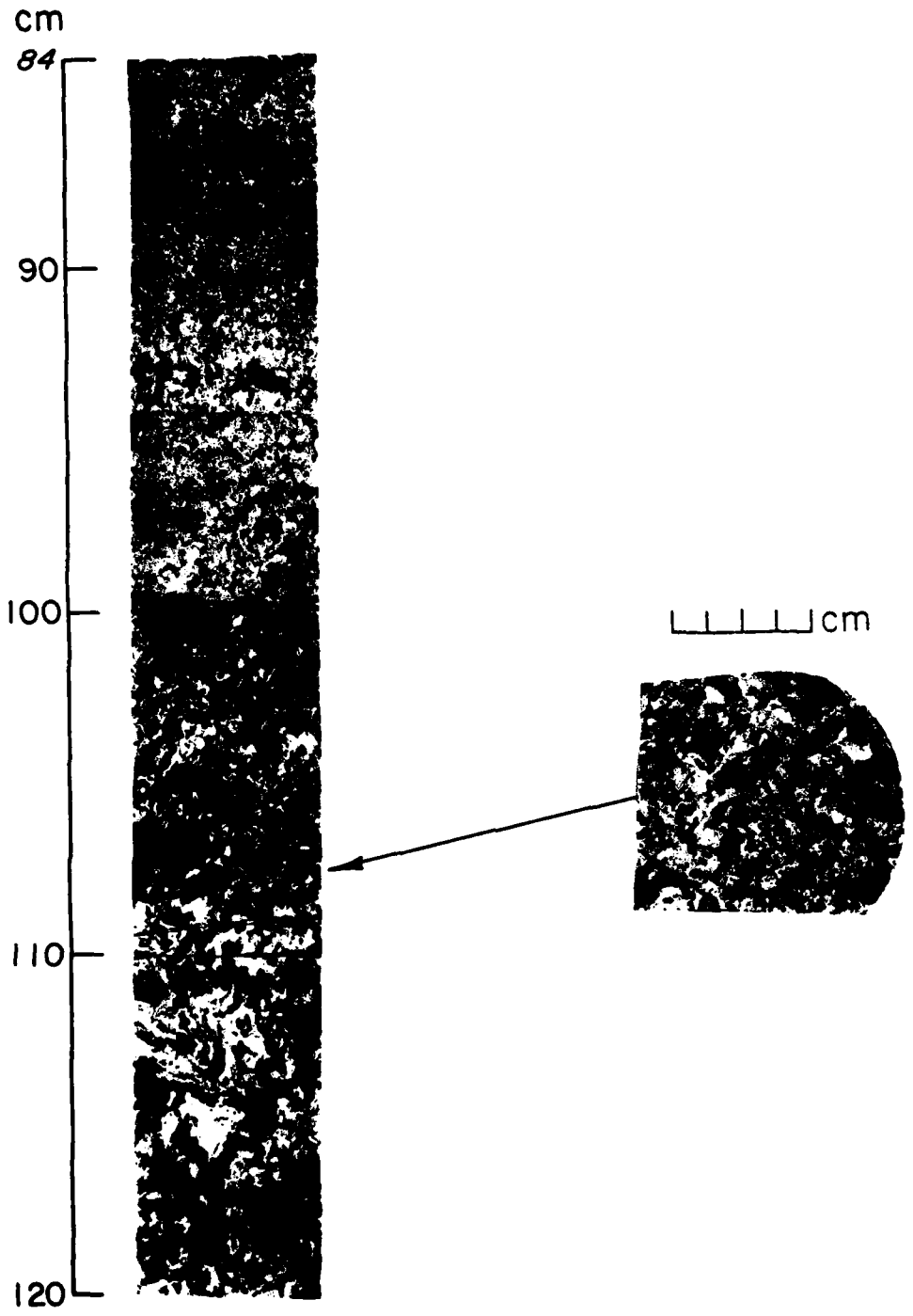
cm
84
90
100
110
120
cm

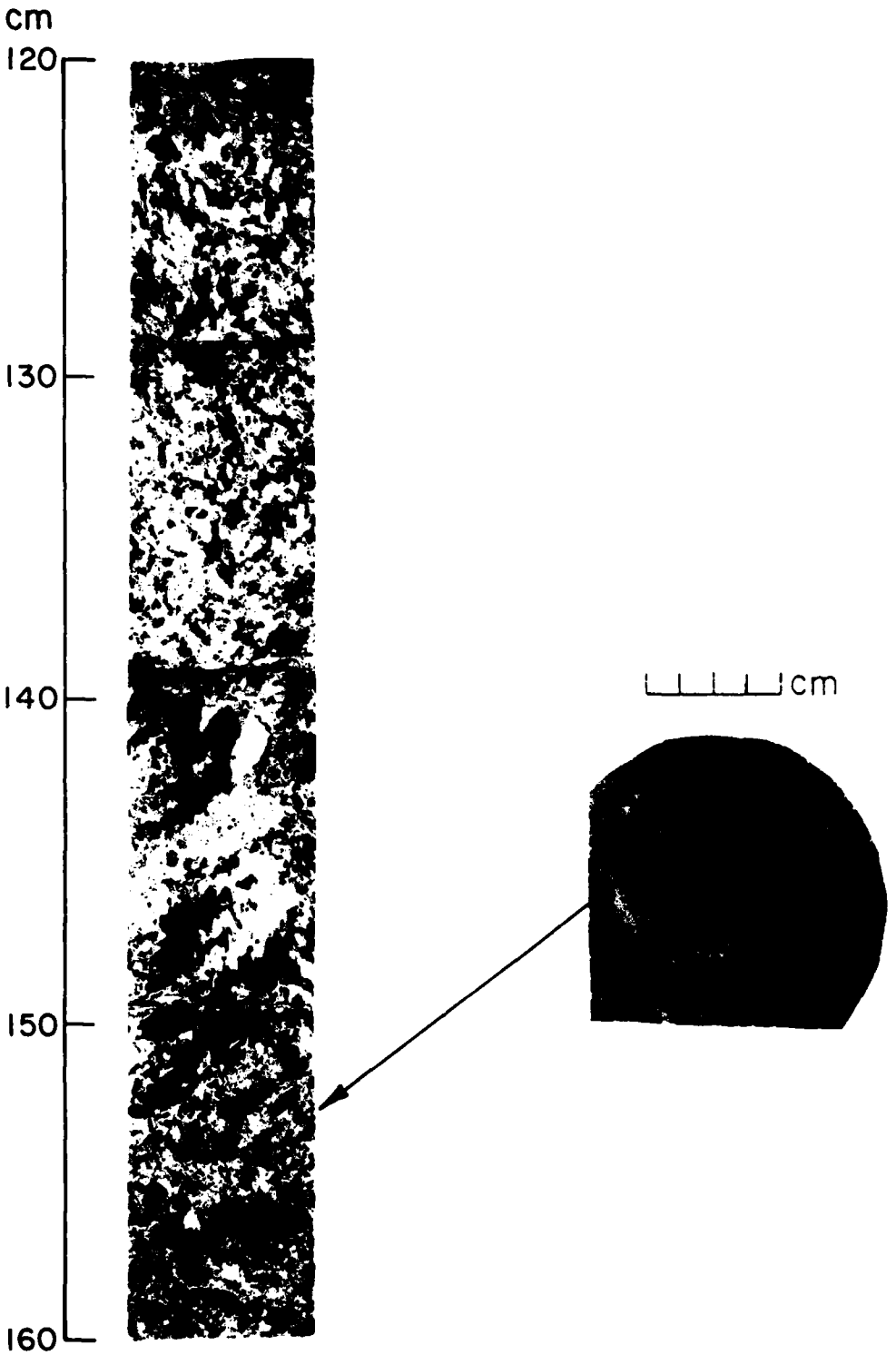
cm
120
130
140
150
160
cm

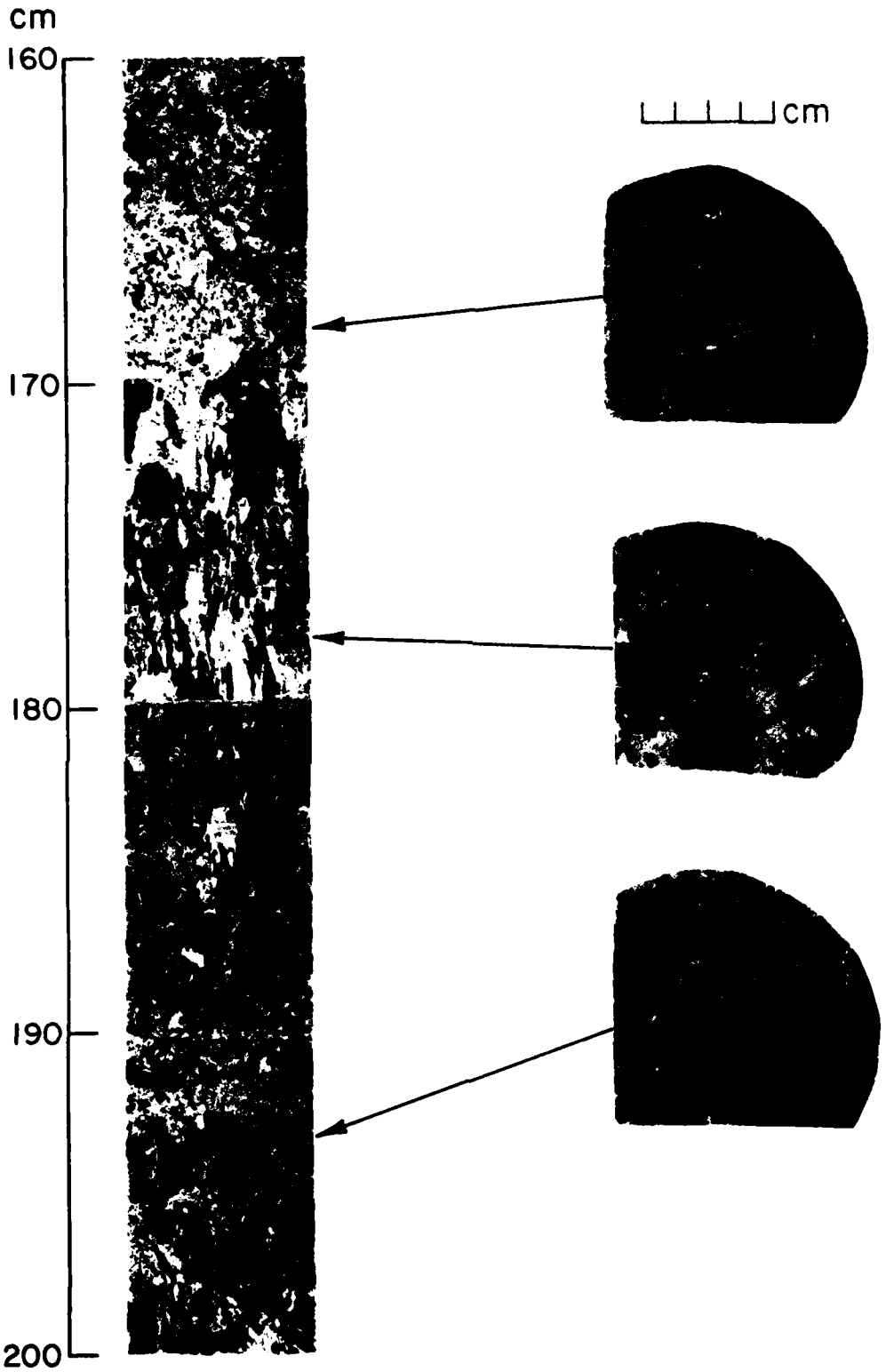
cm
160
170
180
190
200
cm

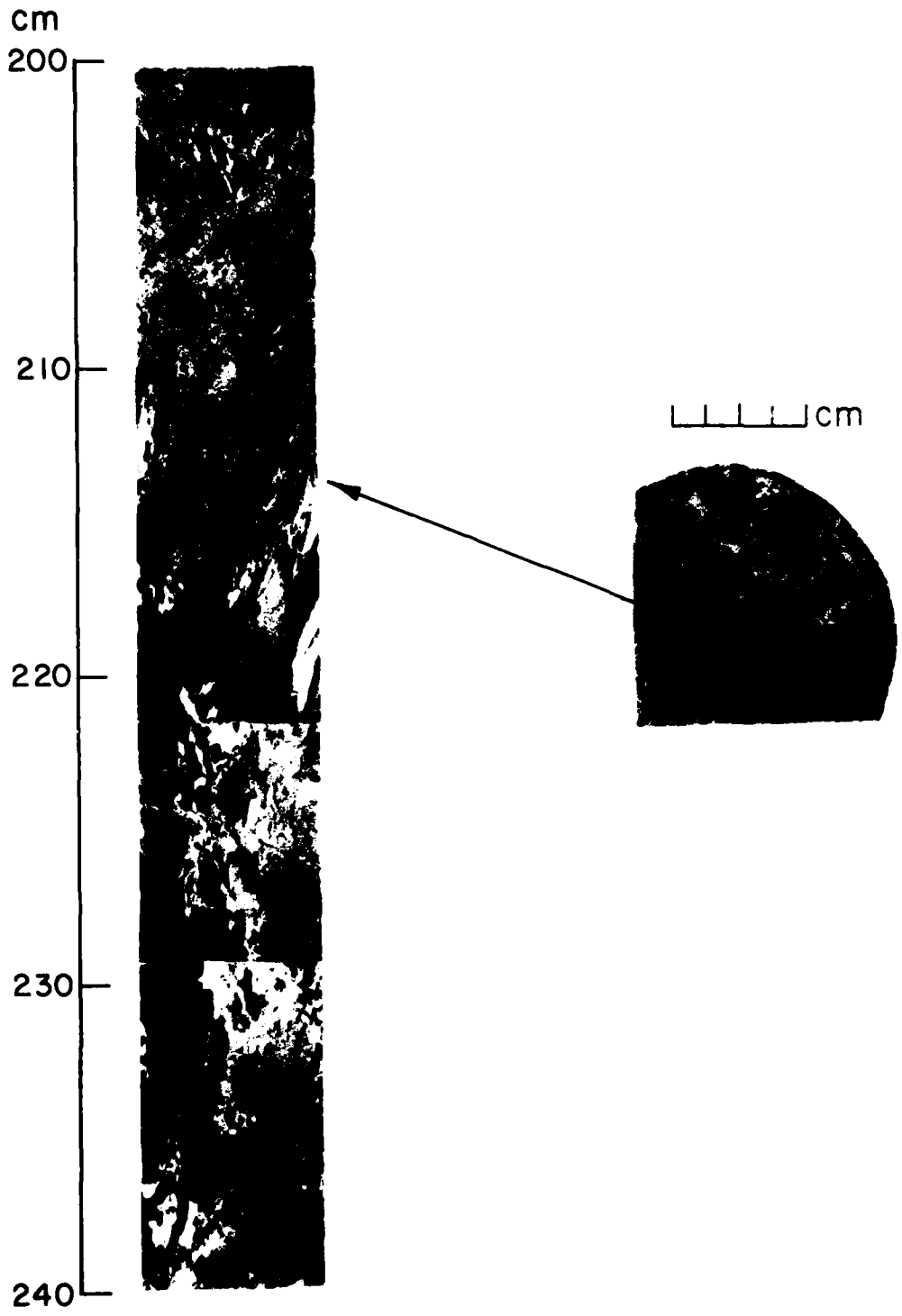
cm
200
210
220
230
240
cm

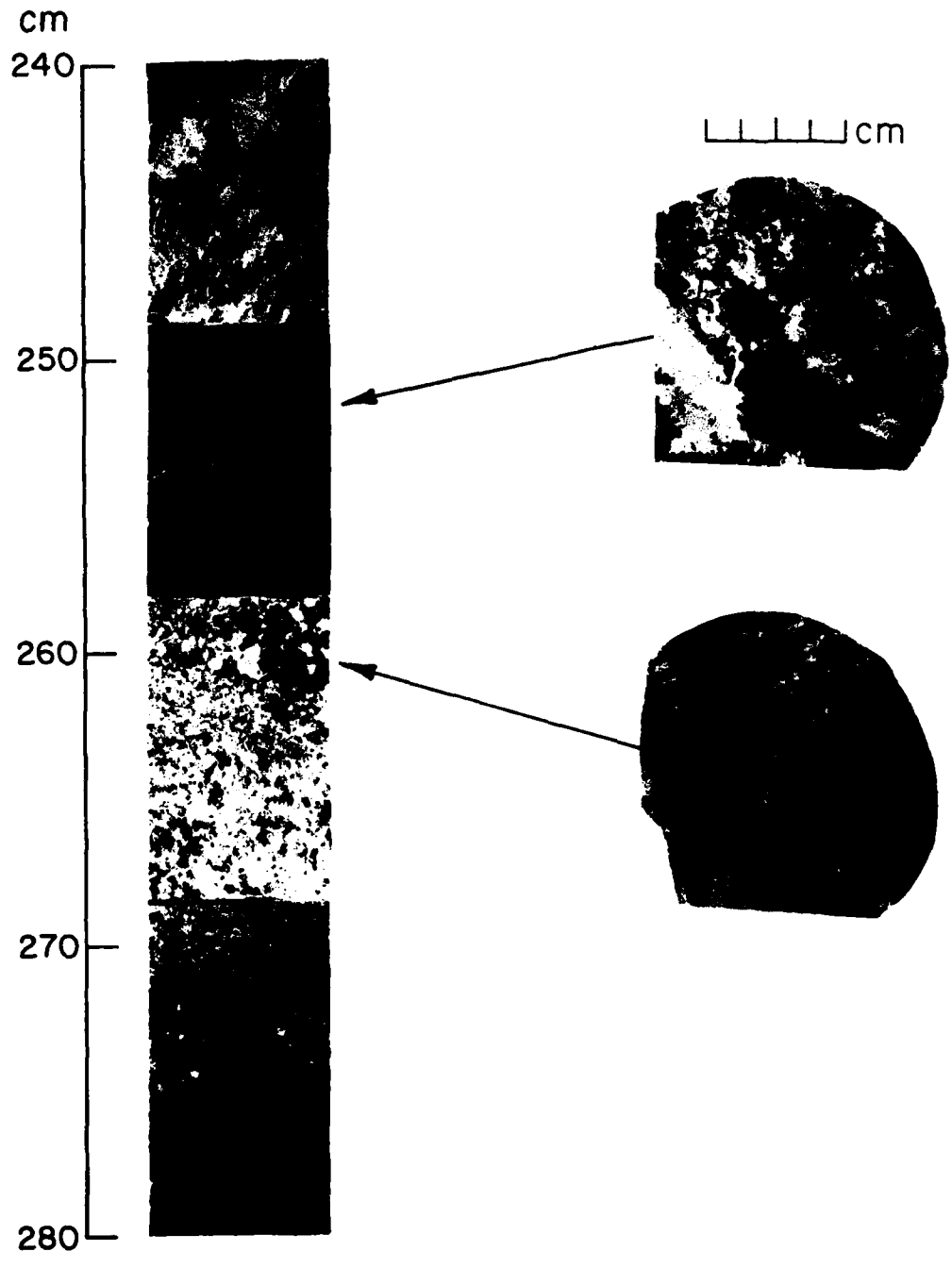
cm
240
250
260
270
280
cm

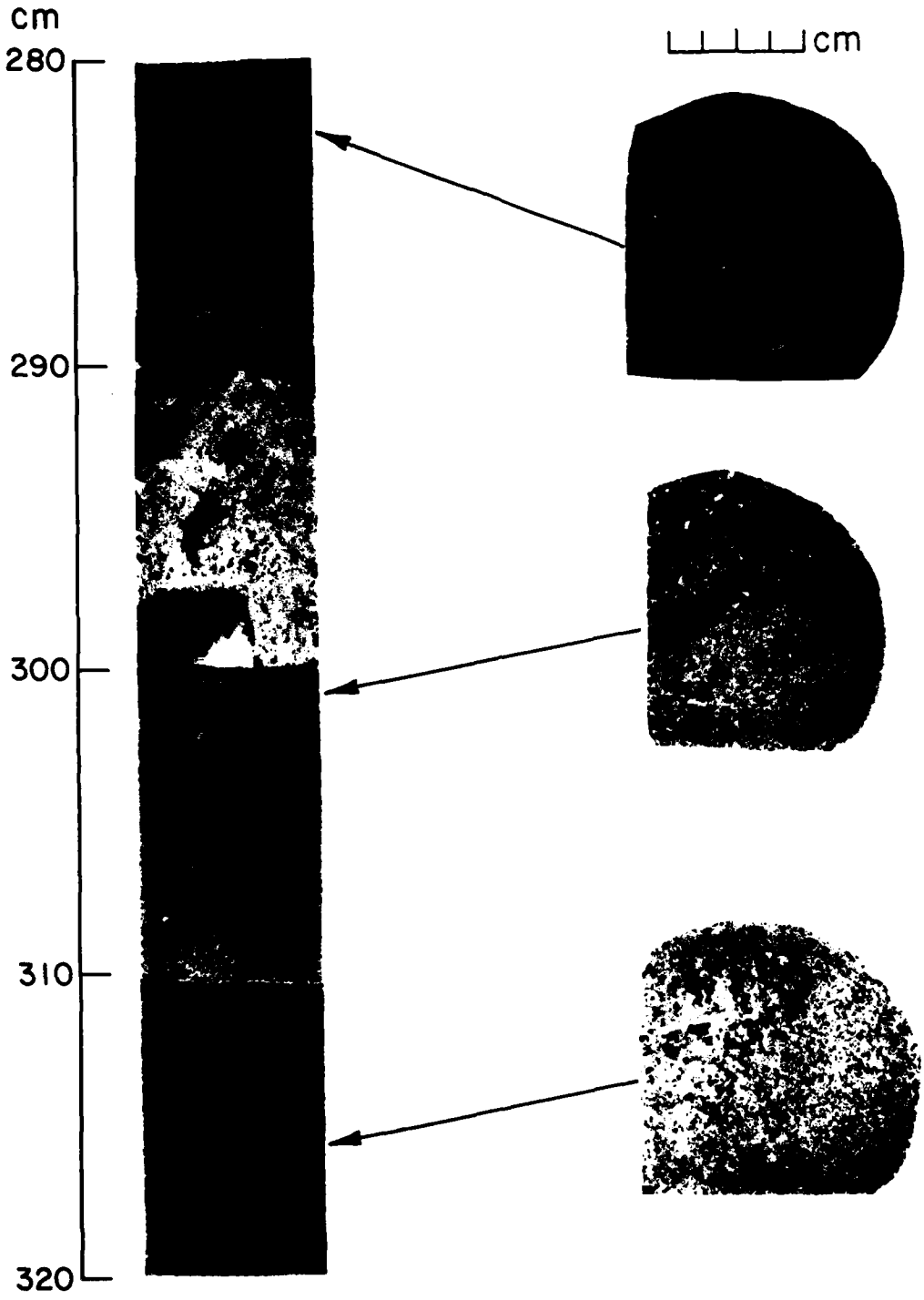
cm
280
290
300
310
320
cm

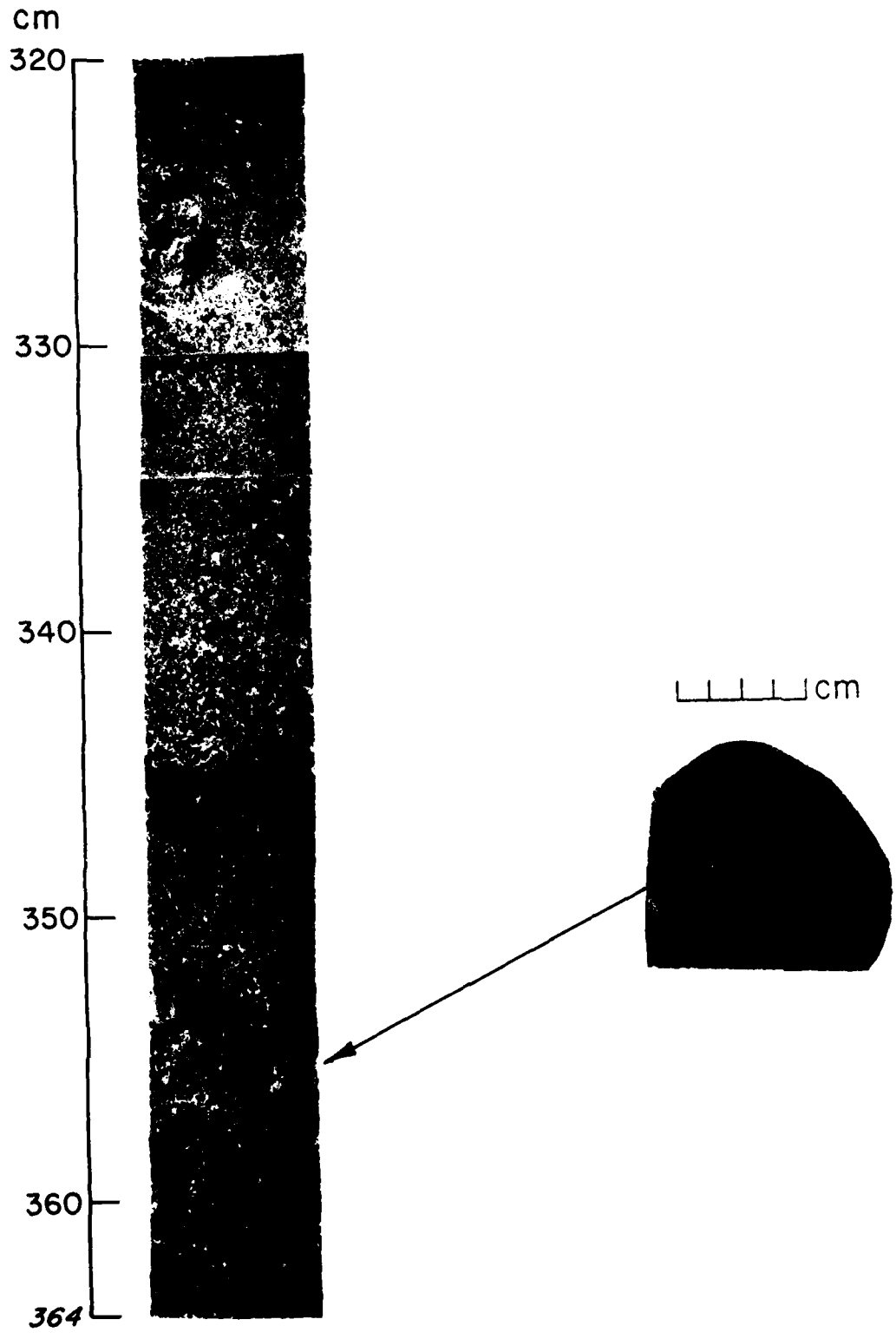
cm
320
330
340
350
360
364
cm

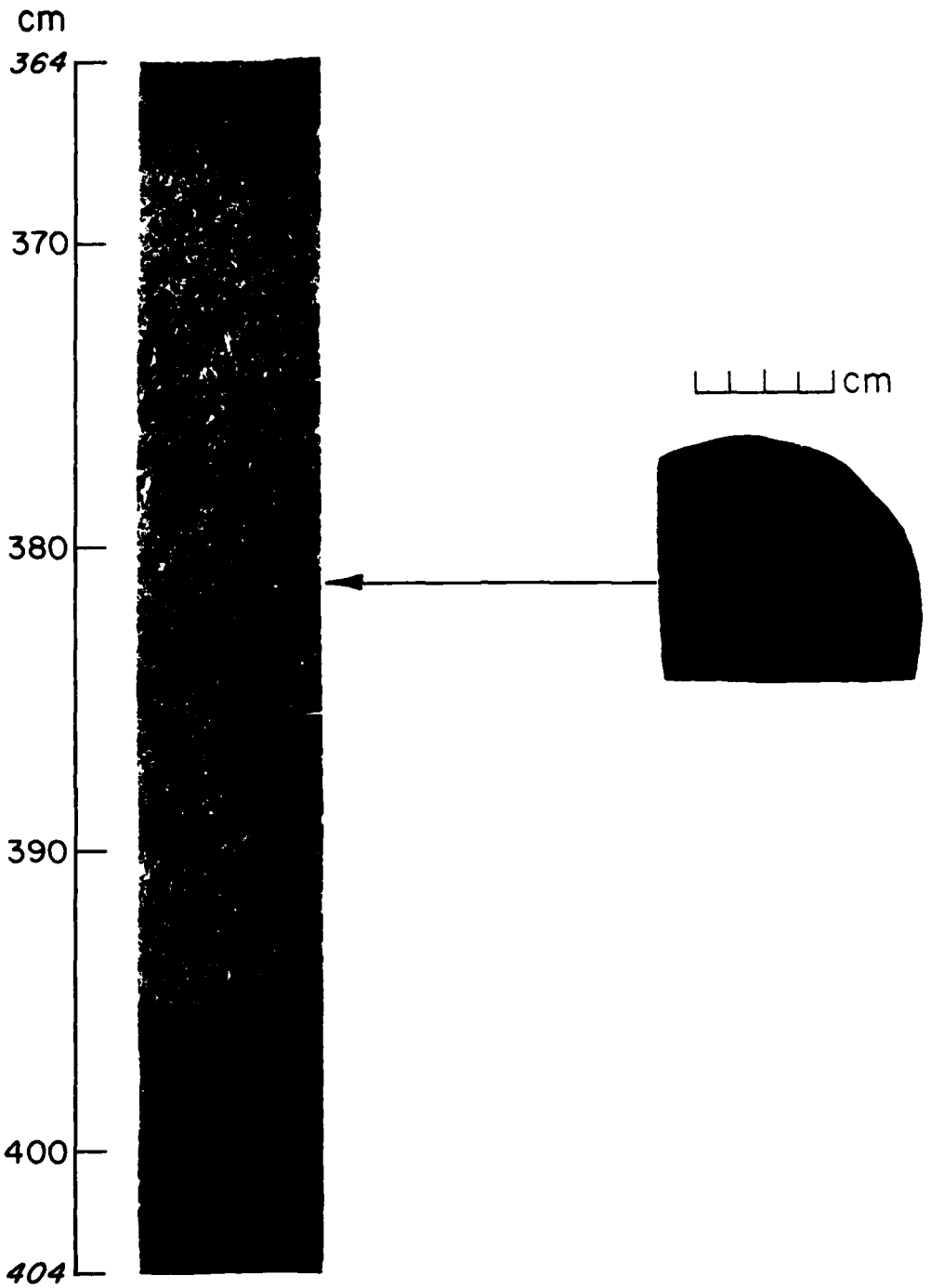
cm
364
370
380
390
400
404
cm

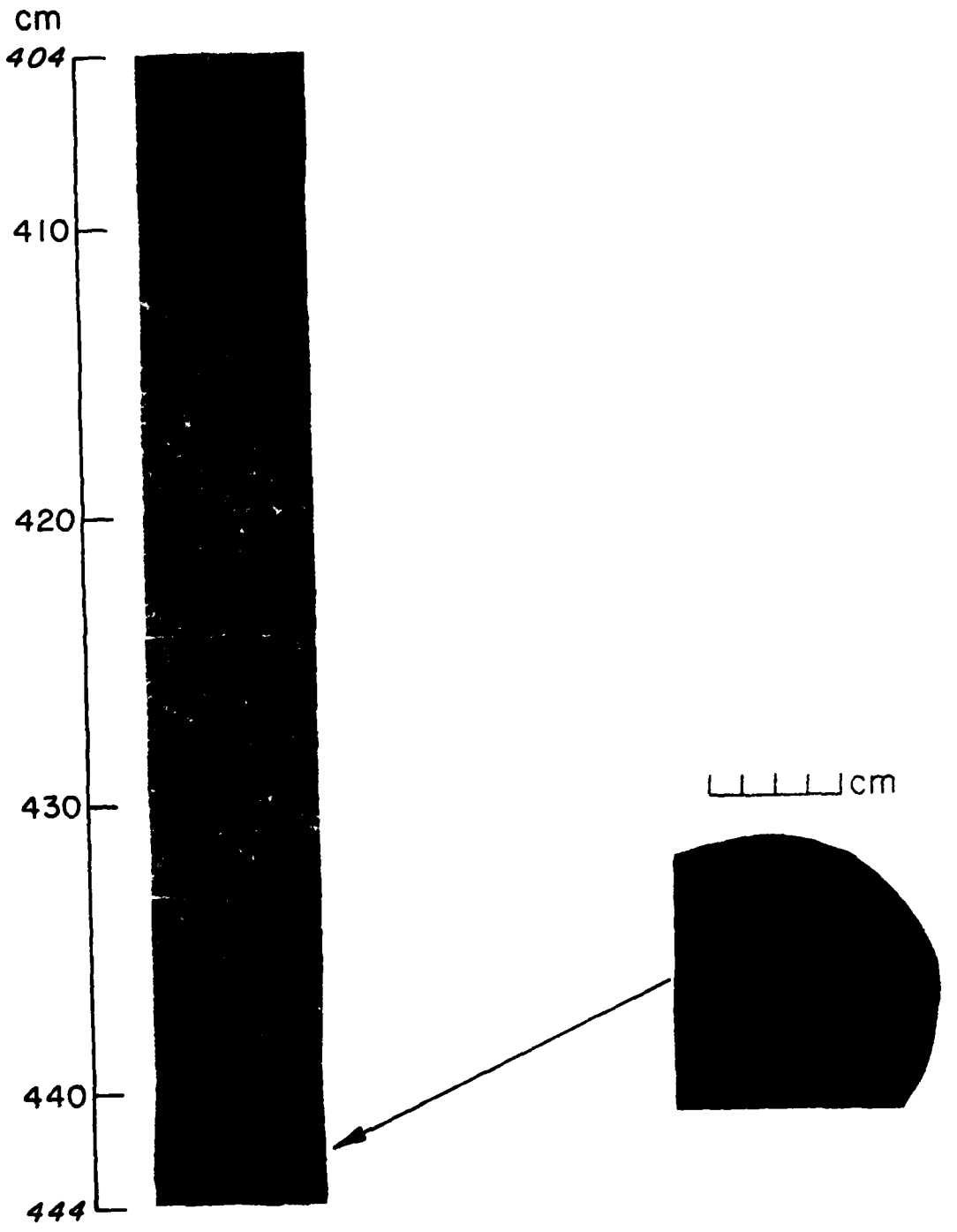
cm
404
410
420
430
440
444
cm

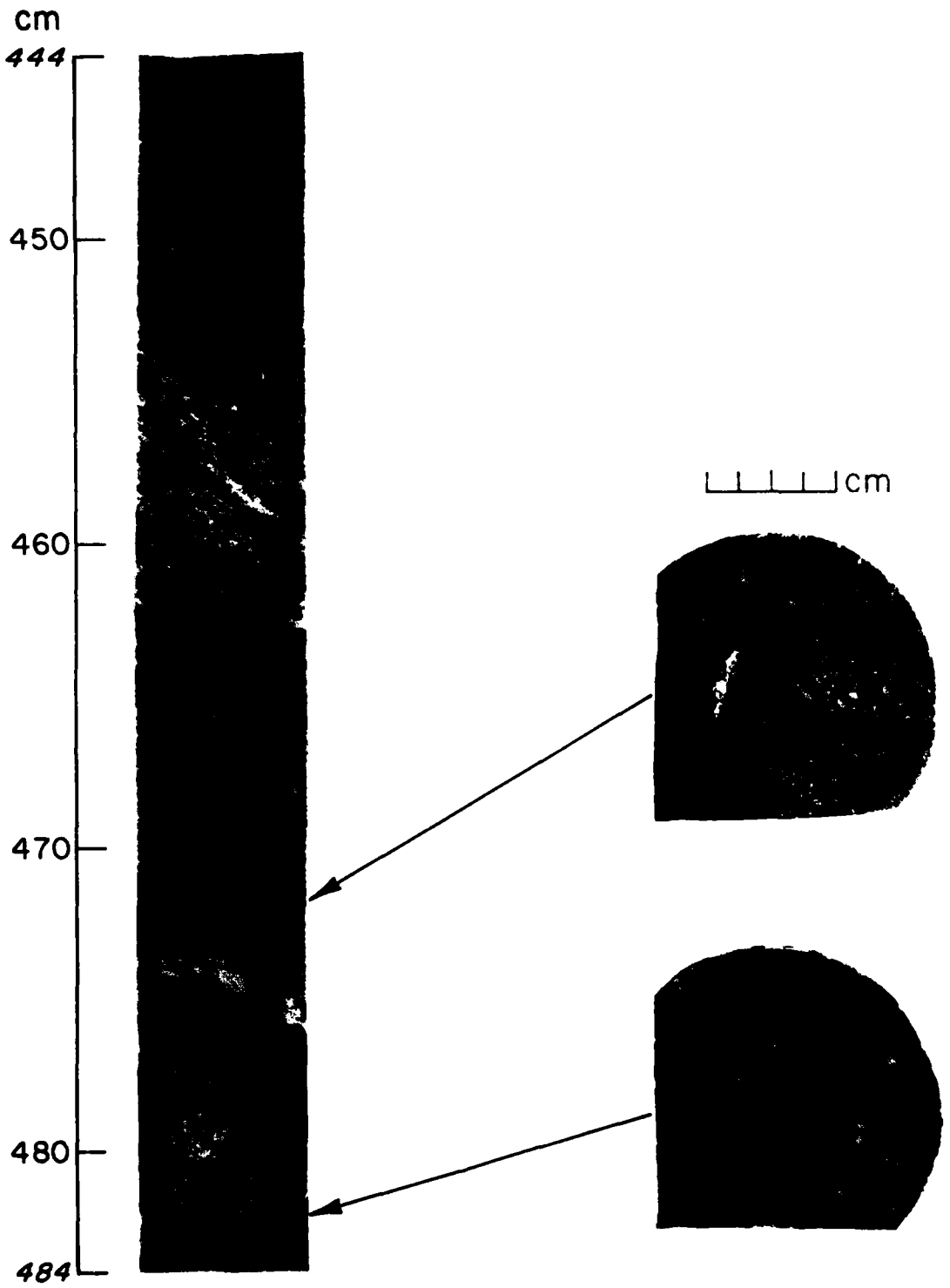
cm
444
450
460
470
480
484
cm

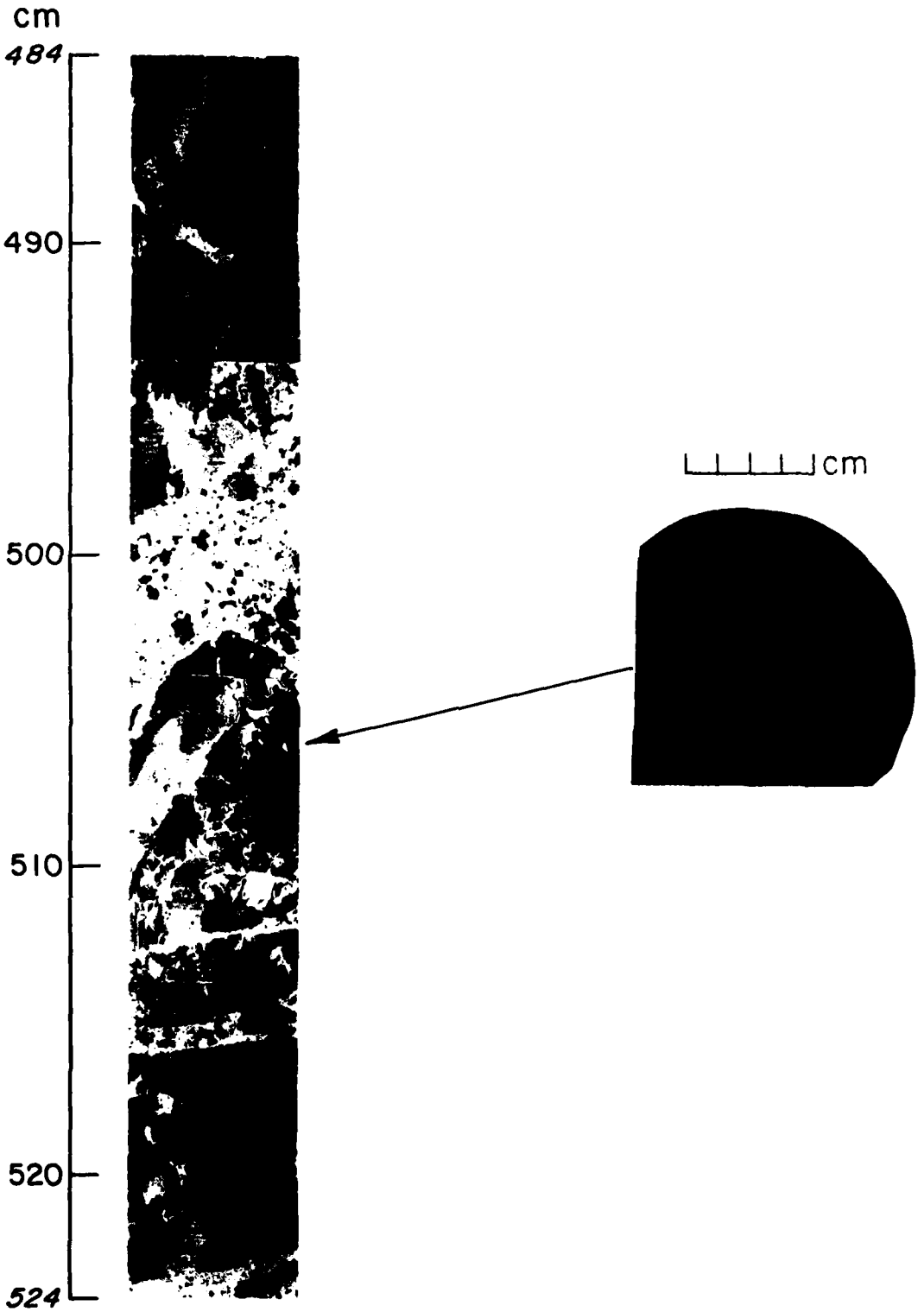
cm
484
490
500
510
520
524
cm

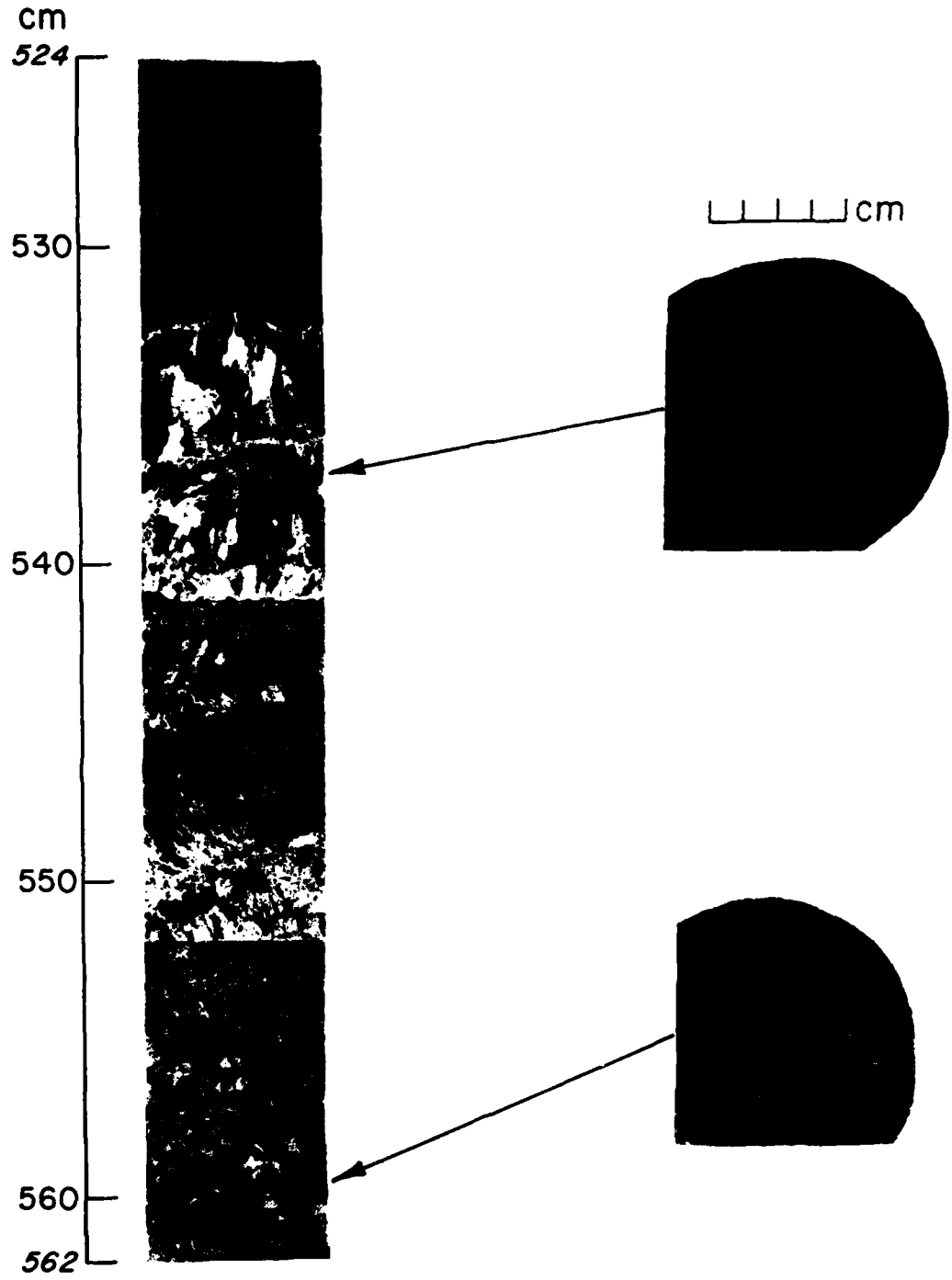
cm
524
530
540
550
560
562
cm

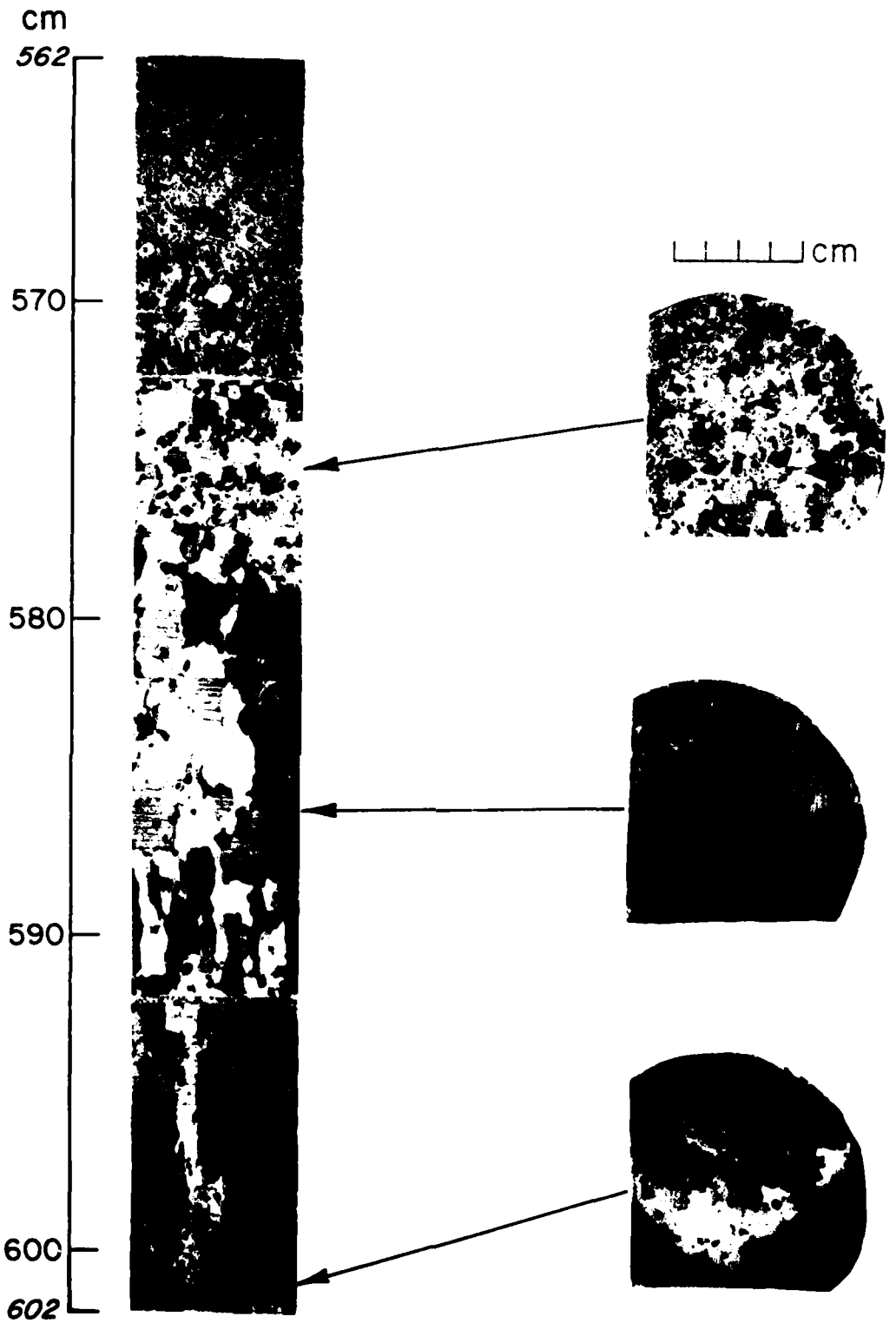
cm
562
570
580
590
600
602
cm

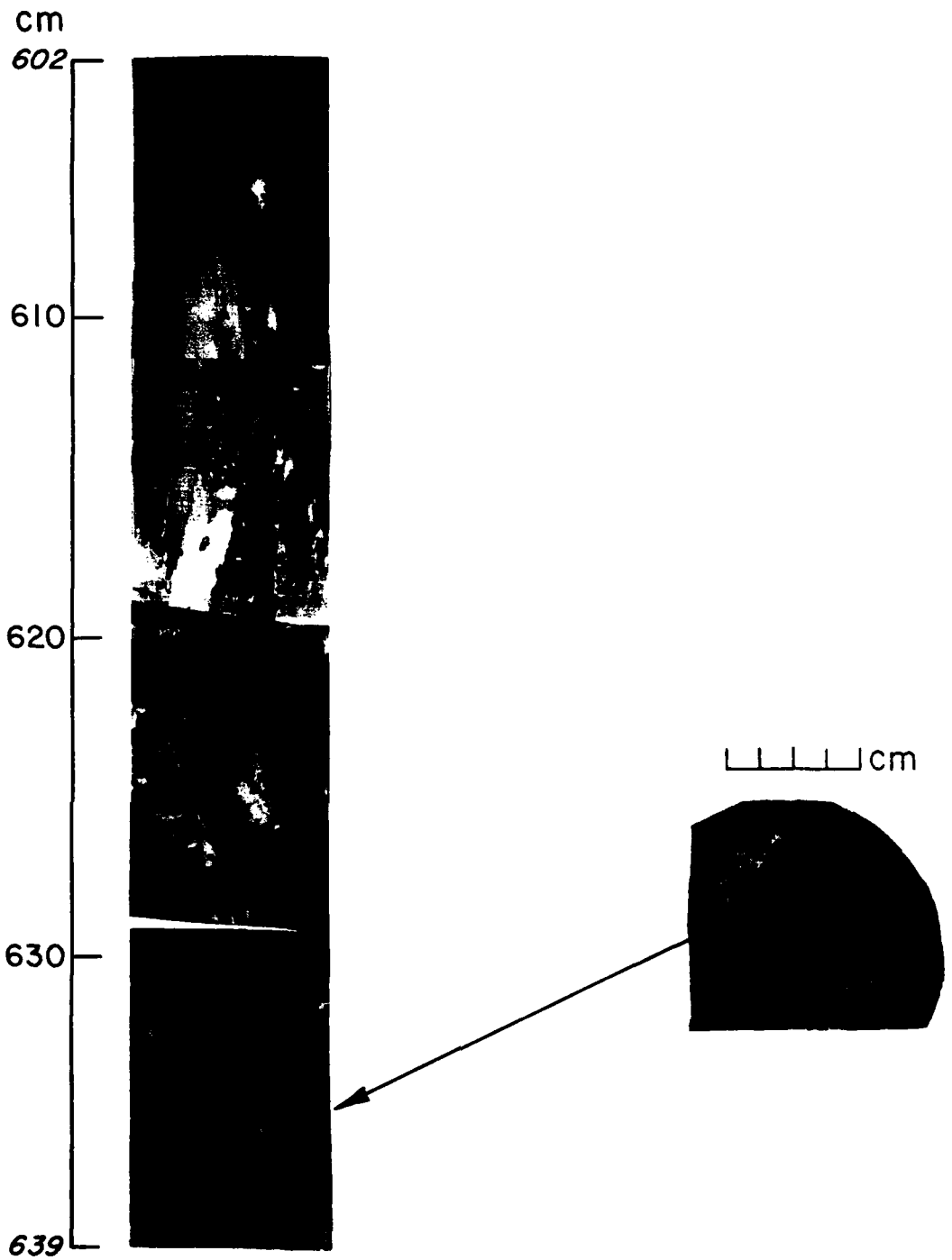
cm
602
610
620
630
639
cm

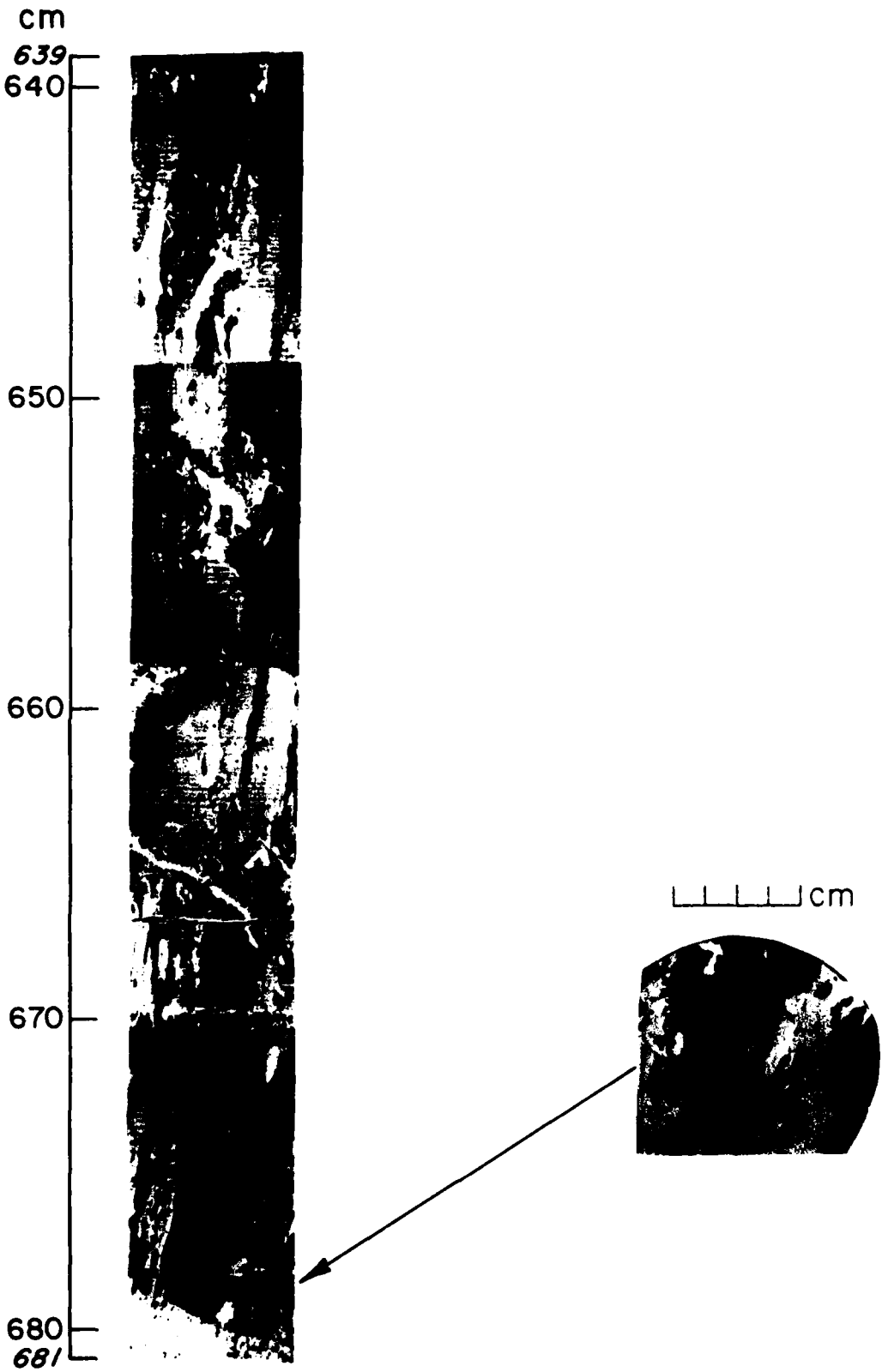
cm
639
640
650
660
670
680
681
cm

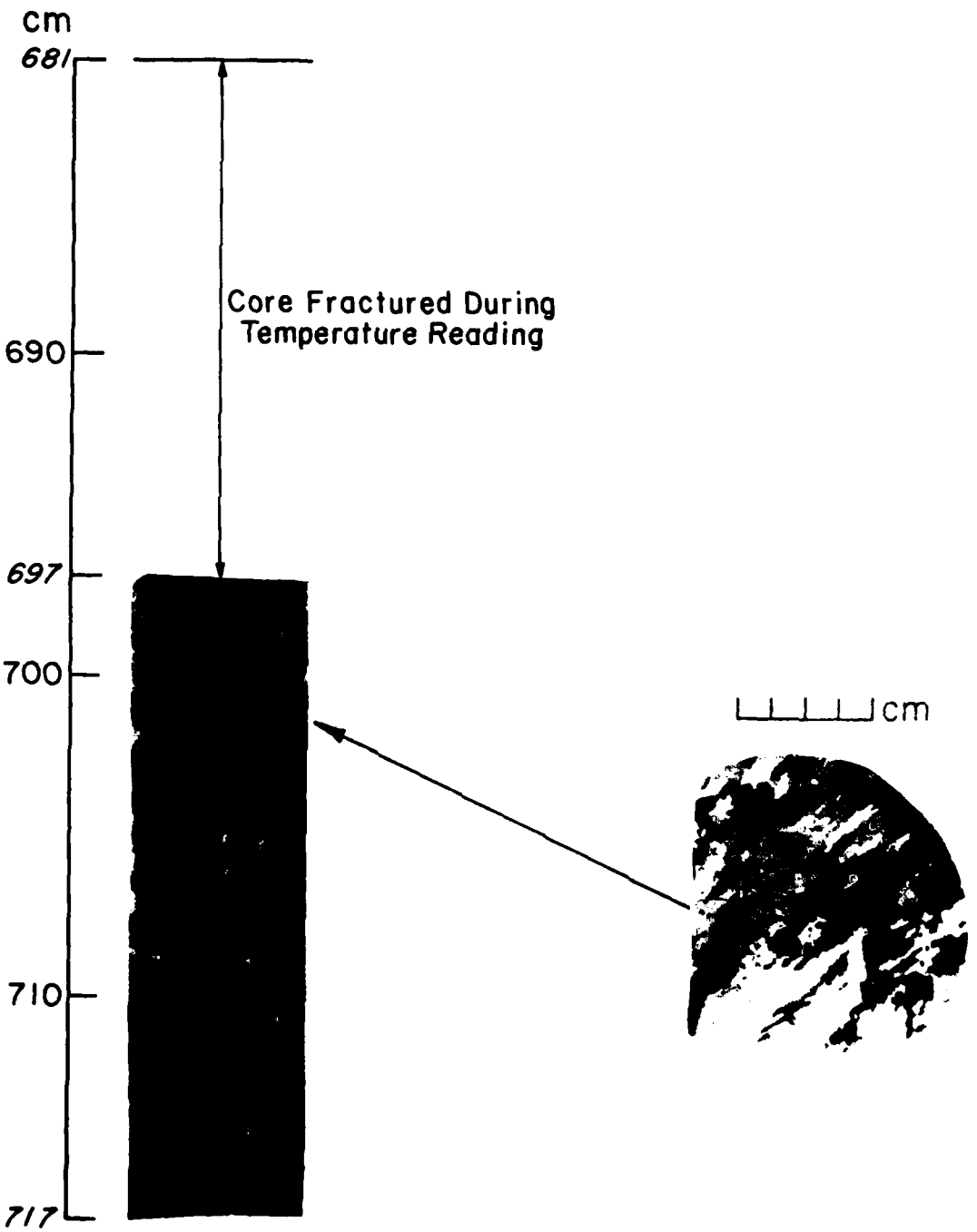
cm
681
690
697
700
710
717
Core Fractured During
Temperature Reading
cm

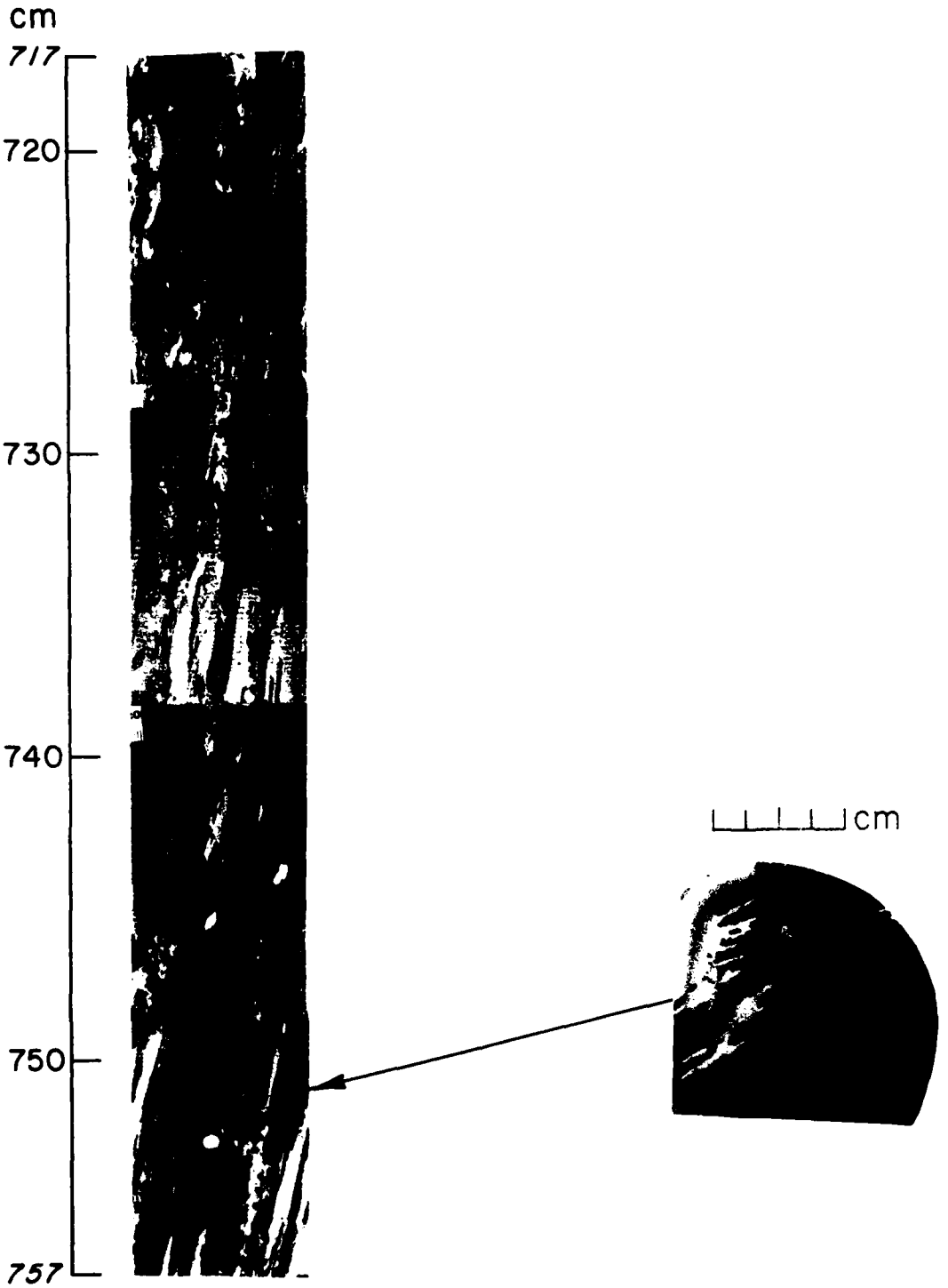
cm
717
720
730
740
750
757
cm

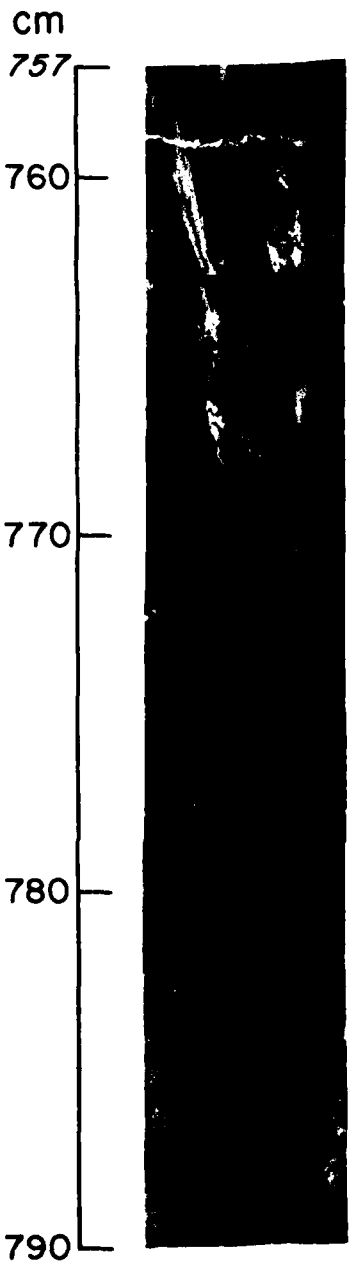
cm
757
760
770
780
790

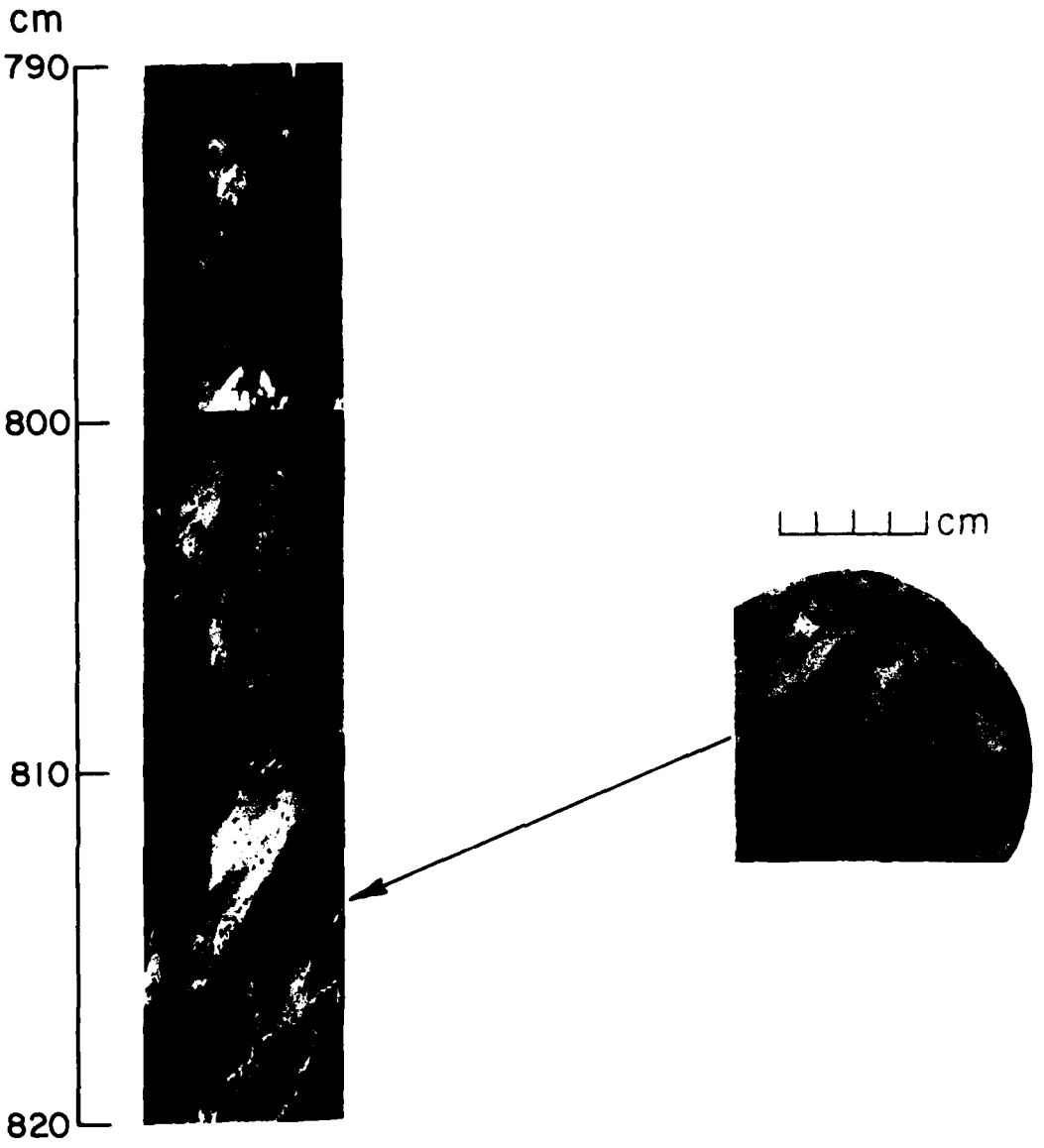
cm
790
800
810
820
cm

APPENDIX B: RIDGE UNIAXIAL COMPRESSION TEST DATA

This appendix contains the results from the constant-strain-rate, uniaxial compression tests performed on the multi-year pressure ridge specimens. The parameters listed for each test are defined in Index B.

INDEX B

Column no.	*Symbol*	*Description*
1	σ_m (psi)	Peak stress, or strength
2	ϵ_m(GL) (%)	Strain at σ_m determined by the DCDTs over a gauge length of 5.5 in.
3	ϵ_m(FS) (%)	Strain at σ_m determined by the extensometer over the full sample length of 10 in.
4	t_m (s)	Time to peak stress
5	σ_e (psi)	Stress at end of test
6	ϵ_e(FS) (%)	Full sample strain at end of test
7	t_e (s)	Time to end of test
8	E_i(GL) (10^6 psi)	Initial tangent modulus determined using strains found over the gauge length
9	E_o(GL) (10^6 psi)	Secant modulus determined using gauge length strains
10	E_o(FS) (10^6 psi)	Secant modulus determined using full sample strains
11	S_i (‰)	Sample salinity at test temperature
12	ϱ (lb/ft^3)	Sample weight density at test temperature
13	V_b (‰)	Brine volume at test temperature
14	V_a(‰)	Air volume at test temperature
15	n (‰)	Porosity at test temperature
16	σ_e/σ_m	Ratio of end to peak stress at 5% full sample strain
17	Ice squareness (in.)	Sample squareness departure after ends are milled
18	End cap squareness (in.)	Sample squareness departure after end caps are mounted
19	Shim (in.)	Amount of shim stock inserted between low end of sample and actuator before testing

Sample Numbers

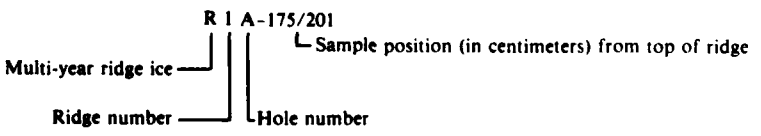

Above Level Ice, $\dot{\epsilon} = 10^{-3}$/s, T = −5°C (23°F)

Sample no	1 σ_m (psi)	2 ϵ_m (GL) (%)	3 ϵ_m (FS) (%)	4 t_m (s)	5 σ_e (psi)	6 ϵ_e (FS) (%)	7 t_e (s)	8 E_i (GL) (10^6 psi)	9 E_0 (GL) (10^6 psi)	10 E_0 (FS) (10^6 psi)	11 S_i (‰)	12 ϱ (lb/ft³)	13 V_b (‰)	14 V_a (‰)	15 n (‰)	16 σ_e/σ_m	17 ISQ (in.)	18 ESQ (in.)	19 SHM (in.)
R1A-175/201	1270	0.14	0.15	1.45	119	5.00	50.00	1.200	0.907	0.847	0.70	56.81	6.9	9.4	16.2	0.094	0.006	0.010	0.010
R1B-131/157	1260	0.16	0.24	2.35	209	5.00	50.00	1.320	0.788	0.525	0.37	56.82	3.6	8.7	12.3	0.166	0.004	0.006	0.004
R2A-110/135	408	0.05	0.04	0.44	408	0.04	0 44	0.868	0.816	1.020	0.20	52.43	1.8	85.0	86.9		0.010	0.009	0.004
R2B-135/161	820	0.11	0.10	1.00	820	0.10	1.00	0.892	0.745	0.820	0.10	55.81	1.0	25.8	26.8		0.009	0.005	0.004
R3A-188/213	970	0.16	0.16	1.64	199	5.00	50.00	1.060	0.606	0.606	1.40	56.85	13.7	9.8	23.5	0.205	0.007	0.007	
R3B-130/155	900	0.14	0.15	1.50	255	5.00	50.00	1.170	0.643	0.600	1.13	56.28	11.0	19.3	30.3	0.283	0.008	0.008	0.004
R4A-283/309	860	0.11	0.10	1.00	860	0.10	1.00	0.973	0.782	0.860	1.30	53.58	12.0	66.7	78.7		0.007	0.013	0.012
R4B-299/325	910	0.14	0.15	1.50	99	5.00	50.00	0.973	0.650	0.607	1.30	54.89	12.3	43.9	56.2	0.109	0.012	0.004	0.004
R5A-135/161	1090	0.10	0.09	0.85	1090	0.09	0.85	1.220	1.090	1.210	0.20	56.10	1.9	20.9	22.9		0.011	0.008	0.006
R5B-141/167	1270	0.11	0.13	1.30	1270	0.13	1.30	1.280	1.150	0.977	0.20	56.20	1.9	19.2	21.1		0.011	0.003	0.002
R7A-005/031	731	0.09	0.11	1.08	731	0.11	1.08	0.781	0.812	0.665	0.02	52.92	0.2	76.2	76.4		0.006	0.002	0.000
R7B-072/098	487	0.06	0.14	1 40	487	0.14	1.40		0.812	0.348	0.48	54.53	4.5	48.9	53.4		0.011	0.007	0.006
R8A-033/059	346	0.06	0.11	1.15	346	0.11	1.15	0.718	0.577	0.315	0.30	53.16	2.8	72.5	75.2		0.008	0.005	0.004
R8B-011/037	811	0.09	0.08	0.80	811	0.08	0.80	0.997	0.901	1.010	0.10	52.48	0.9	84.0	84.9		0.007	0.021	0.020
R2C-049/076	642	0.11	0.15	1.15	139	5.00	50.00	0.806	0.584	0.428	0.17	49.93	1.5	130.6	132.1	0.217	0.004	0.004	0.004
R2D-134/161	706	0.12	0.16	1.70	139	5.00	50.00	0.821	0.588	0.441	0.37	52.64	3.4	81.5	84.8	0.197	0.010	0.011	0.011
R4C-244/271	760	0.07	0.11	1.08	760	0.11	1 08	1.140	1.090	0.691	2.58	56.13	25.0	24.3	49.2		0.006	0.008	0.008

Sample no.	1 σ_m (psi)	2 ϵ_m (GL) (%)	3 ϵ_m (FS) (%)	4 $t_{\neg}$ (s)	5 σ_e (psi)	6 ϵ_e (FS) (%)	7 t_e (s)	8 E_i (GL) (10^6 psi)	9 E_0 (GL) (10^6 psi)	10 E_0 (FS) (10^6 psi)	11 S_i (%)	12 ϱ (lb/ft^3)	13 V_b (%)	14 V_a (%)	15 n (%)	16 σ_e/σ_m	17 ISQ (in.)	18 ESQ (in.)	19 SHM (in.)
R4C-309/336	826	0.16	0.21	2.17	187	5.00	50.00	0.897	0.516	0.393	0.88	55.43	8.4	33.7	42.1	0.226	0.012	0.011	0.011
R4D-228/255	659	0.06	0.09	0.95	659	0.09	0.95	1.110	1.098	0.732	2.51	55.90	24.2	28.1	52.3		0.005	0.007	0.007
R7C-007/034	907	0.12	0.11	1.12	907	0.11	1.12	0.940	0.759	0.825	0.10	54.27	0.9	52.9	53.8		0.005	0.001	0.001
R6A-398/425	764	0.13	0.15	1.45	92	5.00	50.00	0.880	0.588	0.509	0.88	52.18	7.9	90.4	98.3	0.120	0.014	0.004	0.004
R6A-504/531	824	0.16	0.21	2.03	215	5.00	50.00	0.952	0.515	0.392	0.81	53.47	7.5	67.9	75.3	0.261	0.023	0.023	0.023
R7D-088/114	1007	0.18	0.17	1.69	195	5.00	50.00	0.875	0.559	0.592	0.64	55.33	6.1	35.1	41.2	0.194	0.008	0.003	0.003
R9C-080/107	879	0.15	0.19	1.87	235	5.00	50.00	0.973	0.586	0.463	0.46	54.67	4.3	46.1	50.4	0.267	0.011	0.005	0.005
R9D-082/109	816	0.15	0.17	1.69	84	5.00	50.00	0.875	0.544	0.480	0.41	53.72	3.8	62.9	66.7	0.103	0.006	0.002	0.002

Below Level Ice, $\dot{\epsilon} = 10^{-3}$/s, T = −5°C (23°F)

Sample no.	1 σ_m (psi)	2 ϵ_m (GL) (%)	3 ϵ_m (FS) (%)	4 t_m (s)	5 σ_e (psi)	6 ϵ_e (FS) (%)	7 t_e (s)	8 E_i (GL) (10^6 psi)	9 E_0 (GL) (10^6 psi)	10 E_0 (FS) (10^6 psi)	11 S_i (‰)	12 ϱ (lb/ft³)	13 V_b (‰)	14 V_a (‰)	15 n (‰)	16 σ_e/σ_m	17 ISQ (in.)	18 ESQ (in.)	19 SHM (in.)
R2D-220/247	760	0.12	0.14	1.49	760	0.14	1.49	0.900	0.633	0.543	0.37	54.65	3.5	46.7	50.1		0.005	0.003	0.003
R2D-334/371	732	0.13	0.16	1.70	115	5.00	50.00	0.842	0.563	0.458	1.90	54.58	17.9	50.3	68.1	0.157	0.003	0.004	0.004
R4C-414/441	716	0.16	0.16	1.62	191	5.00	50.00	0.905	0.448	0.448	3.03	56.76	29.7	14.1	43.7	0.267	0.005	0.002	0.002
R4C-512/539	816	0.13	0.15	1.54	60	5.00	50.00	0.930	0.628	0.544	1.03	55.85	9.9	26.6	36.6	0.074	0.005	0.012	0.012
R4D-495/522	617	0.11	0.16	1.57	119	0.34	33.60	1.030	0.561	0.386	2.92	57.16	28.8	6.9	35.7		0.006	0.008	0.008
R6C-476/503	852	0.17	0.19	1.87	151	5.00	50.00	0.834	0.501	0.448	0.93	54.44	8.7	51.2	59.9	0.177	0.003	0.008	0.010
R7C-143/170	1015	0.16	0.23	2.23	251	5.00	50.00	0.962	0.634	0.441	0.77	56.27	7.5	18.9	26.4	0.247	0.005	0.002	0.002
R7C-541/568	975	0.17	0.16	1.55	151	5.00	50.00	0.951	0.574	0.609	1.15	56.75	11.3	11.2	22.5	0.155	0.003	0.001	0.001
R7D-223/250	923	0.20	0.24	2.41	207	5.00	50.00	0.875	0.462	0.385	2.04	55.49	19.5	34.5	54.0	0.224	0.007	0.008	0.008
R7D-312/339	963	0.17	0.18	1.76	211	5.00	50.00	0.907	0.567	0.535	1.12	54.82	10.6	44.7	55.3	0.219	0.004	0.006	0.006
R9A-445/482	637	0.13	0.19	1.85	66	5.00	50.00	0.814	0.490	0.335	1.05	54.01	9.8	58.8	68.6	0.104	0.013	0.006	0.006
R9B-329/356	804	0.09	0.10	1.06	804	0.10	1.06	1.000	0.893	0.804	0.78	55.00	7.4	41.0	48.4		0.004	0.004	0.004
R9C-332/359	676	0.14	0.21	2.06	123	5.00	50.00	0.875	0.483	0.322	0.83	54.98	7.9	41.5	49.3	0.182	0.012	0.001	0.001
R9D-249/276	728	0.14	0.18	1.82	76	5.00	50.00	0.921	0.520	0.404	0.96	53.81	8.9	62.2	71.1	0.104	0.003	0.000	0.000
R10A-269/296	971	0.18	0.18	1.84	275	5.00	50.00	0.984	0.539	0.539	0.81	56.39	7.9	16.9	24.8	0.283	0.004	0.006	0.006
R10B-274/301	955	0.17	0.18	1.81	247	5.00	50.00	1.060	0.562	0.531	1.09	56.44	10.6	16.5	27.1	0.259	0.004	0.003	0.003

Sample no.	1 σ_m (psi)	2 ϵ_m (GL) (%)	3 ϵ_m (FS) (%)	4 t_m (s)	5 σ_e (psi)	6 ϵ_e (FS) (%)	7 t_e (s)	8 E_i (GL) (10^6 psi)	9 E_0 (GL) (10^6 psi)	10 E_0 (FS) (10^6 psi)	11 S_i (‰)	12 ϱ (lb/ft³)	13 V_b (%)	14 V_a (%)	15 n (%)	16 σ_e/σ_m	17 ISQ (in.)	18 ESQ (in.)	19 SHM (in.)
R10C-445/472	828	0.11	0.13	1.30	828	0.13	1.30	1.190	0.753	0.637	1.99	56.71	19.5	13.2	32.7		0.008	0.003	0.005
R10D-231/258	903	0.17	0.18	1.77	131	5.00	50.00	0.936	0.531	0.502	1.03	56.61	10.1	13.4	23.5	0.145	0.002	0.003	0.003
R1A-300/326	1580	0.12	0.14	1.38	1580	0.14	1.38	1.430	1.320	1.130	1.00	56.77	9.8	10.5	20.3		0.017	0.006	0.002
R1B-216/241	915	0.12	0.17	1.70	195	5.00	50.00	1.250	0.763	0.538	1.20	57.14	11.8	4.4	16.3	0.213	0.006	0.001	0.000
R1B-243/268	1050	0.15	0.14	1.40	143	5.00	50.00	1.250	0.700	0.750	1.56	57.14	15.4	5.0	20.4	0.136	0.010	0.003	0.000
R2A-285/310	1270	0.16	0.22	2.20	95	5.00	50.00	1.180	0.794	0.577	0.70	56.46	6.8	15.5	22.3	0.075	0.020	0.003	0.002
R2A-383/408	1060	0.11	0.11	1.10	1060	0.11	1.10	1.300	0.964	0.964	2.00	56.81	19.6	11.5	31.1		0.005	0.010	0.016
R2B-351/377	1130	0.14	0.13	1.26	1130	0.13	1.26	1.150	0.807	0.869	2.46	56.37	23.9	19.8	43.8		0.012	0.016	0.016
R2B-438/464	995	0.14	0.18	1.80	149	5.00	50.00	1.020	0.711	0.553	2.70	56.48	26.3	18.3	44.6	0.150	0.012	0.009	0.009
R3A-348/373											1.90	57.08	18.7	6.6	25.3				
R3A-401/427	925	0.16	0.15	1.52	164	5.00	50.00	1.050	0.578	0.617	1.45	57.03	14.3	6.8	21.0	0.177	0.010	0.008	0.004
R3B-239/265	870	0.16	0.16	1.60	255	5.00	50.00	0.997	0.544	0.544	2.00	57.13	19.7	5.9	25.6	0.293	0.011	0.004	0.000
R3B-331/357	971	0.16	0.18	1.75	211	5.00	50.00	1.050	0.607	0.539	2.00	56.79	19.6	11.8	31.4	0.217	0.009	0.005	0.002
R4A-398/423	786	0.14	0.21	2.10	144	5.00	50.00	0.997	0.561	0.374	1.30	56.03	12.6	23.2	36.5	0.183	0.017	0.006	0.004
R4B-358/384	776	0.12	0.17	1.68	99	5.00	50.00	0.892	0.647	0.456	1.96	56.00	18.9	25.5	44.4	0.128	0.011	0.003	0.002
R4B-420/446	910	0.15	0.19	1.85	910	0.19	1.85	1.060	0.607	0.479	3.30	56.39	32.2	20.8	53.0		0.014	0.004	0.004
R5A-473/499	875	0.14	0.17	1.68	169	5.00	50.00	0.949	0.625	0.515	0.91	55.75	8.8	28.3	37.1	0.193	0.005	0.006	0.006

Below Level Ice, $\dot{\epsilon} = 10^{-3}$/s, T = −5°C (23°) (cont'd)

Sample no.	1 σ_m (psi)	2 ϵ_m (GL) (%)	3 ϵ_m (FS) (%)	4 t_m (s)	5 σ_e (psi)	6 ϵ_e (FS) (%)	7 t_e (s)	8 E_i (GL) (10^6 psi)	9 E_0 (GL) (10^6 psi)	10 E_0 (FS) (10^6 psi)	11 S_i (‰)	12 ϱ (lb/ft³)	13 V_b (‰)	14 V_a (‰)	15 n (‰)	16 σ_e/σ_m	17 ISQ (in.)	18 ESQ (in.)	19 SHM (in.)
R5B-287/313	1040	0.10	0.10	1.05	1040	0.10	1.05	1.310	1.040	1.040	4.00	56.96	39.4	12.1	51.4		0.007	0.010	0.004
R5B-370/396	816	0.12	0.14	1.40	149	5.00	50.00	0.989	0.683	0.583	1.26	55.09	12.0	40.4	52.3	0.183	0.017	0.004	0.000
R7A-232/258	736	0.12	0.18	1.83	134	5.00	50.00	0.908	0.613	0.409	3.40	49.76	29.2	136.1	165.3	0.182	0.003	0.007	0.008
R7A-295/321	612	0.11	0.21	2.08	607	0.23	2.33	0.900	0.556	0.291	0.95	54.09	8.9	57.3	66.1		0.005	0.010	0.010
R7B-175/201	557	0.06	0.04	0.43	557	0.04	0.43	0.876	0.928	1.390	0.13	56.03	1.3	22.0	23.3		0.010	0.013	0.012
R7B-440/466	1540	0.17	0.23	2.30	1540	0.23	2.30	1.250	0.906	0.670	2.48	57.08	24.4	7.6	32.0		0.003	0.003	0.002
R8A-305/331	589	0.11	0.11	1.05	243	5.00	50.00	0.728	0.535	0.535	1.50	56.70	14.7	12.6	27.2	0.413	0.008	0.007	0.006
R8A-384/410	1297	0.15	0.17	1.69	1297	0.17	1.69	1.270	0.865	0.763	1.70	57.01	16.7	7.5	24.2		0.004	0.005	0.002
R8B-300/326	587	0.17	0.29	2.93	247	5.00	50.00	1.170	0.345	0.202	0.30	56.61	2.9	12.2	15.1	0.421	0.006	0.004	0.004
R8B-483/509	1440	0.20	0.38	3.78	1440	0.38	3.78	1.140	0.720	0.379	2.10	57.20	20.7	4.9	25.6		0.009	0.005	0.004
R2C-196/223	844	0.15	0.14	1.40	159	5.00	50.00	0.899	0.563	0.603	1.04	55.35	9.9	35.4	45.3	0.188	0.022	0.015	0.013
R2C-278/305	674	0.14	0.19	1.93	230	5.00	50.00		0.481	0.355	2.33	54.66	22.0	49.5	71.5	0.341	0.008	0.006	0.006

Above Level Ice, $\dot{\epsilon} = 10^{-3}$/s, T = −20°C (−4°F)

Sample no.	1 σ_m (psi)	2 ϵ_m (GL) (%)	3 ϵ_m (FS) (%)	4 t_m (s)	5 σ_e (psi)	6 ϵ_e (FS) (%)	7 t_e (s)	8 E_i (GL) (10^6 psi)	9 E_0 (GL) (10^6 psi)	10 E_0 (FS) (10^6 psi)	11 S_i (‰)	12 ϱ (lb/ft³)	13 V_b (‰)	14 V_a (‰)	15 n (‰)	16 σ_e/σ_m	17 ISQ (in.)	18 ESQ (in.)	19 SHM (in.)
R1C-127/154	1520	0.15	0.17	1.66	1520	0.17	1.66	1.400	1.010	0.894	0.31	56.08	1.0	22.8	23.8		0.010	0.004	0.000
R1D-153/178	1270	0.10	0.08	0.84	1270	0.08	0.84	1.520	1.270	1.590	1.00	56.20	3.3	22.1	25.4		0.010	0.006	0.004
R2C-129/156	1580	0.18	0.23	2.45	1580	0.23	2.45	0.709	0.878	0.687	0.63	54.62	2.0	50.5	52.5		0.007	0.015	0.010
R2D-095/122	1230	0 17	0.14	1.54	1230	0.14	1.54	0.951	0.724	0.879	0.20	53.22	0.6	73.3	73.9		0.021	0.009	0.007
R4D-198/225	1140	0.11	0.13	1.30	1140	0.13	1.30		1.036	0.877	2.31	54.72	7.4	49.2	56.5		0.010	0.013	0.013
R6A-531/558	1200	0.20	0.18	1.75	203	5.00	50.00	0.957	0.600	0.667	1.22	54.37	3.9	54.2	58.1	0.169	0.024	0.009	0.009
R6C-134/161	1320	0.18	0.17	1.74	1320	0.17	1.74	0.973	0.733	0.777	0.29	52.48	0.9	86.2	87.1		0.002	0.004	0.004
R7C-092/119	1760	0.05	0.28	2.60	589	1.62	16.50	1.090	3.520	0.629	0.82	55.89	2.7	27.4	30.1		0.007	0.004	0.004
R7D-036/063	1720	0.23	0.24	2.45	1720	0.24	2.45	1.090	0.748	0.717	0.19	55.16	0.6	39.5	40.1		0.002	0.007	0.007
R9A-071/098	1237	0.20	0.23	2.35	231	2.61	2.64	0.941	0.619	0.538	0.04	50.93	0.1	113.0	113.1		0.005	0.005	0.005
R9B-076/103	1110	0.20	0.25	2.45	52	5.00	50.00	1.000	0.555	0.444	0.03	50.68	0.1	117.4	117.4	0.047	0.014	0.010	0.010
R9C-049/076	1480	0.23	0.27	2.76	243	5.00	50.00	1.170	0.644	0.548	0.38	54.81	1.2	45.8	47.0	0.164	0.009	0.003	0.003
R9D-150/177	1530	0.25	0.24	2.55	207	5.00	50.00	1.090	0.612	0.638	1.22	55.68	4.0	31.4	35.4	0.135	0.008	0.008	0.008
R10A-238/265	1838	0.22	0.34	3.33	1739	0.44	4.35	1.270	0.836	0.541	0.81	56.58	2.7	15.4	18.0		0.003	0.004	0.004
R10B-084/111	1510	0.21	0.21	2.28	171	5.00	50.00	1.170	0.719	0.719	0.61	56.33	2.0	19.5	21.5	0.113	0.009	0.004	0.004

Below Level Ice, $\dot{\epsilon} = 10^{-3}$/s, T = −20°C (−4°F)

Sample no.	1 σ_m (psi)	2 ϵ_m (GL) (%)	3 ϵ_m (FS) (%)	4 t_m (s)	5 σ_e (psi)	6 ϵ_e (FS) (%)	7 t_e (s)	8 E_i (GL) (10^6 psi)	9 E_0 (GL) (10^6 psi)	10 E_0 (FS) (10^6 psi)	11 S_i (‰)	12 ϱ (lb/ft³)	13 V_b (‰)	14 V_a (‰)	15 n (‰)	16 σ_e/σ_m	17 ISQ (in.)	18 ESQ (in.)	19 SHM (in.)
R1C-349/375	1440	0.19	0.18	1.80	1440	0.18	1.80	1.310	0.758	0.800	3.42	56.71	11.3	15.6	27.0		0.004	0.008	0.006
R1C-384/410	1020	0.11	0.10	1.02	1020	0.10	1.02	1.100	0.927	1.020	1.94	54.65	6.2	50.0	56.2		0.006	0.005	0.002
R1D-179/206	1640	0.14	0.18	1.84	1640	0.18	1.84	1.450	1.200	0.911	1.03	56.63	3.4	14.7	18.1		0.012	0.011	0.008
R1D-285/312	1650	0.11			1650			1.570	1.500		2.48	57.29	8.3	4.6	12.9		0.006	0.004	0.000
R2C-226/253	1480	0.20	0.26	2.64	199	5.00	50.00	1.080	0.740	0.569	0.89	54.80	2.8	46.4	49.3	0.080	0.020	0.012	0.010
R2C-310/337	1070	0.20	0.33	3.36	466	1.70	17.60	0.904	0.535	0.324	2.63	55.15	8.5	42.0	50.5		0.010	0.000	0.007
R2D-265/292	1410	0.17	0.23	2.28	1410	0.23	2.28	1.030	0.829	0.613	3.01	55.25	9.7	40.6	50.3		0.008	0.004	0.005
R2D-406/433	1100	0.20	0.26	2.72	111	5.00	50.00	0.933	0.550	0.423	1.61	55.13	5.2	41.4	46.5	0.101	0.011	0.010	
R4C-482/509	1420	0.22	0.24	2.40	279	5.00	50.00	1.070	0.646	0.592	1.28	55.92	4.2	27.3	31.5	0.197	0.005	0.008	0.008
R4C-543/570	1400	0.21	0.28	2.84	179	4.22	42.20	1.090	0.667	0.500	1.87	56.16	6.1	23.7	29.8		0.004	0.002	0.002
R4D-382/409	1430	0.22	0.29	2.92	243	5.00	50.00	1.080	0.650	0.493	1.15	56.45	3.8	18.0	21.8	0.170	0.010	0.010	0.010
R4D-414/441	1310	0.16	0.15	1.48	1310	0.15	1.48	1.030	0.819	0.873	0.90	55.25	2.9	38.6	41.5		0.004	0.005	0.005
R4D-525/552	1300	0.20	0.27	2.70	1300	0.27	2.70	1.050	0.650	0.482	0.88	56.19	2.9	22.2	25.1		0.002	0.003	0.003
R6C-559/586	1440	0.24	0.26	2.60	226	5.00	50.00	0.995	0.600	0.554	1.70	55.92	5.6	27.7	33.3	0.157	0.025	0.004	0.004
R7C-457/484	1650	0.24	0.32	3.17	123	5.00	50.00	1.170	0.688	0.516	1.32	57.04	4.4	7.9	12.3	0.746	0.004	0.007	0.010
R7C-572/599	1760	0.23	0.29	2.85	1760	0.29	2.85	1.210	0.765	0.607	1.33	56.73	4.4	13.3	17.7		0.006	0.001	0.001

Sample no	1 σ_m (psi)	2 ϵ_m (GL) (%)	3 ϵ_m (FS) (%)	4 t_m (s)	5 σ_e (psi)	6 ϵ_e (FS) (%)	7 t_e (s)	8 E_i (GL) (10^6 psi)	9 E_0 (GL) (10^6 psi)	10 E_0 (FS) (10^6 psi)	11 S_i (%)	12 ϱ (lb/ft^3)	13 V_b (%)	14 V_a (%)	15 n (%)	16 σ_e/σ_m	17 ISQ (in.)	18 ESQ (in.)	19 SHM (in.)
R7D-254/281	1310	0.23	0.32	3.14	362	5.00	50.00	1.000	0.570	0.409	1.21	55.62	3.9	32.5	36.4	0.276	0.008	0.008	0.008
R7D-546/573	1480	0.23	0.26	2.70	243	5.00	50.00	0.889	0.644	0.569	1.09	56.72	3.6	13.2	16.8	0.164	0.005	0.006	0.006
R9A-424/451	1120	0 16	0.17	1.68	1120	0 16	1.68	0.898	0.700	0.659	0.68	54.00	2.1	60.1	62.3		0.010	0.004	0.004
R9B-417/444	1400	0.20	0.26	2.70	1400	0.26	2.70	0.973	0.700	0.539	0.62	54.37	2.0	53.6	55.6		0.002	0.002	0.002
R9C-507/534	1340	0.21	0.21	2.16	283	5.00	50.00	1.170	0.638	0.638	1.86	56.77	6.2	13.1	19.3	0.211	0.005	0.009	0.009
R9D-348/375	1150	0.13	0.15	1.52	1150	0.15	1.52	1.150	0.885	0.767	1.14	55.39	3.7	36.4	40.1		0.010	0.008	0.008
R10A-407/434	1480	0.21	0.28	2.87	362	5.00	50.00	1.180	0.705	0.529	0.22	56.68	0.7	13.0	13.8	0.245	0.005	0.010	0.010
R10B-449/476	1470	0.17	0.25	2.53	279	5.00	50.00	1.230	0.865	0.588	0.36	56.70	1.2	12.8	14.0	0.190	0.006	0.007	0.007
R10C-506/533	1230	0.20	0.25	2.53	223	5.00	50.00	1.160	0.615	0.492	3.65	57.02	12.2	10.5	22.7	0.181	0.012	0.003	0.003
R10D-508/535	1310	0.19	0.22	2.26	203	5.00	50.00	1.140	0.690	0.596	2.35	57.00	7.8	9.6	17.4	0.155	0.013	0.006	0.006

Above Level Ice, $\dot{\epsilon} = 10^{-5}$/s, T = −5°C (23°F)

Sample no.	1 σ_m (psi)	2 ϵ_m (GL) (%)	3 ϵ_m (FS) (%)	4 t_m (s)	5 σ_e (psi)	6 ϵ_e (FS) (%)	7 t_e (s)	8 E_i (GL) (10^6 psi)	9 E_0 (GL) (10^6 psi)	10 E_0 (FS) (10^6 psi)	11 S_i (‰)	12 ϱ (lb/ft³)	13 V_b (‰)	14 V_a (‰)	15 n (‰)	16 σ_e/σ_m	17 ISQ (in.)	18 ESQ (in.)	19 HM (in.)
R1A-062/089	443	0.31	0.34	344.0	234	5.00	5000		0.143	0.130	1.80	55.05	17.1	41.9	59.0	0.528	0.080	0.028	
R1B-062/089	328	0.11	0.37	365.0	214	5.00	5000	0.973	0.298	0.089	0.30	54.54	2.8	48.4	51.3	0.652	0.022	0.044	0.038
R2A-140/165	388	0.66	0.68	683.0	254	5.00	5000	0.804	0.059	0.057	0.10	56.77	1.0	9.1	10.1	0.655	0.010	0.007	0.006
R2B-094/121	171	0.11	0.16	156.0	176	5.00	5000	0.563	0.155	0.107	0.44	49.35	3.7	139.2	143.0	1.029	0.005	0.004	0.004
R3A-106/131	342	0.46	0.86	855.0	251	5.00	5000	0.654	0.074	0.040	0.60	55.61	5.8	30.1	35.9	0.734	0.007	0.006	0.006
R3B-161/187	308	0.36	0.36	360.0	207	5.00	5000	0.598	0.086	0.086	1.13	56.92	11.1	8.1	19.2	0.672	0.010	0.007	0.006
R4A-312/338	283	0.47	0.47	465.0	193	5.00	5000	0.703	0.060	0.060	1.60	53.92	14.9	61.2	76.1	0.682	0.006	0.019	0.018
R4B-328/354	253	0.40	0.62	615.0	166	5.00	5000	0.411	0.063	0.041	1.57	56.11	15.2	22.9	38.1	0.656	0.011	0.003	0.010
R5A-165/191	619	0.24	0.22	217.0	274	5.00	5000	1.500	0.258	0.281	0.41	56.58	4.0	12.9	16.9	0.443	0.007	0.003	0.002
R5B-075/101	774	0.19	0.20	201.0	246	5.00	5000	1.180	0.407	0.387	1.80	54.26	16.9	55.5	72.3	0.318	0.006	0.001	0.000
R7A-059/085	361	0.47	0.59	588.0	253	5.00	5000	0.804	0.077	0.061	1.70	54.37	15.9	53.6	69.5	0.701	0.003	0.001	0.000
R7B-126/152	240	0.49	0.47	468.0	207	5.00	5000	0.603	0.049	0.051	0.40	51.90	3.6	94.6	98.2	0.863	0.014	0.002	
R8A-133/159	245	0.34	0.33	333.0	208	5.00	5000	0.675	0.072	0.074	1.00	55.95	9.7	24.8	34.5	0.849	0.003	0.002	0.002
R8B-162/189	336	0.37	0.47	473.0	235	5.00	5000	0.560	0.091	0.071	0.82	56.36	8.0	17.4	25.4	0.699	0.006	0.005	0.004
R3C-095/122	268	0.40	0.47	472.0	205	5.00	5000	0.524	0.067	0.057	0.54	54.87	5.1	42.9	48.0	0.765	0.004	0.008	0.008
R3D-159/186	201	0.75	0.72	700.0	201	5.00	5000	0.578	0.027	0.028	0.26	49.39	2.2	138.2	140.5		0.010	0.005	0.005

Sample no.	1 σ_m (psi)	2 ϵ_m (GL) (%)	3 ϵ_m (FS) (%)	4 t_m (s)	5 σ_e (psi)	6 ϵ_e (FS) (%)	7 t_e (s)	8 E_i (GL) (10^6 psi)	9 E_0 (GL) (10^6 psi)	10 E_0 (FS) (10^6 psi)	11 S_i (%)	12 ϱ (lb/ft^3)	13 V_b (%)	14 V_a (%)	15 n (%)	16 σ_e/σ_m	17 ISQ (in.)	18 ESQ (in.)	19 SHM (in.)
R5C-039/066	376	0.47	0.39	416.0	255	5.00	5000	0.875	0.080	0.096	1.27	53.10	11.6	75.0	86.6	0.678	0.006	0.003	0.003
R5D-159/186	384	0.56	0.67	690.0	256	5.00	5000	0.438	0.069	0.057	0.58	56.15	5.6	20.7	26.3	0.667	0.013	0.006	0.006
R6C-166/193	210	0.28	0.31	300.0	223	5.00	5000	0.661	0.075	0.068	0.45	50.74	3.9	114.8	118.8	1.062	0.010	0.006	0.006
R8C-048/075	239	0.31	0.28	278.0	180	5.00	5000	0.637	0.077	0.085	0 56	54.28	5.2	53.4	58.6	0.753	0.008	0.004	0.004
R8D-236/263	331	0.16	0.25	248.0	266	5.00	5000	0.910	0.207	0.132	0.50	54.74	4.7	45.1	49.8	0.804	0.005	0.003	0.003
R10C-063/090	306	0.47	0.43	444.0	236	5.00	5000	0.778	0.065	0.071	0.84	56.25	8.2	19.4	27.5	0.771	0.008	0.002	0.002
R10D-126/153	301	0.50	0.45	484.0	215	5.00	5000	0.770	0.060	0.669	0.83	55.63	8.0	30.2	38.1	0.714	0.007	0.003	0.004

Below Level Ice, $\dot{\epsilon} = 10^{-5}$/s, T = −5°C (23°F)

Sample no	1 σ_m (psi)	2 ϵ_m (GL) (%)	3 ϵ_m (FS) (%)	4 t_m (s)	5 σ_e (psi)	6 ϵ_e (FS) (%)	7 t_e (s)	8 E_i (GL) (10^6 psi)	9 E_0 (GL) (10^6 psi)	10 E_0 (FS) (10^6 psi)	11 S_i (‰)	12 ϱ (lb/ft³)	13 V_b (‰)	14 V_a (‰)	15 n (‰)	16 σ_e/σ_m	17 ISQ (in.)	18 ESQ (in.)	19 SHM (in.)
R1A-226/252	214	0.21	0.17	173.0	124	5.00	5000	0.916	0.101	0.126	1 26	57.00	12.4	7.0	19.4	0.579	0.061	0.035	0.032
R1A-399/425	214	0.29	0.25	248.0	149	5.00	5000	0.751	0.074	0.086	2.40	56.62	23.4	15.4	38.9	0.696	0.007	0.014	0.012
R1B-320/346	1090	0.30	0.25	253.0	189	5.00	5000	1.010	0.363	0.044	1.90	57.08	18.7	6.6	25.3	0.173	0.015	0.005	0.004
R1B-429/455	650	0.27	0.29	285.0	269	5.00	5000	1.150	0.258	0.240	1.80	57.11	17.7	5.9	23.7	0.386	0.004	0.008	0.008
R2A-205/230	443	0.39	0.49	489.0	243	2.98	2975	0.892	0.114	0.090	0 38	55.32	3.6	35.0	38.6		0.021	0.015	0.012
R2A-314/339	308	0.25	0.28	278.0	161	5.00	5000	0.667	0.123	0.110	2.10	56.79	20.6	12.0	32.5	0.523	0.018	0.004	0.004
R2B-408/434	342	0.57	0.60	597.0	261	5.00	5000	0.662	0.060	0.057	0.80	55.82	7.7	26.9	34.6	0.763	0.009	0.005	0.004
R2B-468/494	265	0.42	0.39	390.0	199	5.00	5000	1.070	0.063	0.068	0.70	55.91	6.8	25.2	32.0	0.751	0.006	0.007	0.006
R3A-220/245	253	0.27	0.39	387.0	185	5.00	5000	0.350	0.094	0.065	1.61	57.06	15.8	6.5	22.3	0.731	0.006	0.005	0.004
R3A-430/456	306	0.41	0.53	525.0	215	5.00	5000	0.782	0.075	0.058	2.18	56.21	21.1	22.2	43.3	0 703	0.009	0.017	0.012
R3B-363/389	394	0.51	0.51	507.0	259	5.00	5000	0.787	0.077	0.077	0.89	56.99	8.7	6.5	15.3	0.657	0.010	0.002	0.002
R4A-426/452	322	0.27	0.33	330.0	183	5.00	5000	0.782	0.119	0.098	1.30	55.79	12.5	28.2	40.8	0.568	0.014	0.005	0.000
R4B-391/417	290	0.30	0.31	308.0	185	5.00	5000	0.751	0.097	0.093	2.27	56.42	22.1	18.7	40.8	0.638	0.007	0.004	0.004
R4B-449/475	243	0.42	0.37	368.0	175	5.00	5000	0.521	0.058	0.066	1.83	56.51	17.8	16.4	34.2	0.720	0.004	0.001	0.000
R5A-397/423	314	0.36	0.56	558.0	227	5.00	5000	0.420	0.087	0 056	0.80	56.44	7.8	16.0	23.8	0.723	0.012	0.007	0.006
R5A-442/468	462	0.29	0.28	279.0	218	5.00	5000	1.000	0.159	0.165	1.09	56.73	10.7	11.4	22.1	0.472	0.007	0.012	0.012

Sample no.	1 σ_m (psi)	2 ϵ_m (GL) (%)	3 ϵ_m (FS) (%)	4 t_m (s)	5 σ_e (psi)	6 ϵ_e (FS) (%)	7 t_e (s)	8 E_i (GL) (10^6 psi)	9 E_0 (GL) (10^6 psi)	10 E_0 (FS) (10^6 psi)	11 S_i (%)	12 ϱ (lb/ft^3)	13 V_b (%)	14 V_a (%)	15 n (%)	16 σ_e/σ_m	17 ISQ (in.)	18 ESQ (in.)	19 SHM (in.)
R5A-504/530	327	0.45	0.56	555.0	227	5.00	5000	0.395	0.073	0.058	1.23	56.47	12.0	16.1	28.1	0.694	0.008	0.008	0.008
R5B-341/367	368	0.61	0.61	608.0	264	5.00	5000	0.804	0.060	0.060	0.79	54.57	7.4	48.7	56.1	0.717	0.005	0.002	0.002
R5B-398/423	300	0.40	0.53	525.0	231	5.00	5000	0.609	0.075	0.057	1.13	56.37	11.0	17.7	28.7	0.770	0.011	0.007	0.006
R7A-263/289	68	0.06	0.10	96.00	61	5.00	5000	0.425	0.113	0.068	3.03	50.22	26.3	127.6	153.9	0.897	0.008	0.001	0.000
R3C-296/323	286	0.68	0.64	650.0	271	1.24	1250	0.549	0.042	0.447	1.62	55.91	15.6	26.5	42.2		0.009	0.009	0.009
R3C-380/407	189	0.11	0.19	188.0	131	5.00	5000	0.554	0.172	0.099	1.28	55.33	12.2	36.1	48.3	0.693	0.013	0.002	0.006
R3D-219/246	269	0.33	0.38	380.0	267	5.00	5000	0.628	0.081	0.071	1.28	53.43	11.8	69.3	81.1	0.993	0.004	0.001	0.001
R3D-287/314	334	0.62	0.68	710.0	250	5.00	5000	0.698	0.054	0.049	1.36	56.05	13.1	23.7	36.8	0.749	0.003	0.010	0.010
R5C-219/246	314	0.51	0.56	550.0	223	5.00	5000	0.467	0.062	0.056	1.29	55.67	12.4	30.2	42.6	0.710	0.020	0.003	0.003
R5C-282/30?	279	0.51	0.50	520.0	207	5.00	5000	0.504	0.055	0.056	3.64	56.14	35.3	25.8	61.0	0.742	0.014	0.000	0.000
R5D-225/252	382	0.45	0.50	480.0	245	5.00	5000	0.603	0.085	0.076	1.37	56.35	13.3	18.5	31.8	0.641	0.010	0.005	0.005
R5D-294/321	337	0.42	0.52	548.0	304	5.00	5000	1.090	0.080	0.065	1.73	56.72	16.9	12.7	29.6	0.902	0.008	0.001	0.001
R6A-562/589	223	0.59	0.54	538.0	172	5.00	5000	0.634	0.038	0.041	2.38	54.01	22.2	60.9	83.1	0.771	0.013	0.022	0.022
R6C-529/556	368	0.83	0.82	777.0	269	5.00	5000	0.834	0.044	0.045	0.86	56.14	8.3	21.3	29.7	0.731	0.006	0.004	0.004
R8C-378/405	762	0.17	0.24	245.0	218	5.00	5000	1.430	0.448	0.318	1.44	56.77	14.1	11.3	25.4	0.286	0.016	0.015	0.015
R8C-476/503	148	0.32	0.25	257.0	97	5.00	5000	0.648	0.046	0.059	1.86	57.20	18.4	4.5	22.9	0.655	0.006	0.008	0.008
R8D-446/[illegible]3	226	0.17	0.21	237.0	207	5.00	5000	0.654	0.133	0.108	1.95	56.62	19.0	14.7	33.8	0.916	0.005	0.005	0.005

Below Level Ice, $\dot{\epsilon} = 10^{-5}$/s, T = −5°C (23°F) (cont'd)

Sample no.	1 σ_m (psi)	2 ϵ_m (GL) (%)	3 ϵ_m (FS) (%)	4 t_m (s)	5 σ_e (psi)	6 ϵ_e (FS) (%)	7 t_e (s)	8 E_i (GL) (10^6 psi)	9 E_0 (GL) (10^6 psi)	10 E_0 (FS) (10^6 psi)	11 S_i (‰)	12 ϱ (lb/ft³)	13 V_b (‰)	14 V_a (‰)	15 n (‰)	16 σ_e/σ_m	17 ISQ (in.)	18 ESQ (in.)	19 SHM (in.)
R8D-534/561	240	0.22	0.21	210.0	124	5.00	5000	0.648	0.109	0.114	1.96	56.80	19.2	11.6	30.8	0.517	0.009	0.005	0.005
R9A-341/368	276	0.48	0.48	488.0	205	5.00	5000	0.700	0.057	0.057	0.65	53.71	6.0	63.5	69.5	0.743	0.004	0.003	0.003
R9B-385/412	287	0.77	0.72	704.0	232	5.00	5000	0.609	0.037	0.040	0.72	54.65	6.8	47.2	54.0	0.808	0.008	0.004	0.004
R9C-426/453	283	0.48	0.47	459.0	221	5.00	5000	0.737	0.059	0.060	1.08	56.31	10.5	18.7	29.2	0.781	0.007	0.006	0.006
R9D-181/208	255	0.29	0.29	291.0	209	5.00	5000	1.050	0.088	0.088	1.39	56.67	13.6	13.0	26.6	0.820	0.004	0.001	0.001
R10A-351/378	369	0.77	0.72	721.0	274	5.00	5000	0.722	0.048	0.051	0.27	56.75	2.6	9.8	12.4	0.743	0.004	0.001	0.001
R10B-351/378	331	0.37	0.43	439.0	242	5.00	5000	0.824	0.089	0.077	0.89	56.85	8.7	9.0	17.8	0.731	0.007	0.003	0.003
R7A-342/368	607	0.16	0.26	255 0	195	5.00	5000	0.908	0.379	0.233	1.05	56.57	10.2	14.1	24.4	0.321	0.009	0.004	0.004
R7B-241/267	229	0.34	0.47	465.0	163	5.00	5000	0.523	0.067	0.049	1.30	53.63	12.0	65.8	77.8	0.712	0.007	0.003	0.002
R7B-410/436											1.00	56.73	9.8	11.2	21.0		0.007	0.003	
R8A-164/190	261	0.11	0.29	285.0	175	5.00	5000	0.536	0.237	0.090	1.20	56.45	11.7	16.4	28.1	0.670	0.007	0.010	0.010
R8A-432/458	657	0.16	0.16	156.0	208	5.00	5000	1.070	0.411	0.411	1.80	57.06	17.7	6.8	24.5	0.317	0.004	0.007	0.006
R8B-333/359	344	0.25	0.25	248.0	209	5.00	5000	0.479	0.138	0.138	1.50	57.04	14.8	6.7	21.4	0.608	0.009	0.006	0.004
R8B-515/541	348	0.40				5.00	5000	0.592	0.088		1.80	57 10	17.7	6.1	23.8		0.008		0.004
R10C-316/343	272	0.29	0.30	309.0	204	5.00	5000	0.599	0.094	0.091	2.89	56.58	28.2	17.0	45.2	0.750	0.014	0.008	0.008
R10D-325/352	365	0.28	0.33	340.0	220	5.00	5000	0.693	0.130	0.111	1.61	56.56	15.7	15.2	30.9	0.603	0.004	0.002	0.006

Above Level Ice, $\dot{\epsilon} = 10^{-5}$/s, T = −20°C (−4°F)

Sample no.	1 σ_m (psi)	2 ϵ_m (GL) (%)	3 ϵ_m (FS) (%)	4 t_m (s)	5 σ_e (psi)	6 ϵ_e (FS) (%)	7 t_e (s)	8 E_i (GL) (10^6 psi)	9 E_0 (GL) (10^6 psi)	10 E_0 (FS) (10^6 psi)	11 S_i (‰)	12 ϱ (lb/ft³)	13 V_b (‰)	14 V_a (‰)	15 n (‰)	16 σ_e/σ_m	17 ISQ (in.)	18 ESQ (in.)	19 SHM (in.)
R1C-065/092	617	0.17	0.19	192.0	229	5.00	5000	1.520	0.363	0.325	0.27	55.94	0.9	25.9	26.8	0.371	0.007	0.008	0.006
R1D-071/098	612	0.22	0.22	219.0	193	5.00	5000	1.000	0.278	0.278	0.61	56.61	2.0	14.6	16.6	0.315	0.013	0.004	
R3C-128/155	436	0.35	0.35	341.0	310	5.00	5000	0.847	0.125	0.125	0.74	56.13	2.4	23.1	25.6	0.711	0.010	0.009	0.009
R3D-129/156	289	0.22	0.27	269.0	240	5.00	5000	0.682	0.131	0.107	0.14	49.65	0.4	135.4	135.8	0.830	0.005	0.003	0.003
R5C-097/124	368	0.26	0.36	373.0	280	3.80	3830	0.800	0.142	0.102	0.28	53.38	0.9	70.6	71.4		0.005	0.005	0.005
R5D-121/148	342	0.18	0.26	240.0	291	5.00	5000	1.050	0.190	0.132	0.53	55.91	1.7	26.7	28.5	0.851	0.005	0.005	0.005
R6A-461/488	330	0.27	0.28	278.0	299	5.00	5000	0.745	0.122	0.118	1.05	54.67	3.4	48.8	52.2	0.906	0.010	0.013	0.013
R8C-165/192	522	0.27	0.33	334.0	328	5.00	5000	1.080	0.193	0.158	0.88	54.44	2.8	52.7	55.5	0.628	0.005	0.006	0.008
R8D-192/219	476	0.22	0.25	253.0	301	5.00	5000	0.898	0.216	0.190	0.83	54.72	2.7	47.7	50.4	0.632	0.011	0.003	
R9A-125/152	361	0.43	0.45	449.0	350	5.00	5000	0.875	0.084	0.080	0.04	50.96	0.1	112.5	112.6	0.970	0.010	0.010	0.010
R9B-043/070	337	0.45	0.44	447.0	307	5.00	5000	0.875	0.075	0.077	0.02	51.65	0.1	100.4	100.5	0.911	0.014	0.004	0.004
R10A-195/222	330	0.22	0.26	264.0	236	5.00	5000	0.810	0.150	0.127	0.53	56.20	1.7	21.7	23.4	0.715	0.005	0.005	0.005
R10B-243/270	525	0.10	0.15	154.0	204	5.00	5000	1.120	0.525	0.350	1.35	56.55	4.5	16.4	20.9	0.389	0.010	0.007	0.007
R10C-032/059	484	0.73	0.69	696.0	396	5.00	5000	0.707	0.066	0.070	0.36	55.20	1.2	38.9	40.1	0.818	0.016	0.005	0.005
R10D-157/184	390	0.42	0.47	468.0	301	5.00	5000	0.928	0.093	0.083	0.69	56.76	2.3	12.1	14.4	0.772	0.010	0.002	0.002

Below Level Ice, $\dot{\epsilon} = 10^{-5}$/s, T = −20°C (−4°F)

Sample no.	1 σ_m (psi)	2 ϵ_m (GL) (%)	3 ϵ_m (FS) (%)	4 t_m (s)	5 σ_e (psi)	6 ϵ_e (FS) (%)	7 t_e (s)	8 E_i (GL) (10^6 psi)	9 E_0 (GL) (10^6 psi)	10 E_0 (FS) (10^6 psi)	11 S_i (‰)	12 ϱ (lb/ft³)	13 V_b (‰)	14 V_a (‰)	15 n (‰)	16 σ_e/σ_m	17 ISQ (in.)	18 ESQ (in.)	19 SHM (in.)
R1C-210/236	403	0.22	0.28	282.0	239	5.00	5000	0.769	0.183	0.144	1.10	55.40	3.6	36.1	39.7	0.593	0.003	0.005	0.006
R1C-240/266	443	0.25	0.25	246.0	247	5.00	5000	0.989	0.177	0.177	1.55	55.88	5.1	28.2	33.3	0.558	0.013	0.014	
R1D-209/236	557	0.17	0.28	282.0	254	5.00	5000	0.876	0.328	0.199	0.99	56.01	3.2	25.4	28.6	0.456	0.015	0.010	0.010
R1D-315/342	264	0.22	0.29	285.0	181	5.00	5000	0.712	0.120	0.091	2.21	56.53	7.3	17.6	24.9	0.686	0.008	0.010	0.001
R3C-329/359	433	0.43	0.45	466.0	290	5.00	5000	1.030	0.101	0.096	1.69	55.94	5.5	27.4	32.9	0.670	0.004	0.008	0.008
R3C-411/438	170	0.23	0.25	250.0	116	5.00	5000	0.732	0.074	0.068	1.36	56.55	4.5	16.4	20.9	0.682	0.015	0.004	0.004
R3D-250/277	447	0.27	0.34	350.0	318	5.00	5000	0.854	0.166	0.132	1.59	55.85	5.2	28.8	34.0	0.711	0.006	0.011	0.010
R3D-318/345	468	0.49	0.55	547.0	334	5.00	5000	0.942	0.095	0.085	1.45	56.60	4.8	15.6	20.4	0.714	0.008	0.009	0.010
R5C-250/277	495	0.38	0.40	395.0	286	1.90	1870	0.648	0.130	0.124	1.55	56.55	5.1	16.6	21.7		0.004	0.003	0.003
R5C-328/355	401	0.30	0.30	340.0	223	5.00	5000	0.834	0.134	0.134	3.88	57.00	12.9	11.1	24.0	0.556	0.004	0.010	0.010
R5D-255/282	400	0.44	0.47	490.0	298	5.00	5000	0.700	0.091	0.085	1.69	56.22	5.5	22.5	28.5	0.745	0.010	0.005	0.002
R5D-325/352	474	0.39	0.41	440.0	301	5.00	5000	0.850	0.122	0.116	1.44	56.83	4.8	11.6	16.4	0.635	0.008	0.005	0.005
R6A-661/688	269	0.28	0.26	263.0	207	1.49	1475	0.673	0.096	0.104	2 83	54.39	9.0	55.4	64.4		0.009	0.006	
R6C-589/616	395	0.28	0.28	288.0	255	2.23	2220	0.886	0.141	0.141	1.63	56.52	5.4	12.0	17.4		0.005	0.000	0.000
R8C-444/471	400	0.28	0.29	290.0	202	2.68	2700	0.921	0.143	0.138	1.48	56.56	4.9	16.4	21.3		0.011	0.004	0.004
R8C-508/535	253	0.20	0.20	202.0	110	5.00	5000	0.500	0.127	0.127	2.61	56.84	8.7	12.6	21.3	0.435	0.003	0.006	0.006

AD-A144 132 MECHANICAL PROPERTIES OF MULTI-YEAR SEA ICE PHASE I TEST RESULTS(U) COLD REGIONS RESEARCH AND ENGINEERING LAB HANOVER NH G F COX ET AL. APR 84 CRREL-84-9 2/2

UNCLASSIFIED F/G 8/12 NL

END
DATE FILMED
9 84
DTIC

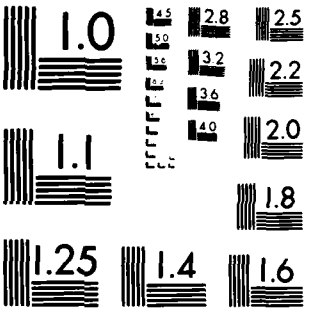

MICROCOPY RESOLUTION TEST CHART
NATIONAL BUREAU OF STANDARDS-1963 A

Sample no.	1 σ_m (psi)	2 ϵ_m (GL) (%)	3 ϵ_m (FS) (%)	4 t_m (s)	5 σ_e (psi)	6 ϵ_e (FS) (%)	7 t_e (s)	8 E_i (GL) (10^6 psi)	9 E_0 (GL) (10^6 psi)	10 E_0 (FS) (10^6 psi)	11 S_i (%)	12 ϱ (lb/ft³)	13 V_b (%)	14 V_a (%)	15 n (%)	16 σ_e/σ_m	17 ISQ (in.)	18 ESQ (in.)	19 SHM (in.)
R8D-477/504	188	0.32	0.40	367.0	135	5.00	5000	0.574	0.059	0.047	1.95	57.10	6.5	7.4	14.0	0.718	0.007	0.009	0.009
R8D-565/592	396	0.23	0.24	254.0	143	5.00	5000	0.824	0.172	0.165	1.45	56.81	4.8	12.0	16.8	0.361	0.011	0.007	0.007
R9A-523/550	411	0.12	0.16	161.0	237	5.00	5000	0.921	0.343	0.257	0.81	55.83	2.6	28.4	31.1	0.577	0.013	0.008	0.008
R9B-449/476	293	0.32	0.30	308.0	209	5.00	5000	0.770	0.092	0.098	1.57	55.09	5.1	42.0	47.1	0.713	0.009	0.006	0.006
R9C-395/422	411	0.34	0.37	363.0	263	5.00	5000		0.121	0.111	1.09	55.77	3.6	29.7	33.3	0.640	0.002	0.001	0.001
R9D-317/344	377	0.63	0.40	394.0	226	5.00	5000	0.844	0.060	0.094	1.11	55.35	3.6	37.1	40.6	0.600	0.005	0.003	0.003
R10A-320/347	466	0.19	0.23	259.0	223	5.00	5000	0.966	0.245	0.203	1.23	56.92	4.1	9.9	14.0	0.479	0.006	0.006	0.006
R10B-418/445	549	0.62	0.69	682.0	436	5.00	5000	0.761	0.089	0.080	0.28	56.62	0.9	14.1	15.1	0.794	0.006	0.005	0.005
R10C-347/374	396	0.25	0.28	286.0	189	5.00	5000	0.959	0.158	0.141	2.65	56.94	8.8	10.9	19.7	0.477	0.009	0.002	0.002
R10D-356/383	377	0.21	0.26	268.0	180	5.00	5000	1.030	0.180	0.145	1.65	56.78	5.5	12.7	18.2	0.478	0.005	0.013	0.013

APPENDIX C: STRUCTURAL PROFILE OF THE CONTINUOUS MULTI-YEAR FLOE CORE

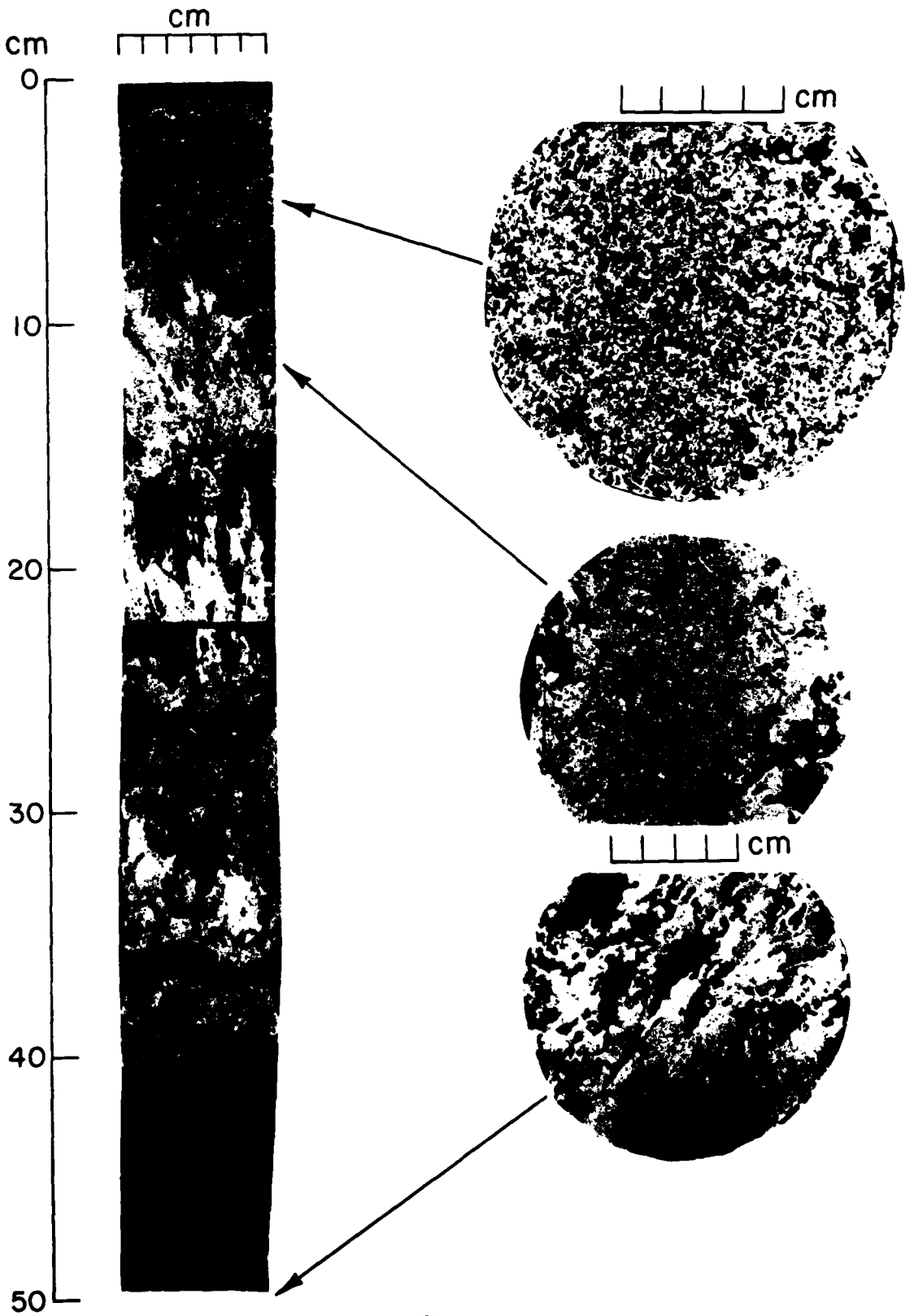

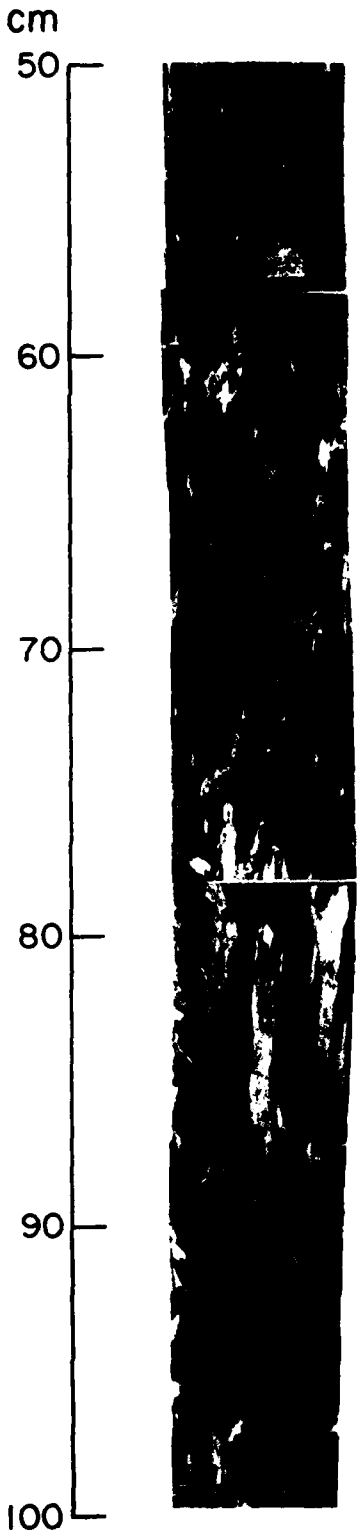
cm
50
60
70
80
90
100

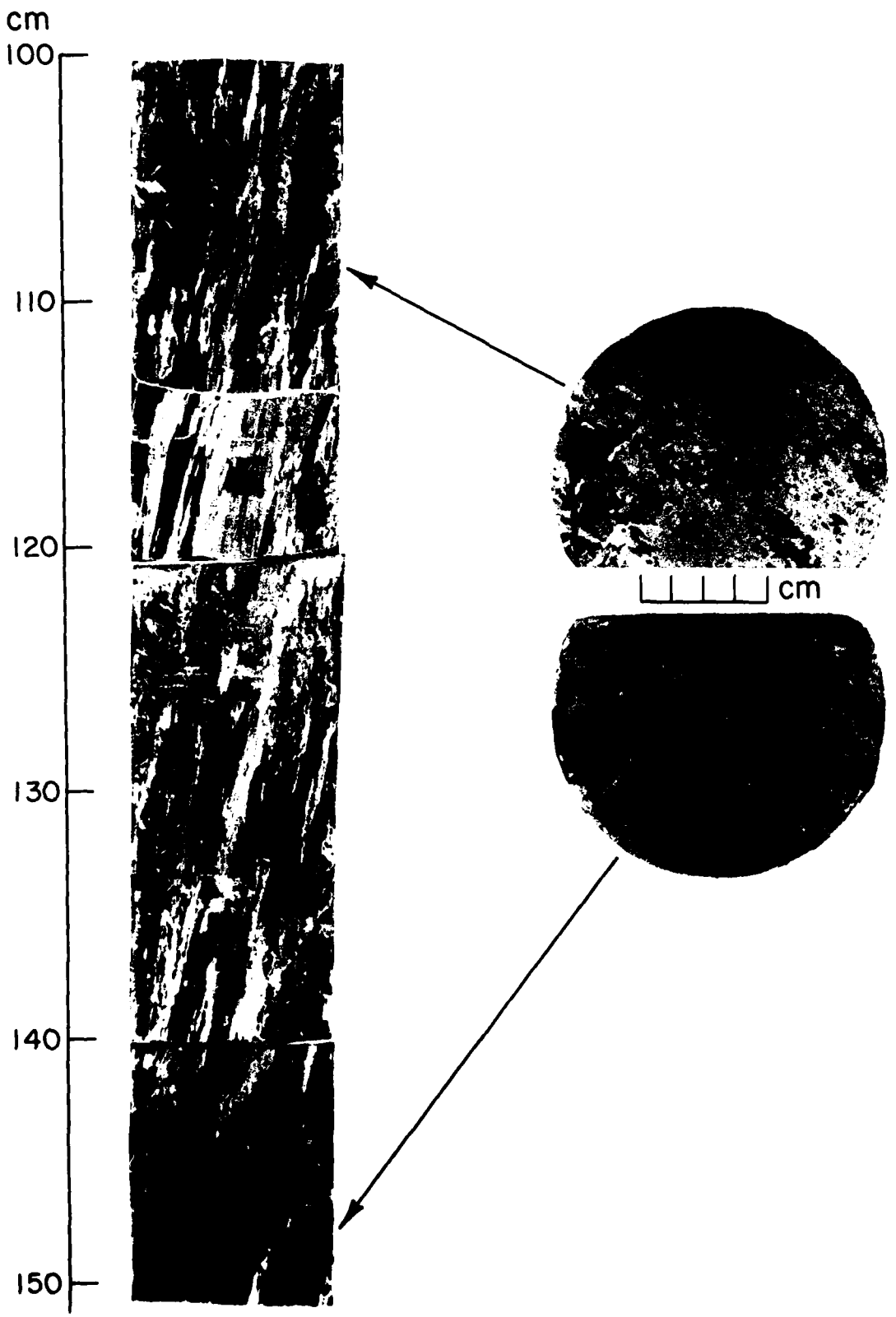
cm
100
110
120
130
140
150
cm

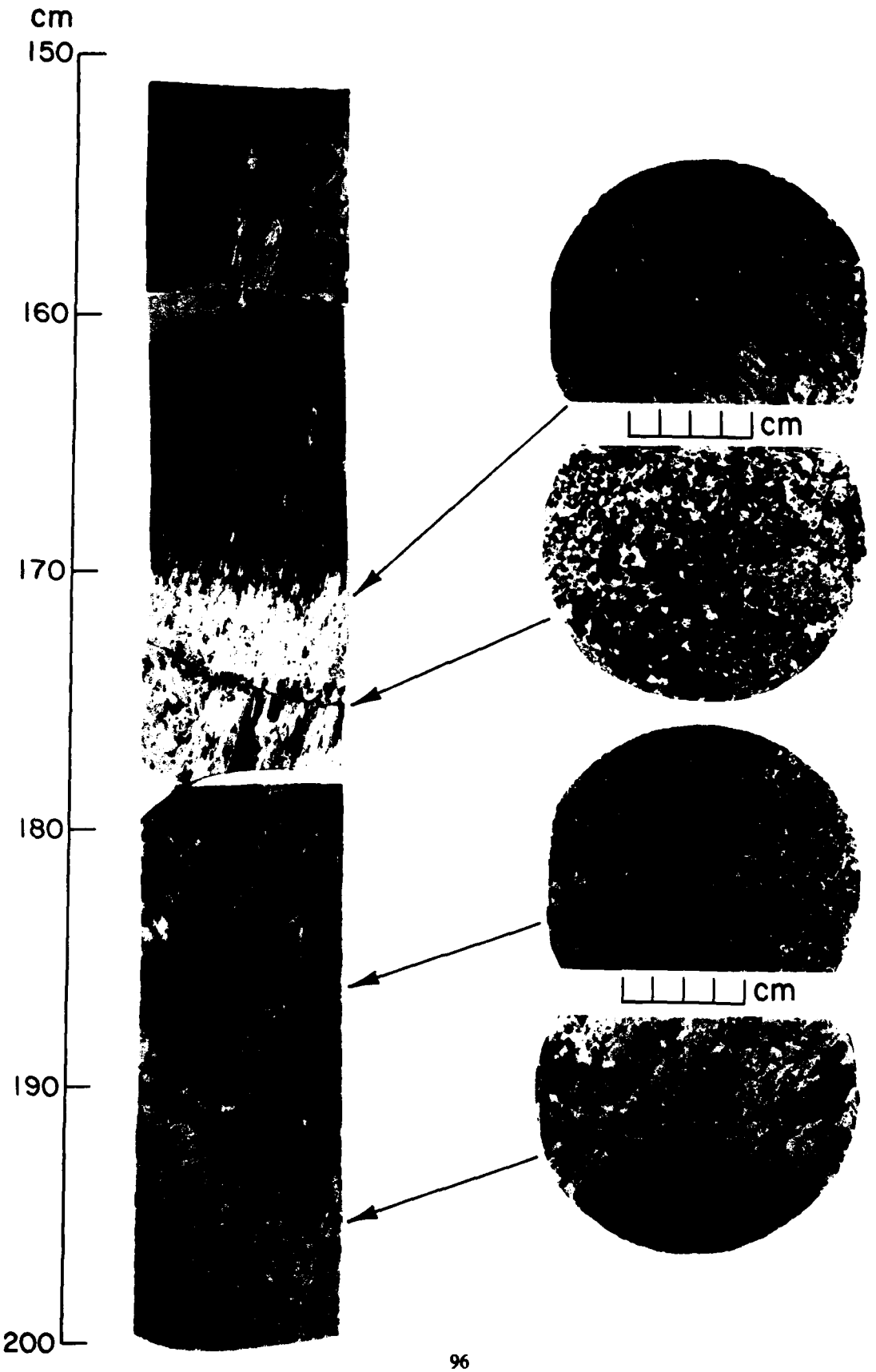
cm
150
160
170
180
190
200
cm
cm

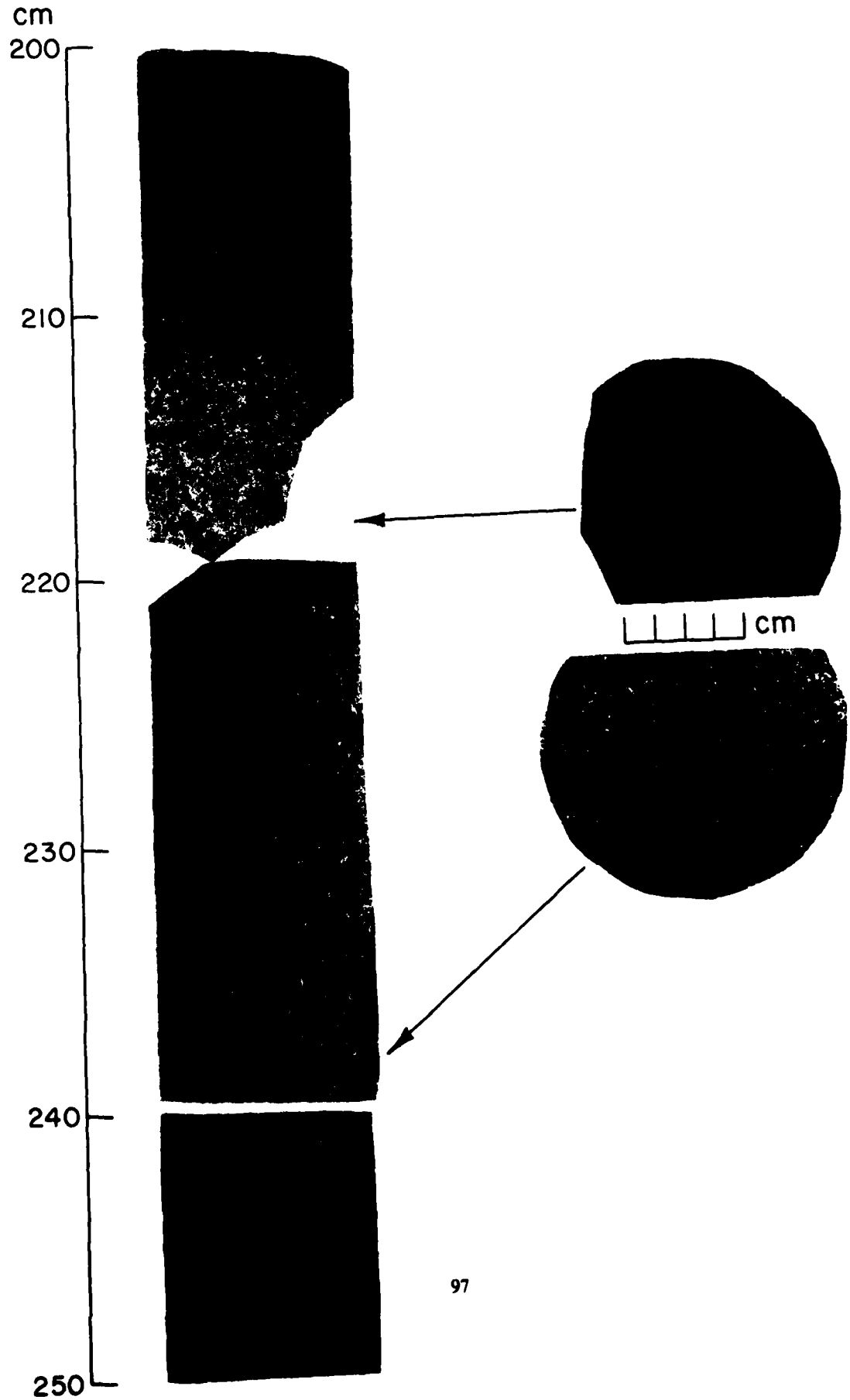
cm
200
210
220
230
240
250
cm

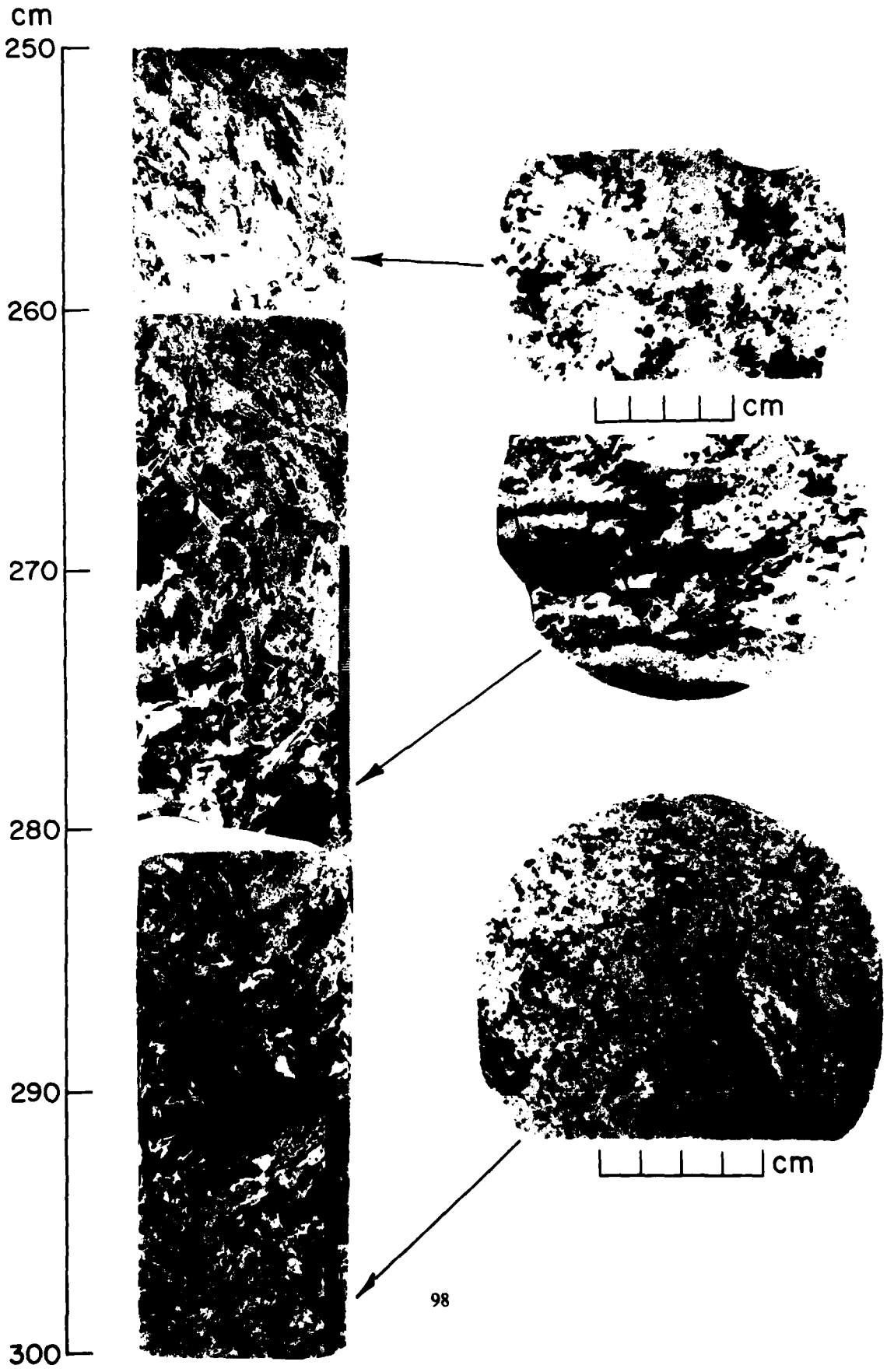
cm
250
260
270
280
290
300
cm
cm

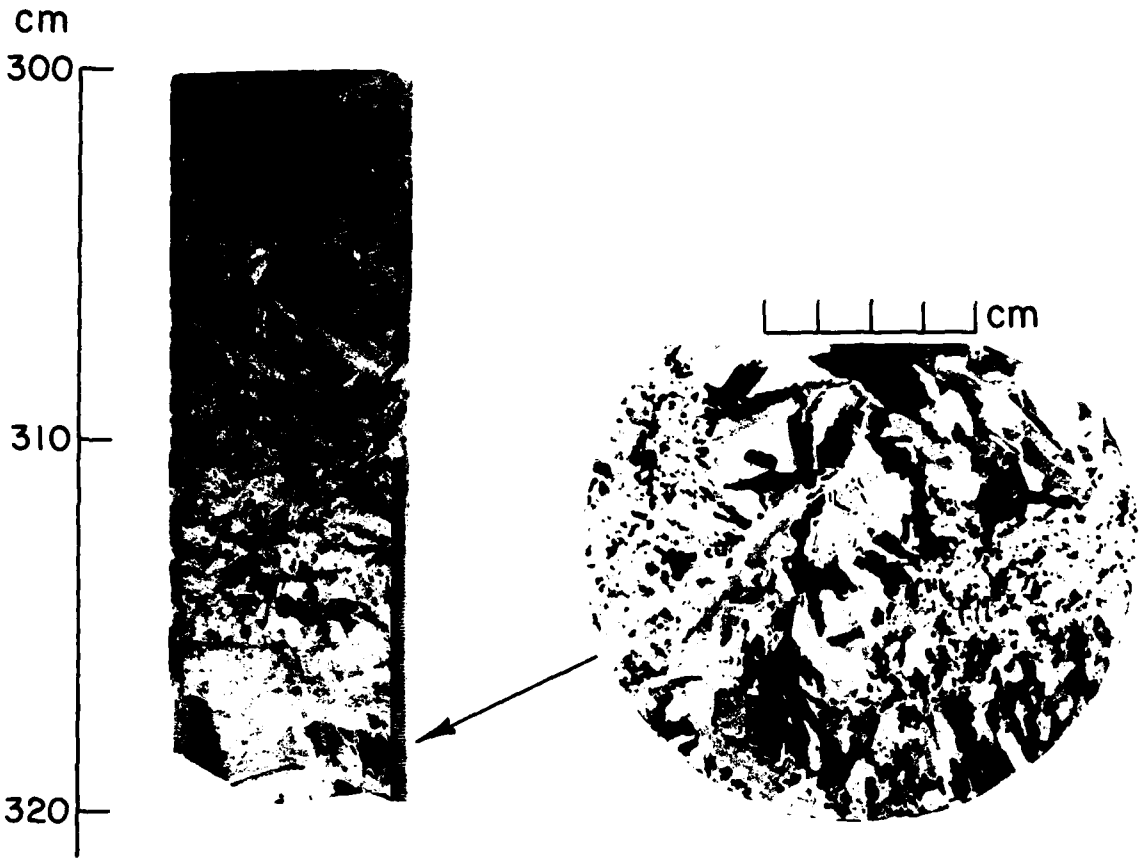
cm
300
310
320
cm

APPENDIX D: MULTI-YEAR FLOE TEST DATA

This appendix contains the results from the tests performed on the multi-year floe specimens. The results are grouped according to the type of test: constant-strain-rate uniaxial compression; constant-strain-rate uniaxial tension; constant-load uniaxial compression; and constant-strain-rate triaxial. Most variables have been defined in Index B, with the following exceptions. In the constant-strain-rate tension test data, the gauge length strains, ϵ_m(GL), were determined over a gauge length of 4.0 inches on the reduced section of the sample. In the constant-load compression test data, σ is the applied stress on the sample, $\dot{\epsilon}_{min}$(FS) is the strain-rate minimum determined from full sample displacement, ϵ_f(FS) is the full sample strain at the strain-rate minimum or failure, t_f is the time to failure, and $\dot{\epsilon}_e$(FS) is the full-sample strain rate at the end of the test.

Table D1. Multi-year floe
constant-strain-rate uniaxial compression test data.

Sample No.	σ_m psi	ε_m (GL) %	ε_m (FS) %	t_m	σ_e psi	ε_e (FS) %	t_e (sec)	E_o (GL)	E_o (FS) psix(10^6)	E_i (GL)	S_i o/oo	ρ lb/ft^3	v_b o/oo	v_a o/oo	n o/oo	σ_e/σ_m	ISQ in.	ESQ in.	SHM in.
$\dot{\varepsilon} = 10^{-3}$/sec, T = -5°C																			
C22-129/156	1373	0.09	0.14	1.45	1373	0.14	1.45	1.53	0.981	1.26	1.80	56.77	17.6	11.9	29.5		0.009	0.003	0.003
C22-159/186	1206	0.15	0.19	1.92	1206	0.19	1.92	0.804	0.635	0.880	1.59	56.27	15.4	20.2	35.7		0.010	0.004	0.004
$\dot{\varepsilon} = 10^{-5}$/sec; T = -5°C																			
C18-167/194	167	0.25	0.23	282	117	5.0	5000	0.0668	0.0726	0.567	1.88	56.43	18.3	17.9	36.2	0.701	0.021	0.001	0.001
C18-269/296	97.5	0.25	0.24	230	71.6	5.0	5000	0.0390	0.0406	0.607	2.20	57.19	21.7	5.3	27.0	0.734	0.007	0.010	0.010
$\dot{\varepsilon} = 10^{-3}$/sec; T = -20°C																			
C23-213/240	1520	0.20	0.22	2.51	187	5.0	50.0	0.760	0.691	1.07	0.80	56.60	12.6	15.0	17.6	0.123	0.008	0.006	0.006
C23-244/271	1556	0.19	0.20	1.86	235	5.0	50.0	0.819	0.778	0.880	1.07	56.75	3.0	12.5	15.5	0.151	0.012	0.012	0.012
$\dot{\varepsilon} = 10^{-5}$/sec; T = -20°C																			
C19-165/192	543	0.19	0.22	234	258	5.0	5000	0.286	0.247	1.01	2.20	56.71	7.3	14.5	21.8	0.475	0.015	0.010	0.010
C18-236/263	258	0.23	0.21	262	90	5.0	5000	0.112	0.123	0.718	1.51	56.81	5.0	12.1	17.1	0.349	0.005	0.008	0.008
$\dot{\varepsilon} = 10^{-2}$/sec; T = -20°C																			
C5-228/254	1345	0.10	0.16	0.20	1345	0.16	0.20	1.345	0.841	1.522	1.78	57.19	5.9	5.7	11.7		0.014	0.009	0.009
C13-236/263	1273	0.11	0.12	0.16	1273	0.12	0.16	1.157	1.061	1.465	2.00	56.84	6.6	12.0	18.7		0.006	0.018	0.018
C23-158/185	2157	0.15	0.20	0.21	2157	0.20	0.21	1.438	1.079	1.644	2.64	56.80	8.8	13.3	22.1		0.004	0.010	0.010

Table D2. Multi-year floe
constant-strain-rate uniaxial tension test data.

Sample No.	σ_m psi	ε_m (GL) %	ε_m (FS) %	t_m (sec)	σ_e (psi)	ε_e (FS) %	t_e sec	E_o (GL) psix(10^6)	E_o (FS) psix(10^6)	E_i (GL)	E_i (FS)	S_i o/oo	ρ lb/ft^3	v_b o/oo	v_e o/oo	n o/oo	ISQ in.	ESQ in.
$\dot{\varepsilon} = 10^{-3}$/sec; T = -5°C																		
C17-228/255	168	0.013	0.018	0.38	168	0.018	0.38	1.292	0.933	1.167		0.70	56.54	6.8	14.1	20.9	0.007	0.003
C17-259/286	185	0.014	0.015	0.41	185	0.015	0.41	1.321	1.233	0.657		0.95	56.90	9.3	8.3	17.6	0.008	0.009
C21-092/119	160		0.014	0.25	160	0.014	0.25		1.143		0.945	1.89	56.56	18.4	15.7	34.1	0.007	0.002
C22-077/104	94.6		0.009	0.17	94.6	0.009	0.17		1.051		1.757	1.11	56.48	10.8	15.8	26.6	0.017	0.006
$\dot{\varepsilon} = 10^{-5}$/sec; T = -5°C																		
C16-224/251	169		0.025	27.6	169	0.025	27.6		0.676		0.849	1.32	56.79	12.9	10.8	23.7	0.005	0.002
C16-256/283	142		0.037	38.3	142	0.037	38.3		0.384		0.650	1.11	56.89	10.9	8.7	19.6	0.005	0.005
C16-288/315	122		0.024	22.8	122	0.024	22.8		0.508		0.815	1.01	56.57	9.9	14.1	24.0	0.005	0.006
$\dot{\varepsilon} = 10^{-3}$/sec; T = -20°C																		
C15-135/162	152	0.011	0.013	0.12	152	0.013	0.12	1.382	1.169	1.377		1.46	57.03	4.9	8.2	13.0	0.009	0.010
C21-198/225	83.2		0.008	0.20	83.2	0.008	0.20		1.040		1.26	1.38	55.08	4.4	42.0	46.5	0.007	0.002
C21-134/161	154		0.012	0.24	154	0.012	0.24		1.283			2.15	56.82	7.1	12.5	12.5	0.009	0.005
$\dot{\varepsilon} = 10^{-5}$/sec; T = -20°C																		
C17-126/153	189	0.018	0.020	3.24	189	0.020	3.24	1.050	0.945	1.223		1.86	57.14	6.2	6.7	12.9	0.018	0.004
C21-166/193	125		0.021	20.9	125	0.021	20.9		0.595		0.666	2.85	56.98	9.5	10.4	19.9	0.009	0.002
C21-266/293	164		0.023	23.2	164	0.023	23.2		0.713		1.047	1.51	56.99	5.0	8.9	13.9	0.017	0.008
C22-236/263	124		0.028	27.5	124	0.028	27.5		0.443		1.247	2.22	57.01	7.4	9.3	16.7	0.005	0.006

Table D3. Multi-year floe
constant-load compression test data.

Sample No.	σ psi	T °F	$\dot{\varepsilon}_{min}^{(FS)}$ sec^{-1}	$\varepsilon_f^{(FS)}$ %	t_f sec	$\dot{\varepsilon}_e^{(FS)}$ sec^{-1}	ε_e %	t_e sec	S_l o/oo	ρ lb/ft^3	v_b o/oo	v_a o/oo	n o/oo	ISQ. in.	ESQ. in.
BELLOFRAM TESTS															
C22-269/296	100	23	1.98×10^{-8}	0.311	1.04×10^{5}	3.24×10^{-8}	1.10	4.10×10^{5}	1.00	56.99	6.8	9.8	16.7	.004	.008
C18-136/163	100	23	3.44×10^{-8}	0.311	5.40×10^{4}	1.61×10^{-7}	4.86	5.78×10^{5}	1.41	56.11	13.6	22.7	36.3	.007	.013
C19-134/161	100	-4	no $\dot{\varepsilon}_{min}$			1.17×10^{-9}	0.04	1.45×10^{6}	1.61	56.78	5.3	12.3	17.6	.008	.004
C14-129/156	100	-4	no $\dot{\varepsilon}_{min}$			1.77×10^{-7}	0.72	3.13×10^{4}	1.16	55.47	3.8	35.0	38.7	.019	.002
MTS TESTS															
C16-134/161	300	23	1.00×10^{-7}	0.180	1.20×10^{4}	5.38×10^{-6}	1.69	5.80×10^{4}	1.64	56.46	16.0	17.0	33.0	.013	.005
C16-073/100	600	23	1.41×10^{-6}	0.168	9.10×10^{2}	7.87×10^{-5}	1.08	2.77×10^{3}	1.89	56.53	18.4	16.2	34.7	.027	.019
C12-267/294	600	23	2.39×10^{-4}	0.187	5.0	3.59×10^{-3}	1.68	2.00×10^{1}	1.80	56.93	17.7	9.1	26.8	.011	.005
C16-165/192	600	-4	5.60×10^{-6}	0.208	2.08×10^{2}	9.51×10^{-4}	2.53	5.84×10^{2}	1.46	56.69	4.8	14.1	18.9	.009	.006
C12-236/263	600	-4	6.67×10^{-5}	0.155	1.07×10^{1}	3.83×10^{-3}	2.55	7.39×10^{2}	1.98	56.61	6.5	16.1	22.6	.009	.009

Table D4. Multi-year floe constant-strain-rate triaxial compression test data.

Sample No.	σ_m psi	ε_m (FS) %	t_m sec	σ_e psi	ε_e (FS) %	t_e sec	E_i (FS) psix(10^6)	E_o (FS) psix(10^6)	S_i o/oo	ρ lb/ft^3	v_b o/oo	v_a o/oo	n o/oo	σ_e/σ_m	ISQ in.	ESQ in.	SHM in.
$\dot{\varepsilon} = 10^{-3}$/sec; T = -5°C; $\sigma_r/\sigma_a = 0.46$																	
C6-228/255	1991	0.56	5.28	1125	5.0	50	0.336	0.356	1.74	56.93	17.1	9.0	26.1	0.565	0.002	0.005	0.004
C6-259/286	1984	0.61	5.97	975	5.0	50	0.553	0.325	1.42	56.92	13.9	8.7	22.6	0.491	0.005	0.007	0.006
C7-129/154	≈4940	≈0.81		1224	5.0	50	0.737		1.09	56.85	10.7	9.4	20.0		0.006	0.013	0.012
C7-267/294	>2041			1060	5.0	50	0.869		1.30	56.80	12.7	10.6	23.3		0.010	0.010	0.010
C24-138/165	2865	0.73	7.25	1034	5.0	50	0.907	0.393	2.74	56.06	26.5	25.7	52.2	0.361	0.009	0.009	0.008
C24-268/295	1474	0.89	8.80	1003	5.0	50	0.394	0.166	2.15	56.88	21.1	10.6	31.6	0.680	0.007	0.003	0.002
$\dot{\varepsilon} = 10^{-3}$/sec; T = -5°C; $\sigma_r/\sigma_a = 0.68$																	
C6-132/158	≈5774	≈1.08					0.700		1.91	56.89	18.7	10.0	28.7		0.012	0.004	0.004
C19-271/298	3099	1.59	16.2	2510	5.0	50	0.700	0.195	0.87	56.59	8.5	13.5	22.0	0.810	0.005	0.009	0.008
C20-188/215	2772	1.61	16.1	1776	5.0	50	0.569	0.172	1.19	56.07	11.5	23.1	34.6	0.641	0.008	0.008	0.008
C20-238/265	>3716						0.639		1.75	56.73	17.1	12.5	29.6		0.003	0.009	0.008
$\dot{\varepsilon} = 10^{-5}$/sec; T = -5°C; $\sigma_r/\sigma_a = 0.46$																	
C7-155/180	1148	0.42	416	486	5.0	5000	0.760	0.273	1.46	56.88	14.3	9.4	23.8	0.423	0.009	0.009	0.008
C7-236/263	479	0.47	467	323	5.0	5000	0.715	0.102	1.76	56.96	17.3	8.5	25.8	0.674	0.008	0.004	0.004
C24-072/099	1512	0.53	536	524	5.0	5000	0.509	0.285	1.14	56.75	11.2	11.2	22.37	0.347	0.010	0.005	0.004
C24-237/264	927	0.69	562	668	5.0	5000	0.268	0.134	2.03	56.75	19.9	12.6	32.5	0.721	0.004	0.007	0.006
$\dot{\varepsilon} = 10^{-5}$/sec; T = -5°C; $\sigma_r/\sigma_a = 0.68$																	
C13-267/294	758	0.88	880	528	5.0	5000	0.328	0.0861	2.94	56.88	28.8	11.8	40.7	0.697	0.010	0.006	0.006
C14-267/294	602	1.03	927	543	5.0	5000	0.356	0.0585	2.93	56.98	28.8	10.1	38.9	0.902	0.014	0.007	0.006
C19-081/108	2535	0.67	670	1034	5.0	5000	0.636	0.378	1.34	56.78	13.1	11.0	24.1	0.408	0.015	0.001	0.000
C24-164/196	1197	0.82	845	877	5.0	5000	0.439	0.146	1.61	56.07	15.6	23.7	39.3	0.733	0.004	0.010	0.010
$\dot{\varepsilon} = 10^{-3}$/sec; T = -20°C; $\sigma_r/\sigma_a = 0.46$																	
C12-072/099	>3716						0.590		1.42	57.01	4.7	8.5	13.2		0.011	0.007	0.006
C14-236/263	3329	1.02	10.54	1523	5.0	5000	0.543	0.326	2.71	57.01	9.0	9.8	18.8	0.458	0.006	0.020	0.020
$\dot{\varepsilon} = 10^{-5}$/sec; T = -20°C; $\sigma_r/\sigma_a = 0.46$																	
C18-072/099	2212	0.60	596	1132	5.0	5000	0.525	0.369	1.42	57.35	4.8	2.6	7.3	0.512	0.009	0.002	0.002
C19-240/267	1429	0.76	762	806	5.0	5000	0.369	0.188	1.06	56.24	3.5	21.5	25.0	0.564	0.008	0.004	0.004
$\dot{\varepsilon} = 10^{-5}$/sec; T = -20°C; $\sigma_r/\sigma_a = 0.68$																	
C6-163/189	2527	3.21	3190	2178	5.0	5000	0.444	0.0787	1.42	56.86	4.7	11.1	15.8	0.862	0.008	0.002	0.002
C20-269/296	2320	1.72	1705	1866	5.0	5000	0.340	0.135	1.74	56.90	5.8	10.7	16.5	0.804	0.006	0.003	0.002

A facsimile catalog card in Library of Congress MARC format is reproduced below.

Cox, G.F.N.
Mechanical properties of multi-year sea ice: Phase I: Test results / by G.F.N. Cox, J.A. Richter-Menge, W.F Weeks, M. Mellor and H. Bosworth. Hanover, N.H.: Cold Regions Research and Engineering Laboratory; Springfield, Va.: available from National Technical Information Service, 1984.
v, 107 p., illus., 28 cm (CRREL Report 84-9.)
Bibliography: p. 51
1. Ice. 2. Ice properties. 3. Mechanical properties 4. Sea ice. I. Richter-Menge, J.A. II. Weeks, W.F. III. Mellor, M. IV. Bosworth, H. V. United States. Army. Corps of Engineers. VI. Cold Regions Research and Engineering Laboratory, Hanover, N.H. VII. Series: CRREL Report 84-9

END

DATE
FILMED

9-84

DTIC